Analysis and Design of a Double-sided Rotor Iron-Cored Radial Flux Permanent Magnet Synchronous Wind Turbine Generator

by

Johannes Hendrik van Wijk

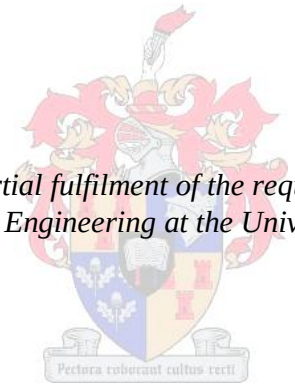

Thesis presented in partial fulfilment of the requirements for the degree Master of Science in Engineering at the University of Stellenbosch

Supervisor: Prof. Maarten Jan Kamper
Faculty of Engineering
Department of Electrical Engineering

March 2012

Declaration

By submitting this thesis electronically, I declare that the entirety of the work contained therein is my own, original work, that I am the sole author thereof (save to the extent explicitly otherwise stated), that reproduction and publication thereof by Stellenbosch University will not infringe any third party rights and that I have not previously in its entirety or in part submitted it for obtaining any qualification.

March 2012

Abstract

Analysis and Design of a Double-Sided Rotor Iron-Cored Radial Flux Permanent magnet Synchronous Wind Turbine Generator

J.H. van Wijk

Department of Electrical and Electronic Engineering

University of Stellenbosch

Private Bag X1, Matieland, 7602, South Africa

Thesis: MScEng (Electrical)

March 2012

The electromagnetic and mechanical design aspects of an optimally designed double-sided rotor radial flux permanent magnet wind generator with non-overlap iron-cored stator windings are analysed in this thesis. The generator topology proposed in this study aims to reduce the strength demand on the generator structural support, caused by the magnetic attraction forces between the rotor and stator iron components, and in so doing reducing the overall generator mass. The proposed design has very good cooling properties. Compared to a conventional iron-cored permanent magnet generator and an air-cored permanent magnet generator, the double-sided rotor iron-cored topology performs the best with reference to mass and efficiency.

Uittreksel

Analiese en Ontwerp van ‘n Tweesydige Rotor Ysterkern Permanente Magneet Sinchroon Wind Turbiene Generator

J.H. van Wijk

Departement van Elektriese en Elektroniese Ingenieurswese

Universiteit van Stellenbosch

Privaatsak X1, Matieland, 7602, Suid Afrika

Tesis: MScIng (Elektries)

Maart 2012

Die elektro-magnetiese en meganiese ontwerp-aspekte van ‘n optimal ontwerpte tweesydige rotor radial-vloed permanente magneet windgenerator met nie-oorvleulende ysterkern statorwindings word in hierdie tesis ontleed. Met die generator topologie wat in hierdie studie voorgestel word, word beoog om die strukturele materiaal wat vir die generator benodig is te verminder. Die magnetise aantrekkingskragte tussen die yster komponente van die rotor en stator word dus aangespreek in hierdie studie, om sodoende ook die algehele massa van die permanente magneet generator te verminder. Die voorgestelde tweesydige-rotor ontwerp het baie goeie verkoelings eienskappe en het ‘n kleiner massa en hoër effektiwiteit as beide ‘n konvensionele ysterkern generator met ‘n enkelsydige-rotor en ‘n tweesydige-rotor lugkern permanente magneet generator met dieselfde drywingsvermoë.

Author Publications

Work done in this thesis can be viewed, in part, in the following publication by the author:

International Conference Papers

J.H. van Wijk, M.J. Kamper, “C - core topology for PM wind generators with non-overlap iron-cored stator windings ", in IET Int. Conf. Power Electron., Mach. and Drives, Brighton, 2010, p. 1-6.

Acknowledgements

Thanks to...

...my God and Heavenly Father for His provision and grace throughout my studies, His gift of salvation through His son Jesus Christ, and His guidance through His Holy Spirit.

…my study leader, Professor Maarten Kamper, for his guidance, counsel, encouragement and prayers.

…the workshop staff of both the SED and SMD for their help with the building of the prototype machine. Special thanks to André Swart, Jos Weerdenburg, Murray Jumat and Pietro Petzer for always being willing to help.

…my wife for her love, support and encouragement through the tough times and late working hours.

…my parents for their prayers, support and for reminding me of my previous victories when I became disheartened.

The financial assistance of the South African National Energy Research Institute toward this research is hereby acknowledged. Opinions expressed and conclusions arrived at, are those of the author and are not necessarily to be attributed to SANERI.

Table of Contents

List of Figures

List of Tables

Nomenclature

Constants

Symbol	Meaning	Unit
μ_0	Permeability of air	($4\pi \times 10^{-7}$ H/m)
π	pi	(3.141 592 653 589)
ρ_a	Density of air at sea level	(1.225 kg/m^3)
ρ_{cu}	Density of copper at room temperature	(8930 kg/m^3)
ρ_m	Density of magnet material (NdFeB) at room temperature	(7501 kg/m^3)
ρ_{fe}	Density of mild steel at room temperature	(7850 kg/m^3)
σ_{fe}	Yield stress of mild steel	(250 x 10^6 Pascal)
$\zeta_{cu\text{-}20}$	Resistivity of copper at room temperature	(17 nΩm)

Variables (in alphabetical order with dimensionless units denoted by '#')

English alphabet symbols:

Symbol	Meaning	Unit
a	Number of parallel connected circuits	(#)
A	Cross-sectional area of the magnetic flux path	(m^2)
B	Average magnetic flux density in the air gap (B_g) and in the steel rotor yoke (B_y). Residual magnetic flux density (B_r) and peak air gap flux density of the fundamental harmonic (B_{p1})	(T)

D_o	Outer diameter of outer rotor yoke	(m)
D_i	Inner diameter of inner rotor yoke	(m)
d_o	Outer diameter of inner rotor yoke	(m)
d_i	inner diameter of outer rotor yoke	(m)
d_i	Average diameter of inner curved permanent magnets	(m)
E	Young's modulus, or modulus of elasticity	(Pa)
E_g	Per phase back-EMF RMS voltage of the generator	(V)
E_{oc}	Open circuit terminal voltage	(V)
f_{fld}	Magnetic field force in air gap	(N)
f	Electrical frequency	(Hz)
f_r	Electrical frequency of wound rotor	(Hz)
g	Air gap length	(m)
g_0	Designed air gap length	(m)
g_c	Air gap clearance	(m)
h	Stator thickness/height measured in the radial direction	(m)
h_m	Magnet thickness/height measured in the radial direction	(m)
h_y	Rotor yoke thickness/height measured in the radial direction	(m)
h_s	Stator thickness/height measured in the radial direction	(m)
i	Magnetic flux excitation current	(A)
I_0	Area moment of inertia	(m^4)
I_{sc}	Short circuit current	(A)
J	Current density	(A/mm^2)
k_f	Copper filling factor	(#)
k_w	Stator winding factor	(#)
l_a	Active length of a stator coil	(m)
l_g	air gap length measured in the radial direction	(m)
L_s	Total system inductance	(H)

m	Number of phases in machine	(#)
N_p	Number of parallel strands in a conductor	(#)
N_t	Number of turns per coil	(#)
n_s	Stator field rotational speed	(rpm)
n_r	Rotor mechanical rotational speed	(rpm)
n_d	Design safety factor	(#)
n_l	Number of slot layers	(#)
n_t	Number of turns per stator winding coil	(#)
p	Number of permanent magnet poles	(#)
P_{cu}	Copper losses in the generator	(W)
P_d	Developed power of the turbine	(W)
P_{gr}	Rated generator power	(W)
p_i	Internal pressure inside the cylinder pressure vessel	(Pa)
p_o	External pressure outside the cylinder pressure vessel	(Pa)
P_o	Designed electrical power output	(kW)
q	Number of stator coils per phase	(#)
Q	Total number of coils in stator	(#)
R_{cu}	Resistance of copper wire	(Ω)
r	Rotor yoke radius, r_i – inner yoke radius, r_o – outer yoke radius	(m)
R_i	Per-phase internal phase resistance of copper stator windings	(Ω)
t	Stator slot closing thickness	(m)
T_0	Designed turbine torque	(Nm)
ΔT	Torque ripple at rated speed	(Nm)
T_{ave}	Average developed torque	(Nm)
THD_V	Total harmonic distortion of the measured voltage waveforms	(%)
V_n	Voltage amplitude of the n^{th} order harmonic frequency	(V)
W_{fld}	Stored co-energy in air gap	(J)

x	Stator eccentricity offset	(m)
x_k	Machine parameter k	(-)
X_i	Internal inductive reactance of the stator	(Ω)
Z_i	Per-phase internal impedance	(Ω)

Greek alphabet symbols:

Symbol	Meaning	Unit
B	Rotor skewing angle	(deg)
η_g	Generator efficiency	(%)
λ	Flux linkage of the concentrated coil	(Wb-turns)
μ_m	Permeability of the magnet material	(H/m)
Φ	Magnetic flux	(Wb)
θ_c	Coil width angle (non-linearised model)	(rad)
θ_m	Magnet angle (non-linearised model)	(rad)
θ_p	Magnet pitch angle (non-linearised model)	(rad)
θ_S	Slot pitch angle (non-linearised model)	(rad)
θ_g	Slot angle (non-linearised model)	(rad)
θ_w	Slot opening angle (non-linearised model)	(rad)
σ_h	Hoop stress in a cylinder pressure vessel	(Pa)
σ_l	Longitudinal stress in a cylinder pressure vessel	(Pa)
σ_r	Radial stress in a cylinder pressure vessel	(Pa)
σ_Y	Yield stress of a material	(Pa)
τ_m	Permanent magnet pole pitch	(#)
$\Delta\tau$	Cogging torque	(Nm)
ω_e	Electrical rotating speed (electrical frequency)	(rad/s)
ω_m	Mechanical angular velocity of the turbine	(rad/s)

Chapter 1
Introduction

The most basic form of energy that humans need to survive is food. However, as population increases and civilization, as we know it today, develops, the demand for energy also increases. It is commonly accepted that a country's energy consumption is a measure of its prosperity and degree of development, since we greatly depend upon mechanical power for industries, agriculture and in almost every aspect of our daily life and work [1]. In recent years however, a lot of concern has been raised with regards to the sustainability of our current energy resources. Likewise the effect these fossil fuel power plants have on the environment and the expected contribution it makes to climate change has created a global shift towards the utilisation of renewable and sustainable energy resources, such as wind.

This chapter presents a comprehensive overview of a literature study done on wind energy conversion, including a historical overview of the development of the modern wind energy converter (WEC), some reasons why there is a shift toward direct-drive generator systems, and finally a summary of the major present and future challenges wind turbine manufactures face. This chapter concludes with the problem statement, objectives for this study, and thesis layout.

1.1 Literature Review

In this section the development of the wind turbine technology is explored; from its humble beginnings - producing primitive mechanical power - to our present-day state of the art structures. Specific attention is given to direct-drive (DD) radial flux permanent magnet (RFPM) synchronous generators with its advantages, disadvantages and design challenges, which are related to the growing power rating demands. In the light of these challenges, a few unconventional concepts, proposed in literature are also discussed.

1.1.1 Humble Beginnings to State of the Art

Although the skill of sailing was already well established among certain civilizations, the use of a mechanism that harnessed the energy of the wind to produce mechanical power was first documented around 640 BC among the Persians [2]. These vertical axis windmills had woven reed sails and were used to drive stone mills for the grinding of grain. Similar structures, utilised to pump water, were also found in the Chinese civilization The introduction of these mechanical wind energy converters to Europe (and later to the West), is speculated to have happened around the time of the first crusades, during the late 11th century (first crusades1096–1099).

In early Europe however, the supply of labour was in abundance and there was no need for the development of new energy sources. As time progressed to the Middle Ages[1], this need took a turn with the fall of the Roman Empire and the introduction of feudalism. It is the opinion of the author that the high rent that peasants were obliged to pay, sparked the search for more energy in order to be more productive with the processing of commodities, which resulted in the rapid development of renewable energy resources. By the eleventh century water mills had become a very common sight in countries such as England and France. Horizontal axis wind energy converters (WECs), also known as windmills, were developed mostly in dryer areas where they were used to grind grain, press olives, process commodities such as tobacco and spices, to mill timber, pump water and operate hammers or the bellows of forges. The Netherlands in particular benefitted from windmills, refining and adapting it for the retrieval of land from its lakes and marsh lands in the 13th century [3]. The windmill was truly the "electrical machine" of pre-industrial Europe, the total converted energy of that time estimated to have been an astonishing 1500 MW; and this being only 600 years since its introduction to Europe [4].

The invention of the steam engine played a key role during the industrial revolution (around 1750), which was focused on mechanisation. It provided power that did not depend upon the flow of rivers or the movement of the wind and made the pumping of water from coal mines possible, allowing miners to dig deeper and retrieve more coal [5] [6]. During this time period the energy consumption of the industrial man rose by a factor 3. The steam engine did consume large amounts of energy, but the advent of the use of coal, which had to be excavated from the earth, produced a lot of work and provided a more reliable source of power that allowed a rapid growth in mankind's wealth.[7] [6].

[1] 5th to 15th Century.

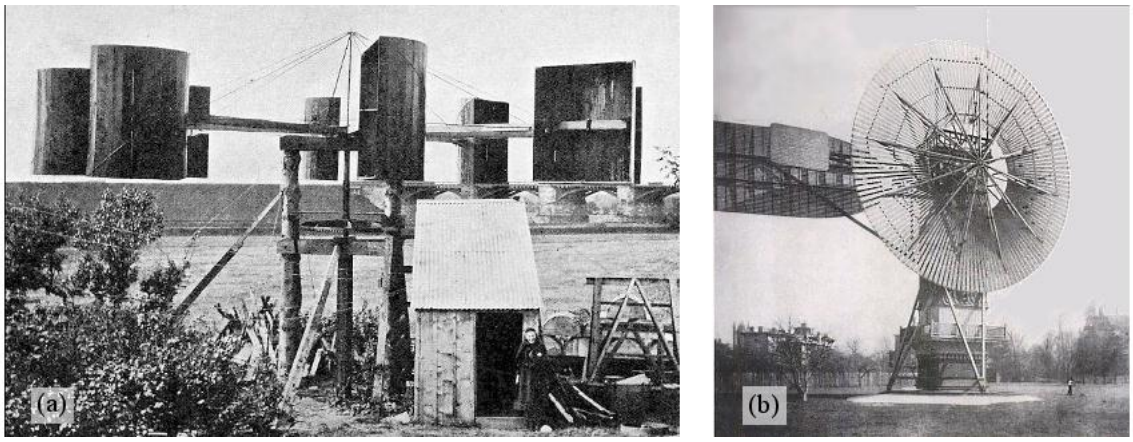

Figure 1: The first two electricity generating turbines – (a) Blyth [10] and (b) Brush [10][11].

Contrary to common belief, the interest in wind energy never dissipated because of the electrification of the industrial world or because fossil fuels became more economical in generating electricity on large scale. The use of the windmill for converting energy to mechanical work did fade, but worldwide theorists and practicians continued to design and build improved windmills which were used for the generation of electricity [6]. Today electricity producing WECs are known as wind turbines.

In the summer of 1887, a Scotsman, Professor James Blyth of Anderson's Collage, Glasgow (today Strathclyde University), was the first to be successful in generating electricity with the use of a windmill [8]. His last of three turbine designs, a 33ft high, cloth-sailed vertical axis wind turbine, powered his home for 25 years [3][9]. About six months later, Professor Charles F. Brush built a 12 kW wind turbine, storing the energy generated in 408 batteries in the cellar of his mansion. His turbine was measured 17 meters in diameter with 144 cedar wood rotor blades and mounted on an 18 meter tower [3][4].These two pioneering structures are shown in Figure 1.

Around the turn of the century, a scientist, Poul la Cour, determined to bring electricity to the rural population of Denmark, discovered that fast rotating wind turbines with fewer rotor blades are more efficient in generating electricity production [8]. He developed a 25 kW four-bladed rotor machine, which was used throughout Denmark by the end of World War I, making Denmark the first country to use the wind for the generation of electricity [2][4].

In the 20's Albert Betz, a professor at the German aero-dynamical research centre in Göttingen, made some path-breaking theoretical studies on wind turbines. His work showed that the fundamental laws of conservation of mass and energy limit the amount of kinetic energy that can be extracted from the wind [6]. This theoretical maximum coefficient of power, also known as the Betz limit, is reached when the wind speed behind the turbine is one third of the undisturbed wind before the turbine [1]. The coefficient of power is furthermore dependent on the blade tip-speed ratio, the

number of blades, blade angle, and the blade design. H. Glauert likewise made numerous contributions to the aerofoil and propeller theories of the time [6]. Both Betz's and Gauert's theoretical contributions have laid the foundation of today's rotor theory. Figure 2 shows that the power coefficient for the most common blade designs varies with the tip-speed ratio.

During the 30's the American market saw a boom in the building and installation of small commercial wind-electric plants all over northern America. Two- and three-bladed turbines with a capacity of 1-3 kW provided farms with lighting, charged crystal radio sets, and later their use was extended to power appliances and farm machinery. The drop in fossil fuel prices and the gradual expansion of power grids throughout rural areas in America soon after World War II, once again resulted in the declined use of these small, electricity generating wind turbines [4].

The late 50's has seen the inventor, Ullrich Hütter from Germany, develop various advanced intermediate size wind turbines. He discovered that slender blades mounted on a rotor with a high tip-speed ratio harnesses more power from the wind. With this discovery, Hütter was ahead of his time, seeing as manufacturing problems with tiny aerofoils and a light yet strong enough material to withstand the complex dynamic forces on the blades were issues at the time. In response to these issues, Hütter investigated shedding these loads as an alternative to withstanding them and introduced a bearing at the rotor hub which allowed the rotor to "teeter" in response to wind gusts and vertical wind shear. He furthermore used fibreglass and plastic in his blade designs, in order to cut back on mass and introduce flexibility for further load-shedding. Hütter also equipped the blades with a pitch that could change in higher wind speeds to keep its rotational speed constant. These novel features he incorporated into a series of advanced intermediate size turbines, which proved to provide greater operating efficiencies. With his aeronautical background, Hütter furthermore developed a theory for blade-element momentum, which is said to be contemporary even today. He was also the first to experiment with wind turbines in the stronger and steadier off-shore winds. [2][4][13].

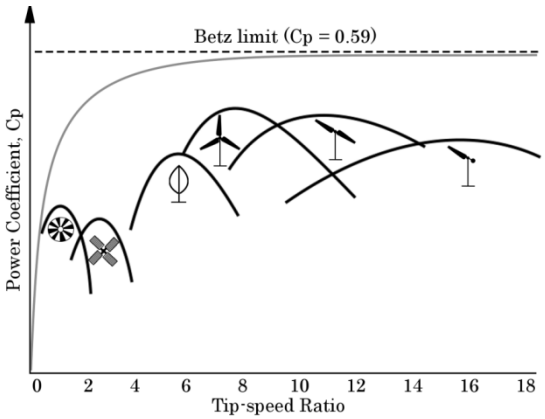

Figure 2: Power coefficient vs tip-speed ratio of different blade designs [12].

The Arab Oil Embargo of 1973-74 brought about a global oil crisis which once again sparked interest in alternative energy resource utilisation. One of the many consequences of the embargo was the oil prices that quadrupled within a few months all throughout the western world [14]. Governments, hoping to make them more independent, showed interest by sponsoring renewable energy research programs in Germany, Sweden, Canada, Great Britain and the United States. As a result, new large scale wind turbines were designed and tested. With over seven decades' theoretical and practical turbine design know-how and with the governments' financial support toward these research programs, it is considered to be a major contributor to significantly reducing the cost of wind power over the following two decades [4][6]. The commercial wind turbine market also witnessed a shift in focus, from small stand-alone machines used primarily in agriculture, to large scale wind turbines arranged in wind farms and connected to the power grid [4].

In recent years climate change, air pollution and related environmental issues have become a growing concern worldwide. As a result, more and more governments are finding interest in greener energy, aiming to reduce greenhouse gasses and other emissions [4], and so stimulating the use of renewable energy regardless of the financial disadvantages that it still might poses. This is evident in that the global wind power capacity has shown an average cumulative growth rate of over 30% in the last decade [15] [16] as depicted in Figure 3.

1.1.2 Modern Generator Systems

Various different turbine systems are operational today, the most common at present being three-bladed, stall or pitch regulated, horizontal axis machines operating at a near-fixed rotational speed [6]. The most common generator system found in wind turbines today consists of a slow rotating rotor shaft connected to a standard/commercial high speed asynchronous generator via a gearbox to step up the rotational speed. Gearless, low speed designs and variable rotor speed designs have recently gained favourable interest in the light of the growing power rating of wind turbines. In this section the three most popular generator systems for wind turbines are explored whilst their turbine-generator coupling, generator-grid connection and power control are also considered. These three systems are represented in Figure 4 - Figure 6.

Probably the oldest wind turbine generator system still used today is the Danish concept. The turbine is connected to a 4 pole, asynchronous squirrel cage induction generator by means of a gearbox. These machines operate typically at speeds of around 1500 rpm, which presents the need for a gearbox to step up the relatively low rotational speed of the turbine to the vicinity of the generator's rated synchronous speed. This system utilises standard, off-the-shelf squirrel cage induction generators and gearboxes, making the design simple and parts readily available.

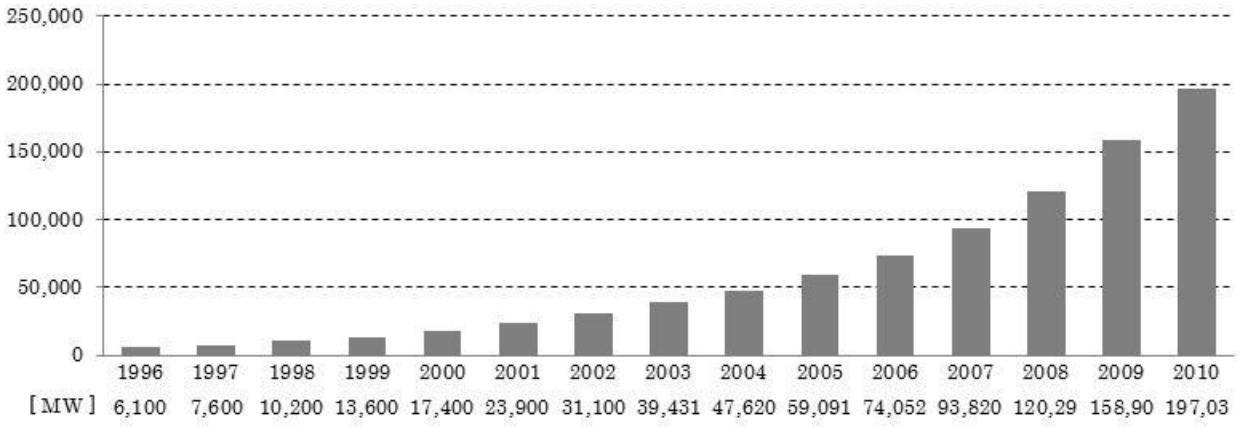

Figure 3: Global cumulative installed wind capacity 1996-2010 [16]

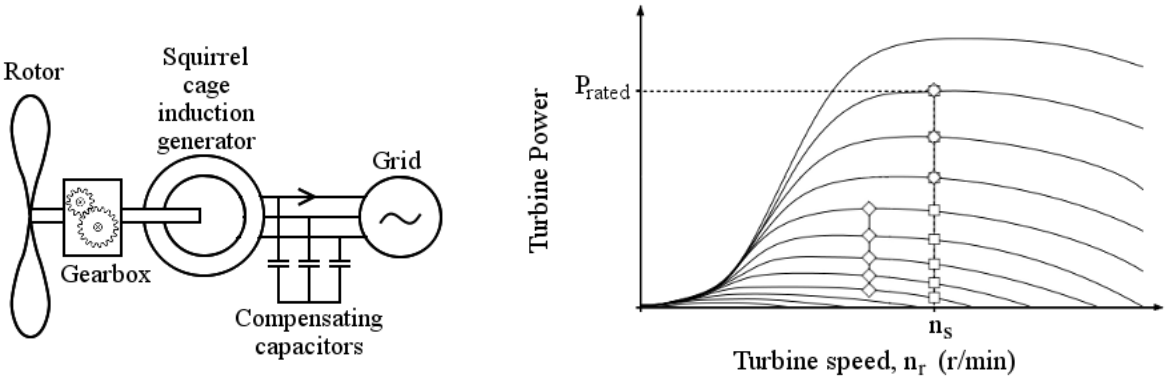

Figure 4: Constant Speed Turbine System (Danish Concept) [17].

Since the squirrel cage induction generator systems can be connected directly to the 50 Hz or 60 Hz utility grid, the grid's frequency determines the generator's synchronous/operating speed. Thus the turbine needs to come up to speed before it can be connected to the utility grid. Once it is connected to the grid, the turbine system operates at synchronous speed for all wind speeds up to rated speed as depicted by the graph in Figure 4. Variations in the rotational speed of the squirrel cage rotor, due to varying wind speeds, become inhibited by the existing slip between rotor and stator fields. This system is thus referred to as a constant speed or fixed speed turbine.

From Figure 4 it is clear that except for rated wind speed, the energy output of the constant speed generator are always below the maximum power point at each wind speed. Induction generators used in these systems are often equipped with two sets of stator windings; each with a different number of pole pairs that enable it to operate at two different constant speeds, thus yielding higher energy. Furthermore, controlling the power output beyond synchronous speed, the squirrel cage rotor is equipped with electronically variable resistances which allow the mechanical load to be reduced

and larger speed variations are therefore possible [19] [20]. This is known as field weakening which reduces the machine's torque. The simplicity and robustness of constant speed wind turbines has made it a favourite for turbines rated below 1.5 MW amongst turbine manufacturers until just before the turn of the 21st century [18]. Because squirrel cage induction generators always consume reactive power, it is detrimental for weak grids with large turbines, and a capacitor bank is often used to partially or fully compensate for the reactive power consumed.

A modern alternative to constant speed turbines is the variable speed wind turbine. Two such systems are in operation today; the first utilising a wound rotor induction generator (also known as a doubly-fed induction generator), and the second utilising a permanent magnet (PM) or electrically excited (EE) synchronous generator. In order to permit wind turbines to operate with variable speed, decoupling of the mechanical rotor frequency and the electrical grid frequency is necessary. In the case of the wound rotor induction generator system, this is accomplished by connecting both the stator and the rotor windings of a wound rotor machine to the utility grid, however, the rotor windings are connected through a back-to-back voltage converter, which in essence then decouples the mechanical and electrical frequency of the rotor.

Figure 5 shows the schematic for the semi-variable speed wind turbine systems with a doubly-fed induction generator. The converter matches the electrical frequency of the rotor with that of the stator by supplying the rotor windings with an alternating current with a frequency, f_r, determined by the following expression:

$$f_r = \frac{p(n_s - n_r)}{120} \tag{1.1}$$

where n_s is the stator field's rotational speed, fixed at 1500 rpm, n_r is the rotor's mechanical speed, and p the number of rotor poles. This enables the wound rotor generator to capture energy over a wider speed range (typically of 60 – 110% of rated speed as shown in the graph of Figure 5) whilst maintaining the rated torque far above its rated speed [20]. This generator system is better described as a semi-variable speed system.

Just as squirrel cage induction machines, standard off-the-shelf wound rotor induction machines are available. They also operate at high rotational speeds, thus requiring a gearbox to step up the rotational speed of the main shaft coming from the turbine. However, a comparative study has shown that this semi-variable speed, wind turbine system is superior because of their higher energy output, lower rating (hence, lower cost) of converter, and better utilisation of the generator when compared to its counterpart using a cage rotor induction machine [20].

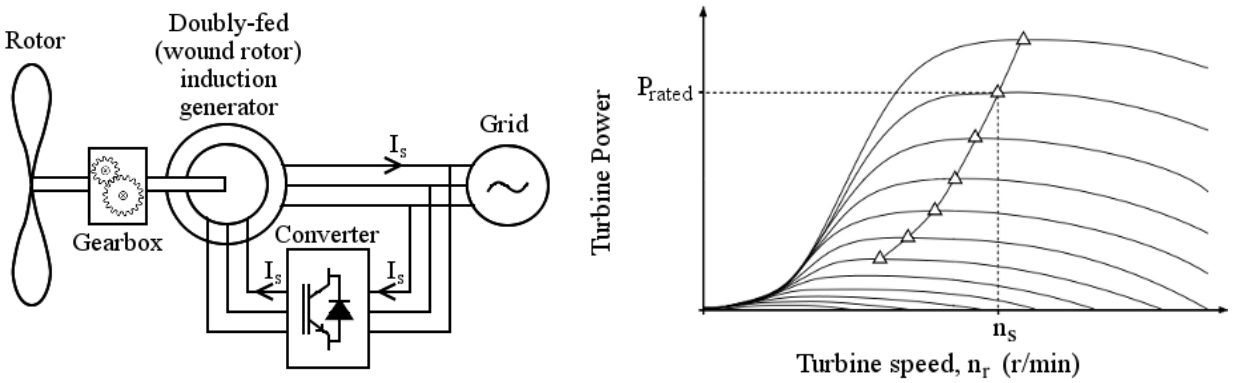

Figure 5: Semi-variable speed Turbine System [17].

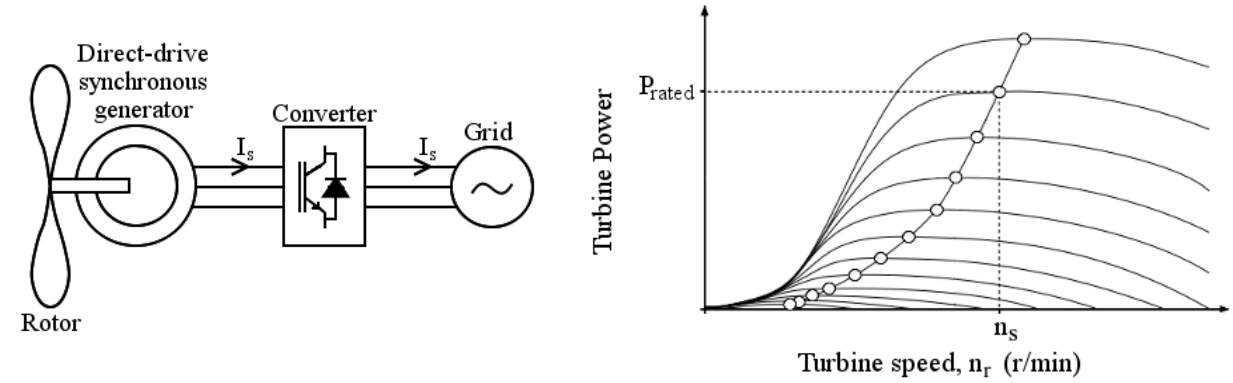

Figure 6: Variable Speed Turbine Systems [17].

The rotor windings can also be supplied with direct current, which makes the generator operate as an electrical excited synchronous machine. Here the mechanical frequency of the rotor is directly related to the stator's generated electrical frequency, because no slip exists between the rotor and stator fields. Wild speed variations thus produce equivalent variations in the electrical frequency produced. Since the rotor field frequency cannot be altered, it is necessary to connect the synchronous generator to the utility grid through a fully rated converter in order to decouple the mechanical synchronous rotor frequency from the electrical grid frequency. The converter thus converts the varying voltage frequency of the generator, due to the varying wind speeds, to the constant grid frequency. The same applies for PM synchronous generators.

Since the converter decouples and matches the synchronous generator and grid frequencies, maximum power point tracking, as shown in the graph of Figure 6, is made possible over the full speed range of the wind turbine. Synchronous generator systems are thus defined as fully variable speed systems. PM synchronous wind turbine generator systems, in particular, have emerged in recent years, due to its ability to operate at the very low rotational speeds of growing wind turbines, and have gained great interest because it eliminates the need for a gearbox, as depicted in Figure 6.

Gearboxes with high gearing ratios have greatly contributed to turbine failures over the last three decades [21]. Synchronous generators for direct-drive (DD) wind turbine applications are discussed in detail in the next section.

1.1.3 Direct-Drive Synchronous Generator Systems

Three-phase synchronous generators are widely used to convert mechanical energy to the electrical energy we consume and are the largest energy converters in the world [19] [21]. The most common topology for these direct-drive machines is known as radial flux (RF), in which the orientation of the magnetic flux produced is in the radial direction. These radial flux machines have inner rotor and outer rotor designs, although the former has shown to be more suitable for large wind energy systems in terms of mass, ease of installation and cooling [21][23][24][25][26]. The simple and structurally stable design of RF machines has made it very popular and widely used in low speed high torque applications. Machines with the magnetic flux directed in the axial direction (AF machines) also exist, but pose more structural challenges, as the air gap diameter increases compared to its RF equivalent.

The shaft power of an electrical machine is directly proportional to the torque produced by the magnetic shear forces in the air gap and the rotational speed of the rotor. For this reason, direct-drive generators are characterised by their large diameters (12 m for the Enercon E112 DD wind turbine). These large diameters are needed in order to produce a high torque in the air gap at their low operating speeds. Their size makes them significantly heavier than the induction generators found in conventional drivetrains, which have diameters of only 1 to 2 meters. As the diameter of direct drive machines increase, so do their air gaps, to ensure proper clearance between rotor and stator. In general, increasing the air gap length depreciates the performance of the machine.

Although gearboxes are well known and widely used in conventional drivetrains, time has shown that they lower the reliability of wind turbine systems by greatly contributing to turbine down time [17][27]. As the power rating of turbines increases, the rotational speed decreases, making the gearing ratios ridiculous; the Siemens Wind Turbine (SWT) 3.6-107 has a gearing ratio of 1:119. Gusty winds translate to great torque fluctuations that consequently have a severe effect on the gear teeth, and demand gearbox designs of at least double the rated torque [28]. Such gearboxes are also very heavy and can contribute to nearly 70% of the system's cost, as shown in Figure 7a.

Direct-drive generator systems, on the other hand, have none of the initial gearbox costs or the regular maintenance routine associated with gearboxes. They are also free of the mechanical noise and losses found in conventional generator systems with gearboxes. Figure 7b shows that, when the reliability and efficiency of the whole drivetrain is considered, heavy direct-drive generator systems for wind turbine applications become very competitive compared to its geared equivalent.

Direct-drive synchronous generators are traditionally electrically excited. The rotor of these machines consists of salient poles with field coils wound around each pole. Direct current (DC) current is supplied to the rotor via slip rings and connected to the field coils in order to produce alternating magnetic rotor poles. The electrically excited rotor poles of synchronous generators are bulky and contribute to the overall mass and cost of the machine. The extra iron and current carrying copper needed for field excitation, furthermore greatly increases the generator's losses.

The development of rare-earth materials over the past two decades have systematically brought a reduction in their price which have made the use of permanent magnets (PM) for field excitation in synchronous generators very economical. The year 2011, however, has seen a dramatic increase in the price of rare-earth materials; the price of Neodymium increased by more than a factor 5.5 between January and June of this year. This sudden price increase is due to legislation matters in China, provider of 95% of the world's magnets. In recent months rare-earth material prices have stabilised and a slight decreasing trend is noticed in the price. PMs will still be considered as an excitation means, because of the advantages it holds.

Using PM excitation eliminates the excitation losses in the rotor and is less labour intensive compared to the rotor windings of generators with electrical excitation. In addition, material volume and mass reduces dramatically (roughly factor 2 in active generator material) which allows these machines to become more compact and have smaller diameters [17][29]. PM excited machines furthermore have no conductor brushes that require regular inspection and replacement. The use of permanent magnets therefore reduce the number of moving parts in direct-drive machines even further, making it a very reliable option [30]. Taking material and labour costs into account, PM excitation definitely becomes very economical compared to electrical excitation, as can be seen in Figure 7a.

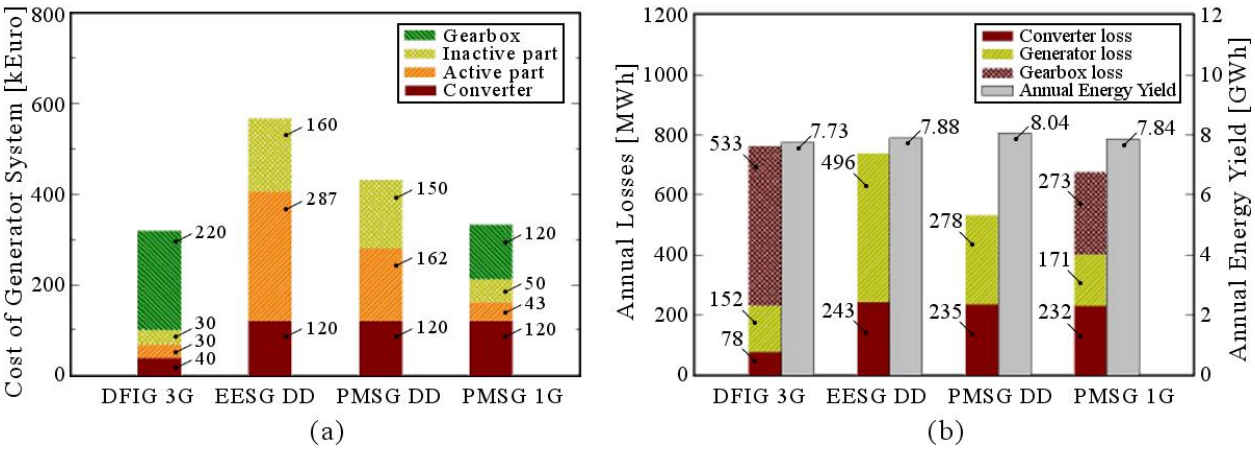

Figure 7: (a) Cost and (b) Annual losses and energy yield of different generator systems [21].

Direct-drive PM generators operate with a good and consistent performance over a wide range of speeds [21][31]. Since PM designs have neither exciter windings nor damper bars, their transient torques in case of sudden short circuit do not exceed their rated values by much. This attribute of PM machines give them tangential magnetic loads during sudden short circuit that is five times lower compared to DC excited designs [29]. Direct-drive RFPM machines are compact and easy to install on top of towers because of its reliable and simple mechanical construction. Unlike electrically excited generators, which reactive power (kva) can be controlled by its field excitation, PM generators require power electronics to control their reactive power, since the field excitation of the magnets are constant [33]. Nevertheless, it's advantages have made PM direct-drive synchronous generators a favourable option in wind turbine applications over recent years [30].

Permanent magnets can either be fully or partially embedded in the rotor yoke or mounted on its surface. Figure 8 illustrates the difference between these three magnet mountings. The advantages of embedding the magnets fully in the rotor yoke are that the magnets are protected against possible damage and that it offers precise magnet placement. By embedding the magnets only partially into the iron yoke, the magnets can be damaged; yet precise magnet position is ensured while the saliency of the rotor offers a marginal increase in torque [31]. Surface mounted magnets require the least amount of iron in the rotor yokes, but precise placement can be cumbersome if a proper mounting method is not used. A common advantage of semi-embedded and surface mounted magnets is that the uneven rotor surface that they create creates a fanlike effect which enhances the natural cooling effect. On the other hand, surface mounted magnets are exposed, which makes them prone to damage.

Finally, direct-drive wind turbine generator systems have shown to be large and expensive, but not unrealistic when compared to the mass of the conventional generator systems [18]. The addition of a fully rated converter, required for grid connection, increases system cost and possibility of system failure further [34]. Nonetheless, when considered on the whole, DD generator systems offer higher efficiencies, operation with similar magnetic flux density in all magnetic circuits, and the construction of compact generators with large number of poles.

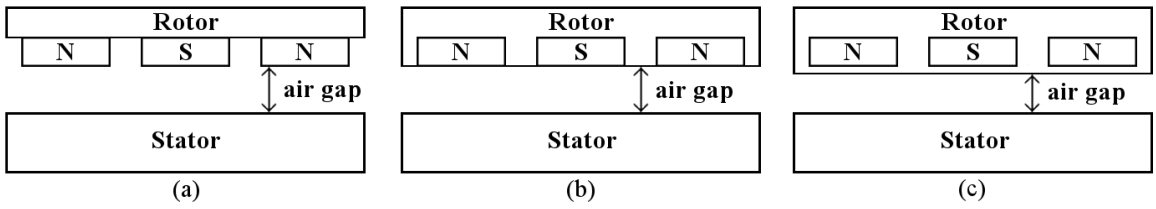

Figure 8: Surface mounted, partially embedded and fully embedded magnets.

1.1.4 Present and Future Challenges

Present and future trends in wind turbine development focus on lowering the cost of energy for this renewable and sustainable energy source. Maximizing the wind energy conversion efficiency and the reliability of these generation systems, while minimising material usage, are therefore three common goals amongst wind turbine developers. Yet, to make wind energy economically feasible means that the power density should also be maximised. Percy H. Thomas, in a study that he performed in the 1940's, concluded that machines in the size range of 6.5 – 7.5 MW were necessary for economic viability [2]. Currently, wind turbines in the size range of 3 -4.5 MW are being installed, but the market has already seen the introduction of turbines in the 5 – 6 MW range, such as the M6 (RE Power) and M5000 (AREVA). Figure 9 shows the rapid growth noticed in the size and power output of wind turbines at market introduction.

Assuming that the blade tip-speed is constant, by up scaling wind turbines, the rotational speed of the rotor reduces proportionally. In such cases, the transmission ratio required to maintain the generator's rated speed in conventional IG drivetrains becomes unfavourable with respect to mass and efficiency [28] and decreases the reliability of these systems. With off-shore wind parks becoming more popular, the mass, transportability and reliability of wind turbine generator systems become important factors in the cost equation.

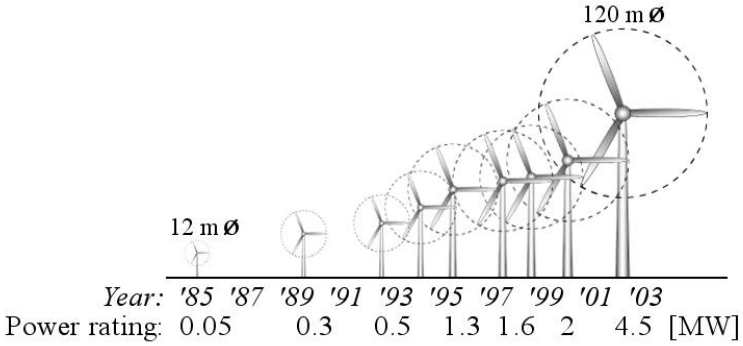

Figure 9: Development of power and size of wind turbines at market level [17]

Hybrid systems aim to combine the advantages of conventional and direct-drive generator systems. Here a much smaller, compact and simpler gearbox, with low stepping ratio, is connected to a compact PM synchronous machine, with a much smaller diameter. This system thus has more moving parts and is therefore less reliable than a direct-drive system, this is clearly evident from Figure 7b. Examples of such turbines are the WWD-3 (WinWind) and M5000 (AREVA).

Reliability of wind turbines, especially those for off-shore applications, has become an important design consideration, seeing as installation and maintenance costs of these turbines are much

higher. The fewer moving parts of the gearless direct-drive generator system has made it an attractive alternative to its conventional counterpart.

As mentioned, direct-drive generators require large bore diameters in order to produce the necessary high torque. Furthermore, because the magnetic attraction forces between the rotor and stator can be 10 times the magnitude of the torque producing shear force, the structural support required to maintain the air gap clearance between rotor and stator becomes bulky and greatly contributes to the mass and cost of synchronous generators [27]. Failing to maintain the air gap clearance will result in the destruction of the system.

In an attempt to simplify the direct-drive system even further, a fixed pitch turbine was suggested by Polinder [18] for a 10 MW DD wind generator. An investigation has shown that this generator system for the turbine with active speed stall control is 60% heavier and more expensive than the generator system of the turbine with pitch control. What is more, a considerable increase in generator system cost is necessary to enable active speed stall control if is desired to keep the annual energy yield at a comparable level.

Finally, challenges during the assembly of PMSGs are also encountered. Because the excitation of magnets cannot be controlled, strong attraction forces are present during the assembling of PM machines. Magnetising the PMs only after the assembling process will ease the handling of the different components, but the magnetising of the magnets are much more strenuous once the machine is assembled.

1.1.5 Unconventional Direct-Drive Topologies

Some of the unconventional generator topologies for wind turbines encountered in literature are presented here. These topologies all aim to reduce the cost of direct-drive wind turbines by suggesting rotor-stator configurations that have the potential to utilise less structural material or reduce the number of components that may fail.

One way to dramatically reduce the mass of a large synchronous machine is to remove all active iron from the stator. These machines are known as air-cored machines and have the advantage of having no direct magnetic attraction forces between the rotor and stator and consequently reduce the structural demand of the inactive components and the load on the bearings. One such ironless RFPM electrical machine is presented in [35]. This light weight, spoked wheel structure proposed is therefore said to be sufficient in supporting both the rotor and stator and to withstand the related operational forces. This design promises to reduce the generator's mass to 20-30% of an equivalent iron-cored design.

The low air gap flux density of 0.25 T, typical to air-cored machines, and consequently its low shear force, nevertheless results in generator efficiency greater than 90%. It is expected that this support structure offers the opportunity to build generators of an unprecedented diameter, which satisfies the very large air gap radii requirement of this machine. Eddy-current and aerodynamic losses are expected to greatly contribute to the total losses of the machine [23], while the natural frequencies of the exposed spoked support (shown in Figure 10a) could become an issue of concern. A modular design can easily be introduced to the proposed topology.

Another air-cored topology presented in literature is the C-GEN [27][37]. Here a second air gap is introduced by means of the modular C shaped core structure, shown in Figure 11. This topology greatly confines the magnetic attraction forces to the flux carrying material (the C structure), and hence allows for a lighter support structure. The three dimensional flux path, provided by the C structure, and shown in Figure 11 b & c, furthermore permits thinner yokes which contribute to the mass reduction characteristics.

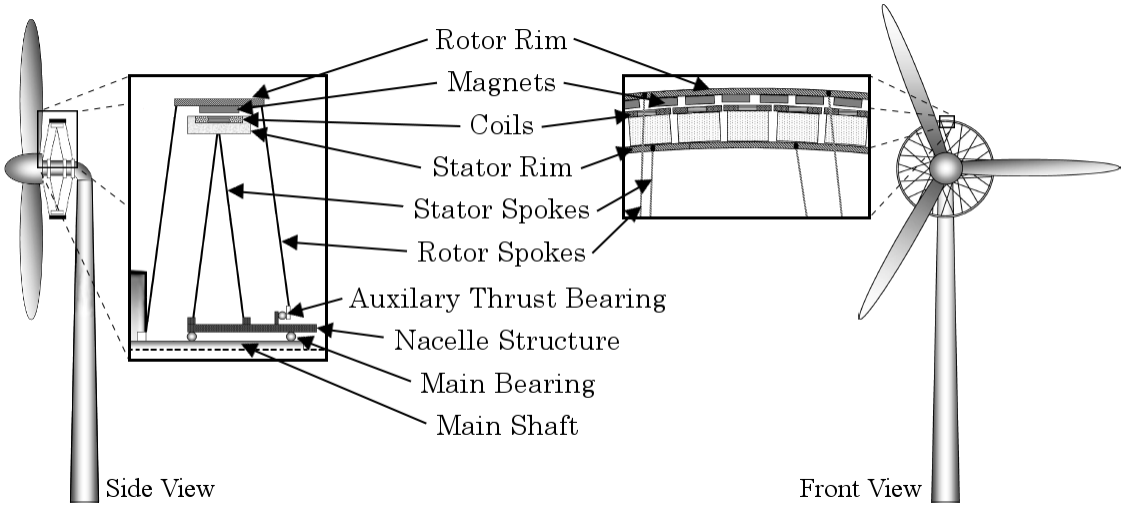

Figure 10: Light weight spoked structure for an air-cored direct-drive PMSG [23].

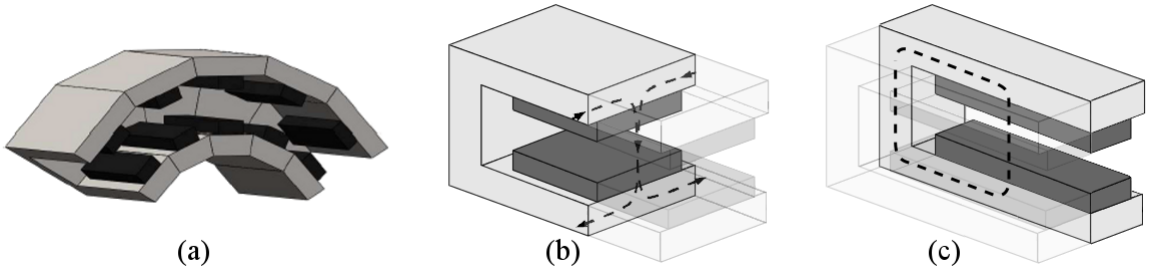

Figure 11: Air-cored PMSG with modular C shaped core structure [27].

Another argument for reducing the cost of direct-drive wind turbines, is to get rid of the full-size back-to-back converter needed for grid connection, which is said to account for more than one third of the whole generating system cost [21][38]. A PM induction generator (PMIG) is suggested to achieve this. The idea of a PMIG was first proposed by Punga and Schon in 1924, but the use of electro magnets on the free rotating rotor, and hence the use of slip rings and brushes to supply the power to the electromagnets, made this system less reliable [38]. However, since the development and reduction in prices of rare earth magnets (before 2011), PM became a logical alternative for the electromagnets.

Recent studies proposed a direct-drive PMIG for fixed speed applications [39]. The idea aims to combine the advantages of induction machines (cheap and robust, direct connection to grid) and PM synchronous machines (high torque and high efficiency, DD) by using a freely rotating PM ring arranged between the rotor and stator for excitation. Although the mass of this system is not reduced, the topology allows for fixed speed, DD applications and direct connection to the electrical grid. Considered as a whole, this topology could offer a great reduction in cost through its simple and robust configuration. Figure 12 shows two rotor configurations for the PMIG concept.

Some efforts have also been made to reduce the mass of large direct-drive generators through removing their large and heavy mechanical bearings and rotor support arms [21]. The rotor ring is designed to offer enough stiffness against radial magnetic force and ovalisation due to gravitational force. It is estimated that for a 5 MW generator the mass can be reduced up to 45%.Various magnetic and hydrostatic concepts have been investigated [21][40]. Magnetic bearings can support large diameter rotors [41][42]. Implementing magnetic bearings into wind turbines can increase the systems reliability, since vibration can be controlled actively and no lubrication is required. It is also expected that magnetic bearings will reduce the generator structural mass. A buoyant-hydrostatic bearing is also claimed to support generator diameters greater than 5m. It is yet still debated whether structural mass reduction is possible with this bearing system. Complexity and lack of technical feasibility have prevented these concepts from being adopted by turbine manufactures.

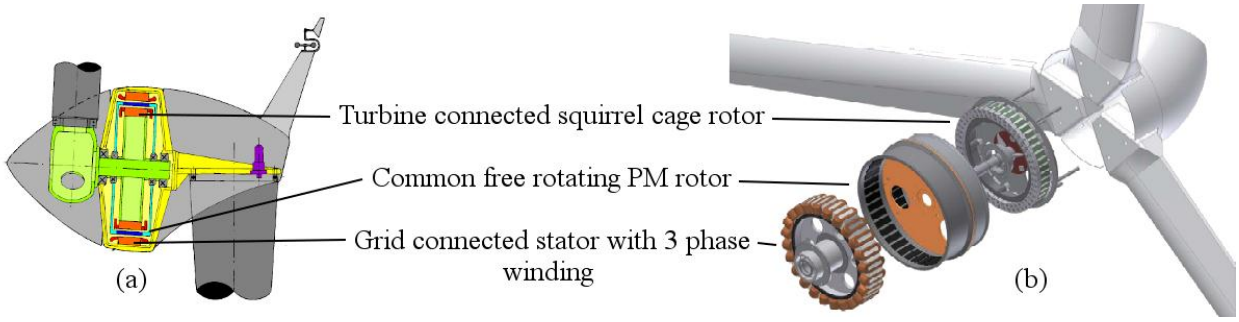

Figure 12: Two different PMIG configurations [38][39].

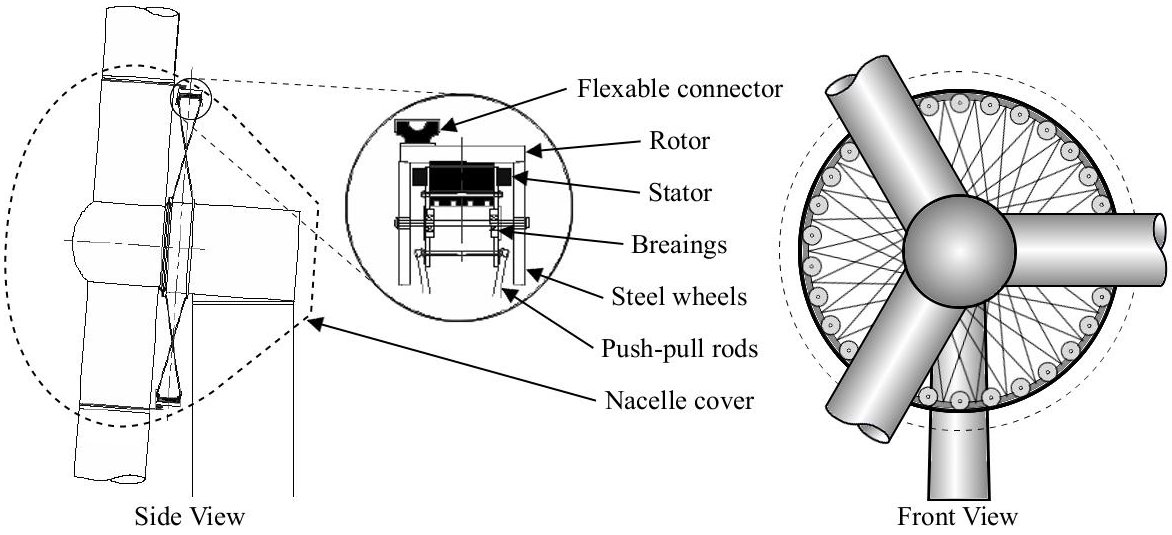

Figure 13: New-Gen generator with mechanical bearings positioned at the air gap [42].

Another idea, proposed in [24], is to move the positioning of the mechanical bearings to be adjacent to the air gap. Contact between the rotor and stator is transmitted by several pairs of steel wheels, shown in Figure 13, fixed to the stator by means of shafts and small mechanical bearings, and acting toward the raceway on the rotor. This bearing arrangement is aimed to reduce the stiffness demand on the rotor and stator. The achievable diameter therefore primarily depends on the bearing stiffness, allowing for thin rotor and stator back iron yokes, and so reduces generator mass. A main bearing is still required to support the wind turbine rotors. Push-pull rods are expected to add enough stiffness and serve as a connection between the stator and hub. A modular design is possible for both the rotor and stator core, which will simplify manufacturing, transport and erecting of the wind turbine structure. A flexible connecting means are used to transfer the torque from the wind turbine rotor hub to the generator rotor ring.

1.2 Problem Statement

From literature it is clear that wind energy is currently seeing a very strong development because of a global environmental awareness, governmental support worldwide, and funding that is available for renewable energy projects such as wind energy. Even though wind energy is the cheapest renewable energy technology available today, it still has a cost disadvantage relative to the well-established fossil energy sources. Wind generated power is not sufficient for modern-day energy needs for two main reasons – the intermittent nature of wind and the low energy density of wind turbines compared to fossil fuels.

Improved materials and design technologies have made it possible to increase wind turbines' energy density considerably. This however, has brought about a diminution of the conventional

geared turbine generator system's reliability. Similarly, direct-drive generators become very large, with structural mass that can be in excess of 80% of the total generator mass [27]. Many studies, aimed to make direct-drive synchronous generators more successful in penetrating the present market, have simply optimised the active material, and have neglected important aspects such as structural design, manufacturability, transportation, and installation in the optimisation and design process [43]. Even the assembly of iron-cored PM machines are made difficult because the magnetic excitation of the PMs cannot be controlled.

Various unconventional structural arrangements for direct-drive generators have been proposed to constrain the load path, and so reduce the unwanted effect that the magnetic loads have on the inactive structure. In addressing the magnetic forces, only ironless generator topologies have been proposed, which in effect eliminate these undesired attraction forces between rotor and stator. The author could find no endeavour in literature to eliminate or minimize these forces in direct-drive iron-cored machines.

Currently, direct-drive synchronous generators are still more expensive than induction generators; not only because they are hefty, but because they need to be specifically developed for every application. Because DD generators are not standard off-the-shelf machines, an effort must be made to find alternative generator topologies which offer the possibilities of further mass and cost reduction [17]. Standardisation or modularisation of direct-drive generator parts or sub-assemblies may assist in overcoming the existing cost barrier [41]. If it is possible to reduce the cost of PMSG DD to or below that of a DFIG with a three stage gearbox, then Figure 7 shows that DD PMSG could be the most suitable generator system for wind turbines [21].

1.3 Study Objectives

The main aim of this thesis is to gain better understanding of the radial magnetic forces that exist in low speed, iron-cored electrical machines. A practical rotor-stator topology, aimed at significantly reduce the structural mass of direct-drive permanent magnet wind turbines, is proposed. This is expected by eliminating or at least reducing the unwanted radial magnetic forces.

In order to demonstrate the potential benefits of this new generator concept, a complete electrical and mechanical design of a 15 kW direct-drive machine is presented and design results show a reduction in mass, whilst maintaining high efficiency at all loads. The design process will incorporate the optimisation of both active and inactive material, whilst considering manufacturability and assembly of the generator. Experimental results of a prototype generator will be illustrated to verify the expected performance. In addition, there will be a description of the building stages of the prototype to demonstrate the benefits for the assembly.

Objectives are summarised as follows:

- To propose a rotor-stator topology that will eliminate/reduce the radial magnetic attraction forces which demand bulky supporting machine structures.
- To optimise the proposed topology, focusing on the reduction of mass by considering both the active and inactive (structural) parts of the machine.
- To explore the manufacturability of the proposed topology and building an experimental machine.
- To compare different machine topologies, with particular reference to the quality of the performance and mass.

1.4 Thesis outline

The next chapter studies the attraction forces between the iron parts of conventional rotor-stator configurations and suggests a topology that has the potential to reduce the structural material, and hence lower overall mass.

Chapter 3 will set out the specifications for the design of a generator with the novel rotor-stator configuration as suggested in the previous chapter. Moreover it will cover the electrical design of the proposed machine and explain the procedures followed for the optimisation of the active material.

Chapter 4 considers various aspects of the mechanical design of the experimental generator prototype.

Chapter 5 presents the actual test results of the experimental machine and compares it with those of a conventional single-sided rotor machine designed and built with the same specifications.

Chapter 6 draws some conclusions to the study presented in this thesis and recommends possible areas for further study.

Chapter 2
Rotor Yoke Topology Selection

The magnetic forces that exist between the rotor and stator of direct-drive synchronous machines consist of two components, namely the shear or tangential forces and radial or normal forces. The shear forces act in the direction of rotation and is quantified in terms of torque, which is required for electricity generation. The radial forces act normal to the rotational direction and are considered to hinder the optimal utilisation of energy by producing unwanted radial vibration in the stator. Furthermore, it also produces the attraction forces between rotor and stator iron parts of iron-cored machines.

The knowledge of the radial forces, generally classified as the unwanted component of force in the iron-cored machine, gives us reason to find ways to alleviate its effect on the structural demand and lessening vibration and acoustic noise [42]. This chapter studies the magnetic circuits in a conventional 300 kW iron-cored PM machine to better understand the radial attraction forces. The objective of this chapter is to find a rotor-stator topology that offers the least attraction between active iron parts of large wind turbine generators.

2.1 Theoretical Concept Development

For this study a basic understanding of electromechanical-energy conversion principles is of essence. Figure 14a shows the general path of magnetic flux in a conventional RFPM synchronous generator (SG). The magnetic flux forms isolated path groupings between adjacent magnets as illustrated in the linear schematic representation in Figure 14b. A linear model can be assumed because of the large air gap diameter of the machine under investigation. For simplification, the effect of the current carrying stator coils is ignored. This allows the removal of the stator slots and teeth, whilst the Carter factor accounts for their effect by increasing the length of the air gap. Figure 14c shows the schematic without magnets, but with the magnet excitation represented by a winding with an excitation current, *i*. Only one pole pitch of the linear model needs to be considered, since the air gap effects are repeated every pole pitch. This simplified model is represented by the electromagnetic circuit in Figure 14d.

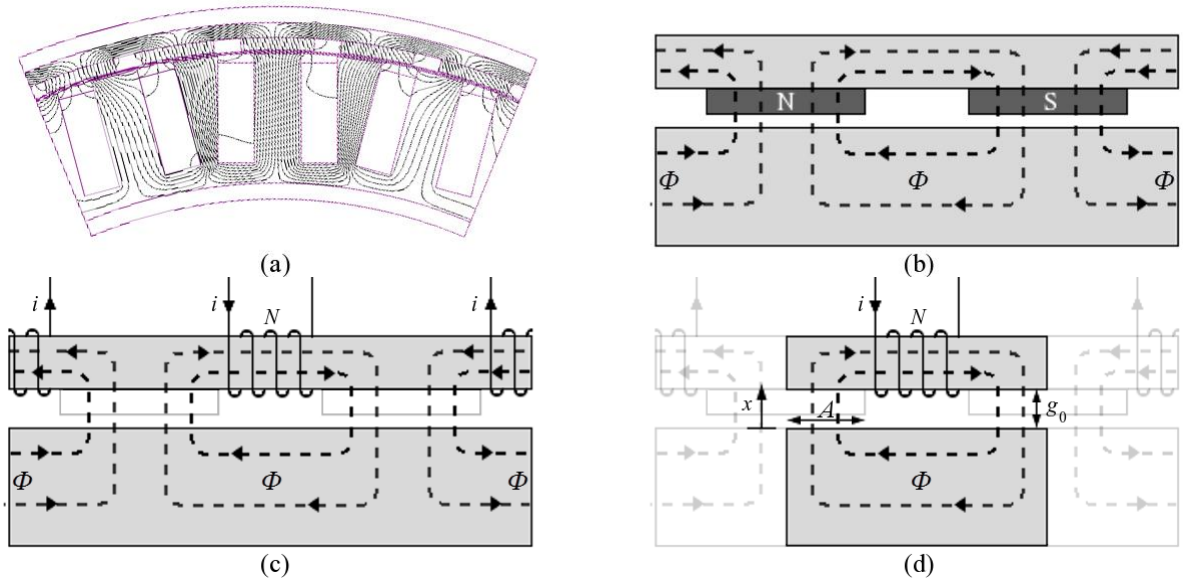

Figure 14: Magnetic flux in a conventional PMSG (a) and its schematic representation(b)&(c) and the schematic of one pole pitch under investigation (d).

To simplify the analysis of the electromagnetic circuit, as presented in Figure 14a, the following assumptions are made:

- Lossless system
- No flux leakages around magnet sides
- No flux fringing
- Linear magnetic system
- Saturation in the iron yokes are ignored

The stored co-energy, W'_{fld} in the field (or air gap) is a state function, where i and x are its two independent state variables. The field attraction force, f_{fld} produced by the magnetic field is defined as the partial derivative of the magnetic stored co-energy, W'_{fld} in the air gap, g with respect to a displacement, x, whilst keeping the excitation current, i constant. This is written as

$$f_{fld} = \frac{\partial W'_{fld}(i,x)}{\partial x}\bigg|_i. \tag{2.1}$$

Because of the dominant air gap, the system is assumed to be linear ($\lambda = Li$) [45]. Consequently the stored co-energy in the air gap can be defined as

$$W'_{fld} = \frac{1}{2}L(x)i^2. \tag{2.2}$$

The circuit inductance, L is a function of the reluctance of the magnetic flux path, Φ and hence inherently dependent on the effective air gap length, $g(x) = (g_0 - x)$. The expression for inductance is

$$L(x) = \frac{N^2}{\mathcal{R}(x)} = \frac{\mu_0 A N^2}{g(x)}. \tag{2.3}$$

The cross-sectional area of the flux path, is represented by A. From Equation (2.1) - (2.3) the field attraction force, f_{fld} is defined as

$$f_{fld} = \frac{\mu_0 A N^2 i^2}{2} \frac{\partial}{\partial x}\left(\frac{1}{g(x)}\right). \tag{2.4}$$

The schematic in Figure 14 shows the total effective air gap length, $g(x)$ for the flux path to be

$$g(x) = 2(g_0 - x). \tag{2.5}$$

The constant, g_0 is the designed air gap length. Substituting Equation (2.5) into Equation (2.4) and differentiating, gives

$$f_{fld} = \frac{\mu_0 A N^2 i^2}{4(g_0 - x)^2}. \tag{2.6}$$

Equation (2.6) is a good approximation of the magnetic field force in one pole pitch of a conventional PMSG and can be rewritten to give the following well known expression for the force on the stator in terms of the air gap flux density, B_g

$$f_{fld} = \frac{{B_g}^2 A}{\mu_0}. \tag{2.7}$$

It is clear that the force produced by the magnetic field is inversely proportional to the square of the effective air gap length of the generator. Any deformation of the rotor or stator thus results in a quadratic increase in the field force, according to Equation (2.6). Consequently the structural integrity of large diameter direct-drive machines becomes compromised, requiring bulky mechanical structures for these machines to ensure sufficient stiffness of the rotor and stator. On the other hand, any closing of the air gap due to eccentricity results in an opening of the air gap at the opposite side of the PMSG, which results in a force imbalance on the stator and rotor.

Air-cored PMSGs are a logical solution for addressing the unsolicited effects of the magnetic field force. The absence of the stator iron in essence makes the state function, W'_{fld} independent of the stator position, x. Hence W'_{fld} is only dependent on the excitation current, i which is constant in PM machines. The flux linkage of such an air-cored machine, presented in Figure 15a, is much poorer. Air-cored machines require a large amount of magnetic material (it could easily exceed a factor of 4 compared to conventional iron-cored PMSGs) to produce the air gap flux densities equivalent to those in iron-cored PM machines [23][46][47]. By introducing a second rotor with magnets, as in [47], a return path for the magnetic flux is provided by the rotor yoke whilst the magnets improve the magnetic flux distribution in the air gap and hence improve the flux linkage of air-cored machines. Figure 16a shows the magnetic flux paths in such a double-sided rotor air-cored machine, with p magnets mounted on each rotor yoke.

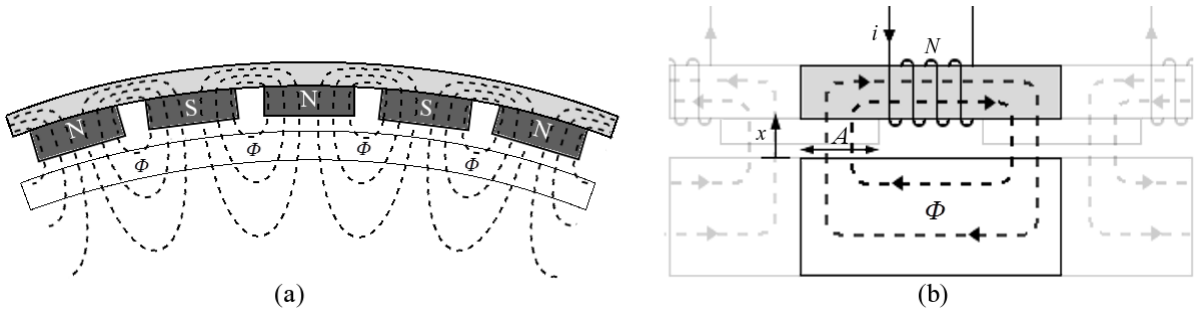

Figure 15: Magnetic flux in an air-cored single-rotor PMSG (a) and its magnetic circuit (b).

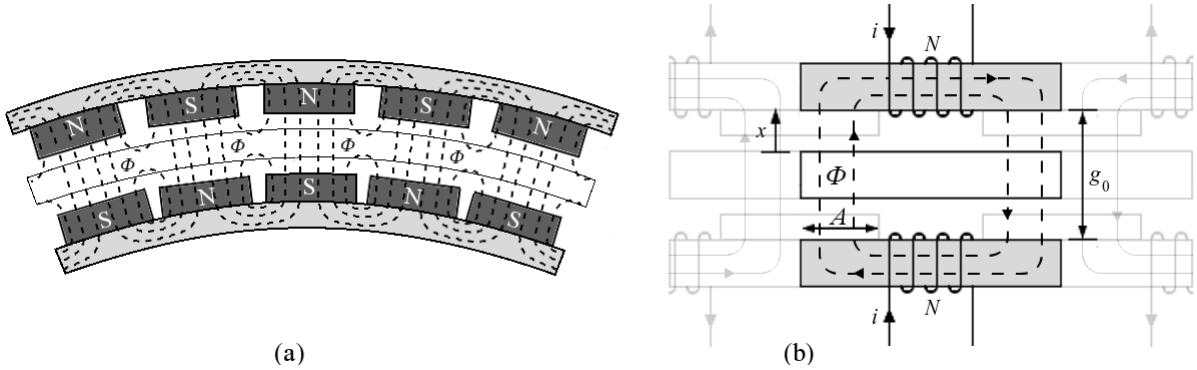

Figure 16: Magnetic flux in an air-cored double-sided rotor PMSG (a) and its magnetic circuit (b).

Figure 16b shows a schematic of magnetic circuit of the double-sided rotor air-cored PM generator. It is clear that the stator position, x, has no influence on the magnetic field force, since the effective air gap length is constant at g_0. The attraction force is only experienced between the two rotor yokes and is much more manageable structurally because the load path is much shorter; the load on the mechanical structure simply runs from the one rotor yoke to the other though a common connector.

It would be ideal to find a PMSG topology that keeps the air gap stored co-energy and hence the field force, independent from the stator position, x, but that requires a lower magnet volume. The latter is achieved when iron is again introduced to the stator. Figure 17a is a cross-section of a double-sided rotor (also referred to as dual-rotor in literature) iron-cored RFPM machine. This specific machine has back-to-back stator configuration which shares a common yoke and employs toroidally wound stator windings. Such topologies have been investigated for both single- and dual-outputs [48][49][50][51]. Figure 17b shows the magnetic flux paths of the machine presented in Figure 17a.

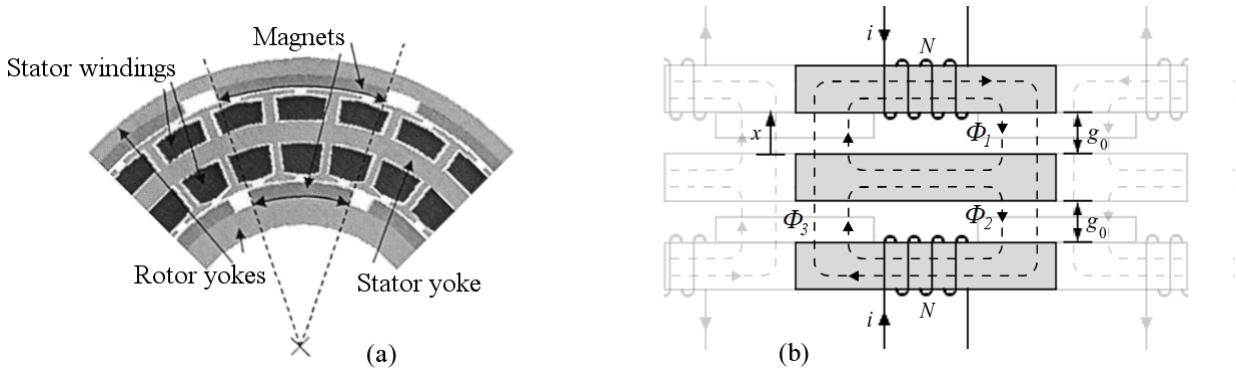

Figure 17: (a) Double-sided rotor, radial-flux, toroidally wound PM machine [48][49] and (b) its magnetic circuit.

With the stator iron introduced into the magnetic circuit, magnetic flux will follow the path indicated by Φ_3, and will thus be mutual to both rotor yokes. A closing of one air gap translates to a proportional opening of the other. The effective air gap seen by flux path Φ_3 is constant ($g = 4g_0$) and so too the total reluctance of Φ_3, making its induced field force, f_{fld} independent of x.

A significant amount of magnetic flux "leaks" back through the stator iron and adjacent magnet to the rotor yoke that it originated from as illustrated with flux paths Φ_1 and Φ_2. The effective air gap length, $g_1(x)$ for flux path Φ_1 is given by Equation (2.5) and the magnetic field force, f_{fld1} experienced in the air gap is described by Equation (2.6). Flux path Φ_2, in the opposite air gap, experiences the inverse. The effective air gap length, $g_2(x)$ and the magnetic field force, f_{fld2} in the second air gap are represented by the following equations respectively.

$$g_2(x) = 2(g_0 + x). \tag{2.8}$$

$$f_{fld2} = -\frac{N^2 i^2}{\mu_0 A \mathcal{R}^2(x)} = -\frac{\mu_0 A N^2 i^2}{4(g_0+x)^2}. \tag{2.9}$$

From Equation (2.6) and (2.9) it can be seen that when the two air gap lengths are equal ($x = 0$), the resultant force on the stator is theoretically zero. Any shift of the stator will decrease the reluctance of the closing air gap, therefore resulting in a quadratic increase in the attraction force. The opposite is true for the opening air gap, which experiences an increase in reluctance and therefore a quadratic fall in the field attraction force.

A way to impede the flow of flux in the closed loops of flux paths Φ_1 and Φ_2 is to eliminate the magnetic paths that create these undesired and unstable field force effects. By replacing the toroidal coils with concentrated coils, the common yoke of the stator can be removed. This reduces the active material and creates an air gap barrier between the iron-cored stator teeth, thus decoupling the stator position, x from the field force, f_{fld} to some degree. When a stator tooth is between two magnets, leakage flux such as Φ_1 and Φ_2 in Figure 17b is expected to occur, thereby making f_{fld}

periodically dependent on x. Figure 18 shows the FE model, with flux paths, of a double-sided rotor, yokeless stator PM machine.

The modular C-shaped rotor core structure for air-cored machines, such as presented in [27] and in Figure 11 of the previous chapter, offers both transverse and longitudinal return paths for the magnetic flux. By introducing this notion of a transverse flux path to the iron-cored model, as an alternative to the longitudinal flux path, adjacent magnet pairs are magnetically detached from each other and thereby making the field force in both air gaps completely independent of the stator positions. This is illustrated in Figure 19.

The schematic model in Figure 19 shows how the iron yoke between the neighbouring magnets is removed and thereby also the longitudinal flux path. The effective air gap length for flux path Φ_1 and Φ_2 thus becomes $2g_0$ and for Φ_3, $4g_0$. The field force, f_{fld} is thus essentially decoupled from the stators position, x in the air gap between the magnets. To prove the feasibility of this topology

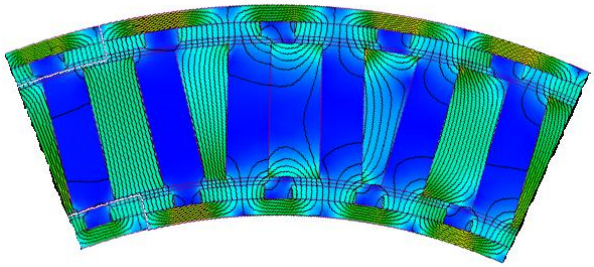

Figure 18: Magnetic flux of a double-sided rotor PMSG with a slotted stator iron.

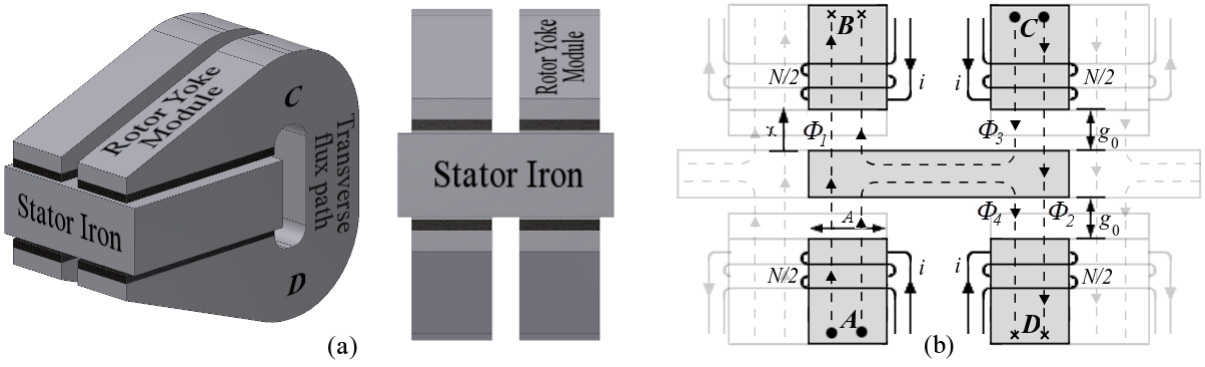

Figure 19: Schematic of the magnetic flux in a modular C-shaped rotor yoke PMSG.

2.2 Analysis of Proposed Concept

The modular C-shaped rotor yoke structures seem to be most effective in decoupling x from f_{fld}. To verify whether it is practically viable, this concept is analysed mechanically and magnetically in this section. Figure 20b shows the conventional single-sided rotor 300 kW radial flux PMSG which was design and manufactured locally, whilst the proposed topology is implemented in the conceptual radial flux PMSG of equal rating, illustrated in Figure 20a.

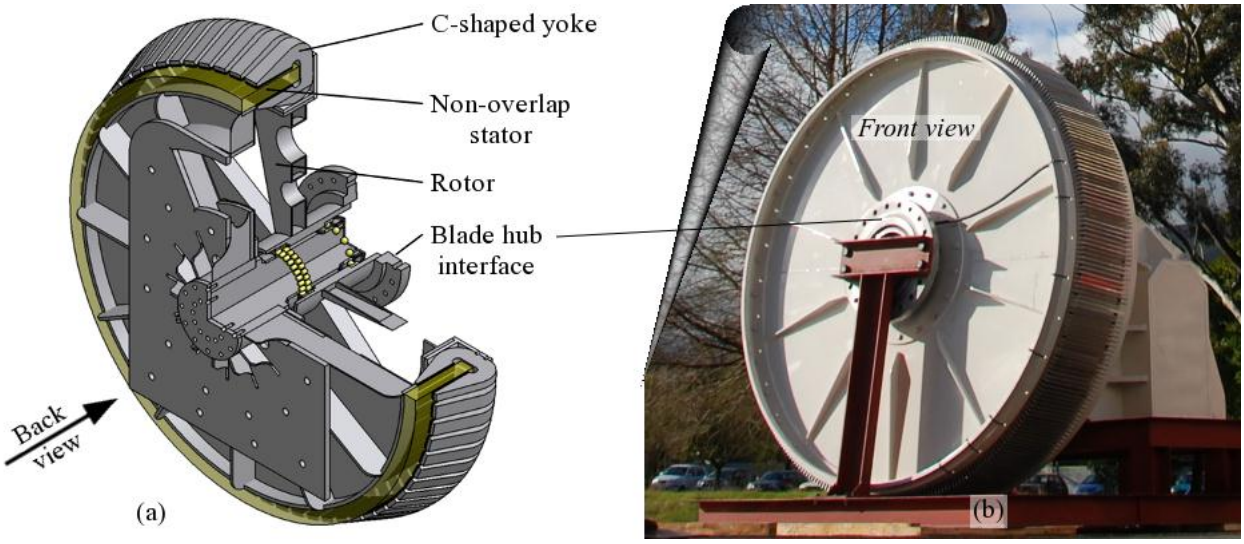

Figure 20: 300 kW RF PMSG - (a) Conceptual double-sided rotor [52] and (b) Actual single-sided rotor.

2.2.1 Magnetic Analysis

Due to the fact that the direction of the rotor's motion components and the magnetic flux path operate in plains perpendicular to each other, a 3D Finite Element software program is necessary to do a thorough electromagnetic analysis of this proposed modular topology. The absence of such a software program therefore limits the analysis of the model to only a magneto static FE analysis. The stator iron and copper content can consequently not be optimised. The FE stator model is simply taken as a solid iron section with the same height as the stator teeth.

The analysis considers a linear model which resembles a two pole pitch section of the C-shaped rotor yoke topology. The outcome is that attraction forces do exist between the rotor and iron-cored stator of the generator when $x \neq 0$. Further investigation into the source of the attraction forces confirms, as expected, that leakage flux does exist around magnet sides and greatly contributes to the existence of the radial attraction forces in large RFPM wind turbines. To put the magnitude of

these attraction forces into perspective, similar machine sections of two other PMSG topologies are considered; they are the conventional single–sided rotor PMSG, used for the purpose of benchmarking, and the double-sided rotor topology PMSG. These three FE models are shown in Figure 21.

A 2-pole pitch section of each topology is modelled with a solid iron piece as the stator. The magnet pitch of the double-sided rotor model is taken to be the same as that of the conventional machine's; the model with the C-shaped rotor yoke modules has a smaller magnet pitch due to a mechanical/physical limitation that is explained in the next section. The magnet height of the two models investigated is adjusted to give the same air gap flux density as that found in the benchmark model. The force on the stator for the conventional topology FE model is found to be 12,9 kN, which is taken as unity in the comparisons to follow.

Three scenarios are considered in this comparison. For the first scenario the stator is positioned with the designed air gap length, that is $g = g_0$. The attraction forces that exist between the active components (rotor and stator) are then calculated by the FE software. The second scenario considers these forces when the stator has an off-set so that the air gap has a 10% closing ($x = 0.1g_0$). For the two models with two air gaps, this closing is only applied to one of the air gaps, while the other air gap experiences an opening of $x = 0.1g_0$. Turbine manufacturers consider this to be the maximum allowable air gap closing [29]. Finally an extreme case is considered where the air gap closing is one fourth of g_0 ($x = 0.25g_0$). The results of this study are tabulated in Table 1.

From Table 1 it is noticeable that both the double-sided rotor and the C-shaped rotor yoke topologies are very effective in reducing the large field forces found in conventional generators. From these results it can be deduced that by introducing a second air gap in iron-cored machines, the field forces in the two air gaps oppose each other and for all practical reasons eliminate the strong resultant force present in conventional PM wind turbine generators. Even with the stator not centred between the magnet pairs, the opposing magnetic field forces greatly reduce the resultant force experienced by the stator.

It is further expected that a solid iron stator (no slots or copper) will experience the greatest attraction forces compared to slotted stators at a specified stator position, x. For the C-shaped rotor yoke topology, the forces on two stator designs are compared to that of a solid iron stator and tabulated in Table 2. Figure 22 shows the different stator configurations used in this analysis. The effect that the slot-closing thickness, t, has on the attraction field force is also investigated and shown in Table 2.

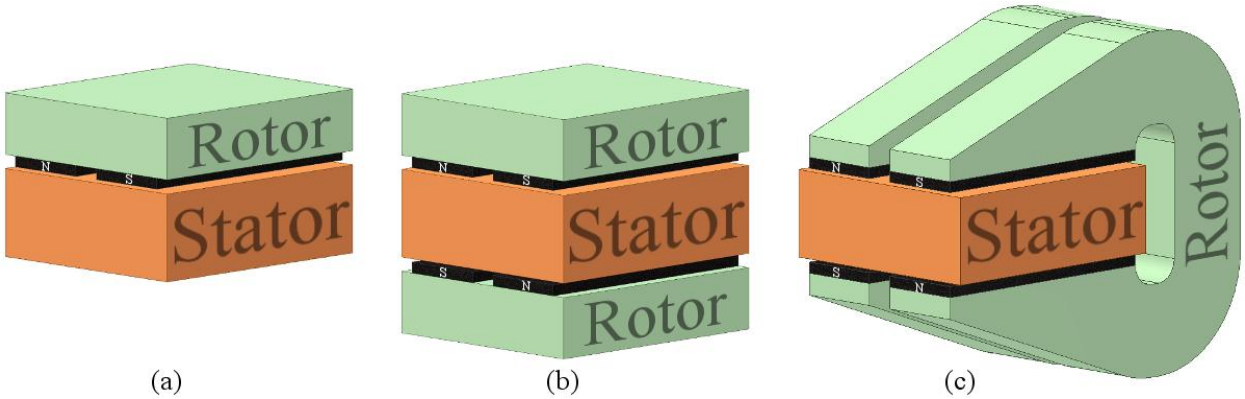

Figure 21: Three PM machine FE models – (a) single-sided, (b) double-sided, (c) C-shaped rotor yoke.

Resultant force (pu) on solid iron stator			
Topology	$x = 0$	$x = 0.1g_0$	$x = 0.25g_0$
Conventional	1	1.06	1.16
Dual-rotor	< 0.01	0.1	0.27
C-core	< 0.01	0.065	0.19

Table 1: The resultant force on stator at three different stator positions (pu) [52].

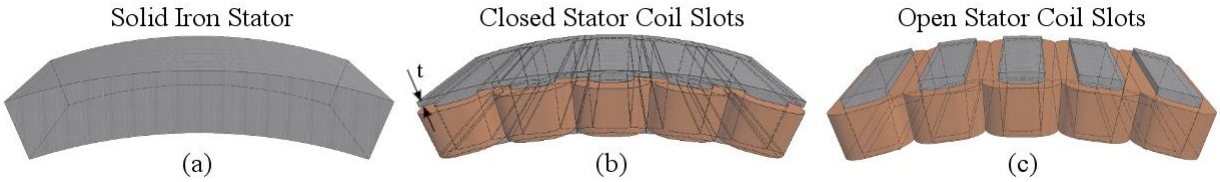

Figure 22: Solid iron stator, closed slot stator and open slot stator design.

Resultant force (pu) on iron stator	
Stator Design	Force (pu)
Solid stator	0.19*
Closed slot – t = 2.5mm	0.1
Closed slot – t = 2 mm	0.08
Open slot – t = 0 mm	0.03

* value taken from Table 1 for the C-core topology.

Table 2: Stator design force results at x = 0.25g0 [52].

2.2.1 Mechanical Analysis

During the operation of an iron-cored machine, the armature reaction produces a non-static distribution of the magnetic flux in the rotor yokes. Iron-losses in the rotor yokes of these machines are therefore noteworthy. Constructing the rotor yokes so that is consists of thin laminated silicone steel sheets, insulated from its neighbour by a thin layer of non-conducting material, reduces the iron-losses caused by the fluctuating magnetic flux through the steel yokes. The use of laminated steel for the construction of the modular C shaped yokes limits it to having a uniform width. When these modular yokes are mounted on the rotor support structure in their circular array, it is apparent that the inner diameter of the yoke arrangement, where they are closest to each other, governs the pole pitch, p_p. This can be seen in the close-up view of the illustrated 300 kW PMSG with the implemented C-shaped rotor yoke modules, shown in Figure 23. To ensure that the individual yokes stay magnetically insulated, a spacing that is larger than $2g_0$ at the inner diameter needs to be accounted for. The maximum allowable width of the C shaped yokes and hence width of the magnets is calculated to be 68.8 mm (a magnet pitch to pole pitch of 0.77). This limitation is expected to diminish the generated torque with no more than 5% [53].

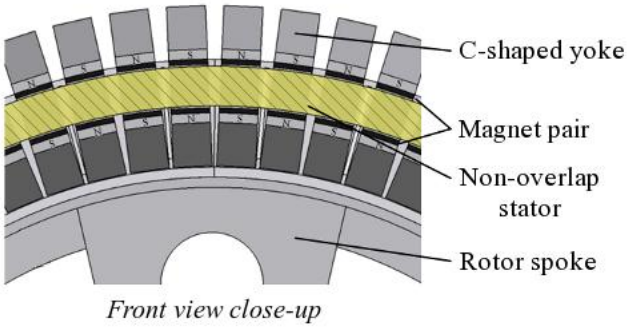

Figure 23: 300 kW C-core PMSG and C shaped yoke arrangement

The resultant forces on the yoke modules, obtained from the FE tests in the previous section, when the maximum allowable air gap closing 10% has occurred, is used to calculate the expected deformation of the yoke modules. With the back of the modules fixed to the rotor structure, the load carrying system can be approximated by two cantilever beams with forces. Deformation calculations done on a cantilever with uniform cross section, obtained from the FE modelling in the previous section, show that the air gap closing reaches a maximum of 2.27%. Although the tapering ends of the yoke, seen in Figure 24, are not accounted for, FE strength analysis confirms this result by predicting an air gap closing of 2.95%. Figure 24b shows an exaggerated graphic FE result, representing the deformation of the C-shaped rotor yoke. For these extreme conditions it is

interesting to note that the yoke's cross-sectional area or height, h_y, is governed by the electromagnetic requirements and not the mechanical requirements. The height of h_y = 85 mm is 63% more than what is structurally required.

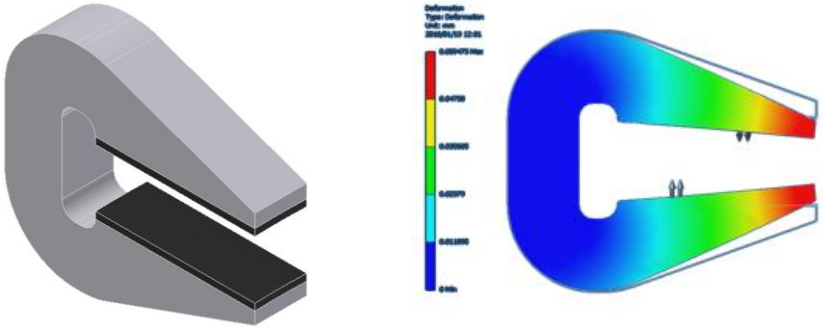

Figure 24: (a) C-core module with (b) illustration of mechanical deformation.

2.3 Mass Comparison

To determine whether the proposed C-shaped rotor yoke topology alleviates the demand on the generator's structural components, a simple comparison study is performed. The conceptual design is compared to an equally rated direct-drive PM conventional synchronous wind turbine as shown in Figure 20b. The author was only provided with the dimensions of the active components due to the confidentiality of the structural information. The comparison is therefore limited to the approximated mass of the active materials.

The active mass of the conventional RFPM direct-drive synchronous generator is estimated from the dimensional information available. The mass of the rotor iron and the magnets of the dual air gap topologies (that is the double-sided rotor and C-shaped rotor yoke topology) are calculated with dimensions derived from the models analysed in the previous section. It is furthermore expected that the copper volume will not change significantly and is accepted to be the same for all three generator topologies. The stator of the two dual air gap machines has no iron yoke, which lessens the stator iron by nearly two thirds. The mass of the various active materials are tabularised in Table 3. Taking the mass of the active material in the conventional generator as unity, the mass s of the two unconventional generators under investigation are put in better perspective by Figure 25.

300 kW RFPM Synchronous Generator			
Active Component	Weight of Active Components (kg)		
	Conventional	Dual-rotor	Modular C-core
Magnets	233	453	194
Rotor Iron	480	1056	2349
Copper	780	780	780
Stator Iron	1412	530	530
Total	**2905**	**2819**	**3853**

Table 3: Active mass of two PMSG topologies

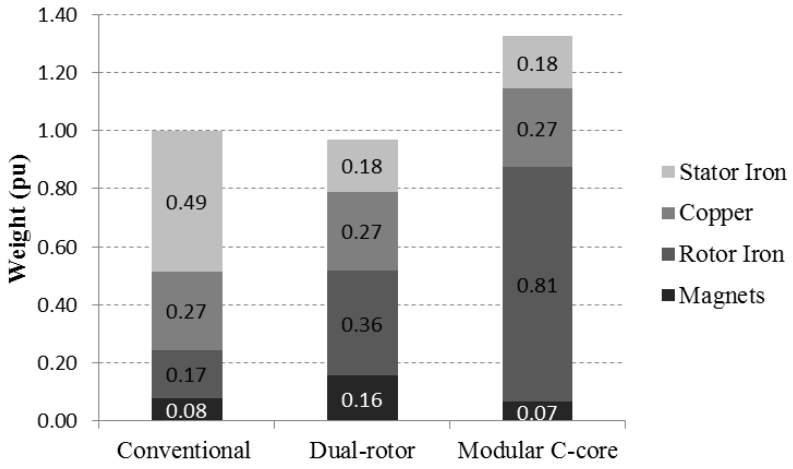

Figure 25: Active mass distribution in PMSG topologies.

Magnet material of the double-sided rotor is, as expected, about double that of the conventional single-rotor machine. It is surprising to see that the magnetic material usage of the machine with the modular C-shaped rotor yokes is less than that of the benchmark machine. The greatest contributor to this result is the smaller magnet pitch (0.77 compared to 0.9) and the uniform yoke module (or magnet) width. The total magnet height required for the C-shaped modules to produce the same magnetic flux density in the air gaps as that produced in the conventional machine, is the same as the magnet height of the benchmark machine. The magnet sizes differences of these two machine volume of these two PM machines can be seen in Figure 26, showing their active components which overlap and share the same air gap diameter. Figure 25 also shows that the C-shaped rotor yoke topology uses about 33% more active mass than the conventional generator, whilst a hefty 61% of its mass is contained in its modular yokes alone, which is nearly five times more than that of the benchmark. On the other hand, although the double-sided rotor topology uses twice as much magnetic material, it promises the possibility of mass reduction as can be seen from Figure 25 and Table 3.

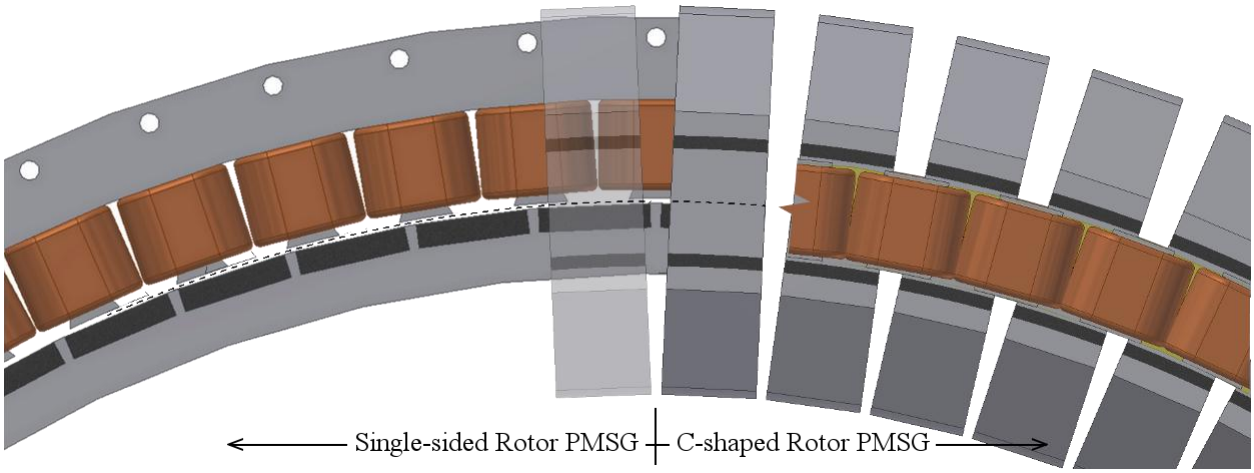

Figure 26: Magnet difference

2.4 Conclusion

In this chapter the electromechanical-energy conversion is studied in order to gain a better understanding of the radial attraction forces that exist in direct-drive generators and demand bulky structural support to maintain the desired air gap clearance. Although these attraction forces between the rotor and stator of iron-cored generators cannot be eliminated, the analytical method used suggests two topologies that promise to greatly reduce the resultant force on the iron-cored, yokeless stator. FE analysis results support this finding.

The results of the magneto-static tests performed in this chapter are expected not to correlate with real world result, but the FE models do provide some mean to do a comparison study. These tests have shown that the C-shaped yoke topology's calculated mass is unfavourable, compared to that of a conventional machine's. The weighty modules are found to be a result of the yoke height which is determined by the electromagnetic design of the core and not the mechanical strength criterion. The C-shaped yoke furthermore also posed various construction challenges and design limitations.

The double-sided rotor topology on the other hand, reduces the resultant effect of the magnetic field forces on the stator structure, whilst reducing the required active material. In conclusion, it can be said that a double-sided rotor iron-cored PMSG is theoretically an unequalled topology for reducing the effect of the magnetic field forces on the iron components in wind turbine generators, and maintaining a very high efficiency due to the iron-cored stator. The extent of the reduction of structural mass of direct-drive wind turbines with the double-sided rotor topology need to be confirmed by a thorough generator design and thus will be examined in the following chapters.

Chapter 3
Electrical Design of the Double-sided Rotor PMSG

This chapter deals with the first, and not necessarily the optimum, electrical design of the Double-sided rotor PMSG prototype. Firstly, some design specifications are set for the experimental machine. Thereafter, design choices with regards to iron losses, magnetic excitation, winding arrangement and pole-slot combination are motivated. The model is then optimised and the simulations analysed before the final design is presented for manufacture.

3.1 Generator Specification

As one of the objectives of this study is to compare the double-sided rotor PMSG to a conventional single-sided rotor PMSG on the bases of their performance, the quality of their output parameters and their mass, it is important to set good design specifications and constraints for the prototype machine. One thought is to put no constraints on the dimensions of the machine and optimise it for mass, whilst ensuring that the power output satisfies its specified rated output. This however makes the optimisation very intensive. The alternative is to put constraints on the outer diameter, D_o and the axial length, l and then maximise the inner diameter, D_i of the RFPM generator so as to minimise mass whilst still meeting the specified rated power output. The generator is therefore optimised within a confined volume. The latter ideology is adopted for this study. This allows the same turbine blades, used for the conventional generator, to be used for the experimental double-sided rotor machine.

With D_o fixed, D_i is determined by the rotor yoke and magnet heights of the inner and outer rotors, the two air gap clearances and the stator height. The air gap clearance, g_c for both air gaps are taken to be constant and each are equal to the air gap clearance of the conventional machine. Furthermore, the rotor yoke height, h_y of the inner and outer rotors are accepted as equal, and so too the heights of the inner and outer magnets, h_m. Both the magnet and slot widths are defined by the magnet pitch, θ_m and slot width pitch, θ_g respectively. The actual widths of both the magnets and

slots are consequently also determined by their radial placement, since their pitch is defined as an angle. The slot width is constant or uniform and does not taper toward the machine's centre. The magnet and slot pitches can additionally be represented as a fraction of the pole pitch, θ_p and slot pitch, θ_S respectively and are indicated by the symbol σ. These ratios are expressed in per unit (pu) values as in Eq.1.

$$\sigma_m = \frac{\theta_m}{\theta_p} \; ; \quad \sigma_g = \frac{\theta_g}{\theta_S} \tag{3.1}$$

where

$$\theta_S = \frac{2\pi}{S} \; ; \quad \theta_p = \frac{2\pi}{p} \; , \tag{3.2}$$

while S is the number of stator slot and p the number of magnetic poles.

The number of dimensional variables are five, namely, rotor yoke height, h_y, magnet height, h_m, stator height, h_s, the ratio of the magnet pitch to the pole pitch, σ_m and the ratio of the slot opening pitch to the slot pitch, σ_g. These are given by $\boldsymbol{X}$.

$$\boldsymbol{X} = \begin{bmatrix} h_r \\ h_m \\ h_s \\ \sigma_m \\ \sigma_g \end{bmatrix} \tag{3.3}$$

The performance output parameters are the electrical power output, P_O, the rated rotational speed, n_r (determined by the turbine's power curves and its rated speed), and the output or electrical frequency, f. These performance parameters are given by $\boldsymbol{U}$.

$$\boldsymbol{U} = \begin{bmatrix} P_O \\ n_s \\ f \end{bmatrix} = \begin{bmatrix} 15\ \text{kW} \\ 150\ \text{rpm} \\ 50\ \text{Hz} \end{bmatrix} \tag{3.4}$$

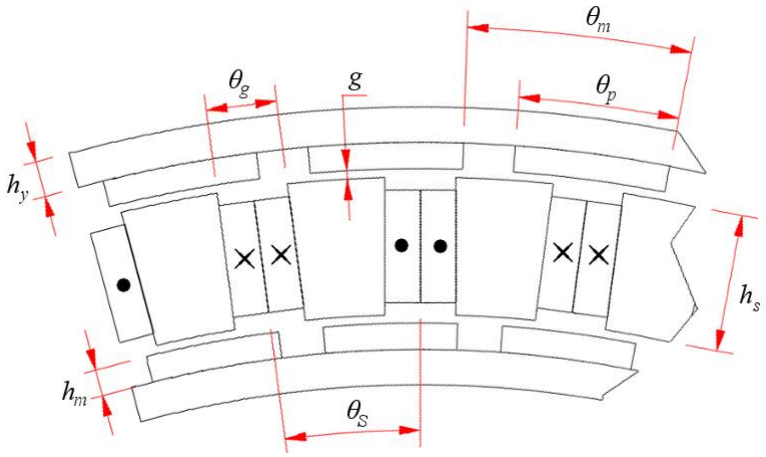

Figure 27: Section of double-sided rotor PMSG model

With P_0 and n_s known, the required developed air gap steady state torque, T_0 can be calculated as

$$T_0 = \frac{P_0}{\omega_r} \tag{3.5}$$

The number of poles, p in a synchronous generator is determined by the rated synchronous speed, n_s and the required electrical frequency, f with the following expression:

$$p = \frac{120\,f}{n_s} \tag{3.6}$$

Although the conventional generator used a 40-48 pole-slot combination with a single-layer winding configuration, no requirement is placed on the number of slots in the stator or on the winding configuration of the experimental double-sided rotor machine. From the requirements in $\boldsymbol{U}$ and their relationship in Equation (3.6), it becomes evident that the pole number for the double-sided rotor PMSG will also be 40. The selection of a pole-slot combination and winding layout is discussed in the following section. The only other performance output requirement is that the peak line-to-line voltage should be 400 V.

During the design process of all direct-drive wind generators, numerous features dominate the design. Some of the primary features are cost, mass, simplicity of design, robustness, maximum power output and satisfactory quality of the output parameters, such as voltage and torque. Cost is most often linked to the mass of the machine and the simplicity of the design. The mass of the generator furthermore determines the structural requirements of both the tower on which it is mounted and the tower foundation, and hence greatly influences the labour costs of manufacturing and erecting such a structure. A simpler and lighter design will reduce the generator's manufacturing cost and help decrease the maintenance cost. Seeing that the objective of the topology choice in the previous chapter was to reduce generator structural mass and indirectly cost, the electrical design will likewise account for the generator mass in the optimisation process. Active mass will be optimised in this chapter, whilst the mechanical design in the next chapter will focus on original and simplistic structural design in order to reduce the machines mass even further.

3.2 Motivation of Design Choices

3.2.1 Iron losses

The two cylindrical steel yokes of the double-sided rotor radial flux PM generator serve as a return path for the magnetic flux between adjacent magnets. The magnetic flux density in the rotor yokes is not static like air-cored machines, and due to the magnified armature reaction of the iron-cored stator, is expected to have a sinusoidal fluctuation around a mean value. The stator iron or stator teeth also experience fluctuating flux densities as the magnet pairs sweep across them. The

stator iron, however, experiences a completely reversed sinusoidal flux density fluctuation. These magnetic flux density fluctuations induce eddy currents in the iron components which increase their temperatures (a result of ohmic power loss) and can consequently be detrimental to the generator's performance. For this reason stator iron are always laminated to reduce the flux that the eddy currents enclose. The rotor yokes iron are also laminated, since non-overlap stator windings are known to have much more sub-harmonics than overlap windings, which is also a source of losses.

Furthermore [39] has shown that reducing the rotor yoke height, not only reduces the active material volume, but also brings about a significant reduction in the eddy current losses in the yoke and permanent magnets. From an electrical point of view, the thinnest possible yoke height will be the optimum; mechanical strength of the yoke structure, however, also needs to be considered in the search of an optimum yoke height.

3.2.2 Field Excitation

Rare earth permanent magnets (PMs) are used for the field excitation in the experimental generator of this study for two reasons. Firstly, by using PMs, the rotor uses less material, making the overall machine lighter and compact. Secondly, the lesser rotor iron reduces the iron losses in the rotor, and the excitation losses found in wound rotors are eliminated. Since a study has shown that using stronger magnets does not necessarily increase the cost of the magnets [47], sintered neodymium-iron-boron ($Nd_2Fe_{14}B$) magnets, with a N48 grade are used.

It has been shown that by segmenting the magnets of PMSGs, the eddy current losses in the magnets are reduced, which has a noticeable effect on increasing these machines' performance [55][56][57]. By restraining magnet losses, less magnet material is needed to produce the required magnetic flux density in the air gap, and as a result the cost and mass of the machine reduces. Fully segmented magnets will therefore be used in the double-sided rotor PMSG. Double-sided partially segmented magnets are just as effective in reducing magnet losses, while manufacturing promises to be less cumbersome and hence cheaper [55].

Maximum external MMF, with which the magnetic circuit might come into contact, occurs during a winding short circuit – therefore there must be a certain minimum magnet height in order to prevent the magnets from demagnetisation.

3.2.3 Winding Configuration

The winding layout of a stator can be defined as the placement of the conductors of each phase in the stator slots. Various types of stator winding layouts exist for AC machines. While the actual phase conductor placement is determined by the pole-slot combination, discussed in the next section,

the winding layouts can be categorised into two main configurations, namely, an overlapping or distributed winding arrangement, and a non-overlap or concentrated winding arrangement.

The most common winding arrangement for iron-cored radial flux PM machines is the overlapping or distributed winding layout. Because the coil of a phase must cross over the other phase coils, overlap winding configurations have long and bulky end-windings, which exceed the coil height. With a small air gap clearance between the double-sided rotor magnets, the overlap winding configuration makes the axial insertion of the stator in a double-sided rotor topology practically impossible.

An alternative winding configuration is the non-overlap or concentrated winding arrangement where each coil is wound around a stator tooth. The simpler coil structure, shorter end-windings and lower torque ripple of non-overlap stator windings have made it a very attractive option for direct-drive PM machines with a high pole number [26][30]. It has also been shown that the slot fill factors, which directly affect the performance of a machine, are much higher for non-overlap winding configurations than it is for overlap winding configurations [59]. Furthermore, since the end-windings of non-overlap coil configurations do not exceed the coil height, it allows for easy axial insertion of the stator between the outer and inner rotor yokes, which makes this winding configuration a much better choice for the double-sided rotor topology.

Non-overlap windings can either have one or two layers per slot. When the conductors of a single coil fills two slots as it is wound around every second stator tooth, it is classified as a single-layer non-overlap winding configuration. On the contrary, the stator coils of a double-layer non-overlap winding layout only fill half of two adjacent stator slots (in other words a single coil fills the area of one slot) as they are wound around every stator tooth. Although the double-layer arrangement has twice as much coils as the single-layer arrangement (one slot per coil vs. two slots per coil), it has much less sub-MMF harmonic content [59], more sinusoidal back-EMF waveforms [58] and lower Joule losses.

The end-winding axial length of single-layer non-overlap windings is approximately twice the length compared to those of double-layer windings, while double-layer windings have twice the number of coils as single-layer windings. A machine with a double-layer non-overlap winding configuration has the greatest potential to be the most compact unit of the three described winding types for electrical machines [59]. The copper losses are thus expected to be the lowest for concentrated windings when a double-layer is compared to a single-layer.

When two phases share a slot, as in a double-layer winding configuration, more insulation material is needed compared to when only one phase occupies a slot. For this reason it is said that a single-layer winding arrangement offers a higher slot fill factor than the double-layer configuration.

This is true for conventional iron yoked stators, whilst for the yokeless iron-cored stator of the double-sided rotor PMSG topology, a fill factor, k_f as high as 0.53 was proven possible. This is 26% more copper in the slot compared to its iron yoked counterpart. This improvement is owed to the new winding procedure, discussed in the next chapter, and is made possible by the modularity of the cored coil. A cross-sectional view of the copper filled stator slot with die designed number of coil turns is showed in Figure 28. In conclusion, a double-layer non-overlap winding topology is proposed for the double-sided rotor PM generator in this study, due to its various advantageous properties discussed.

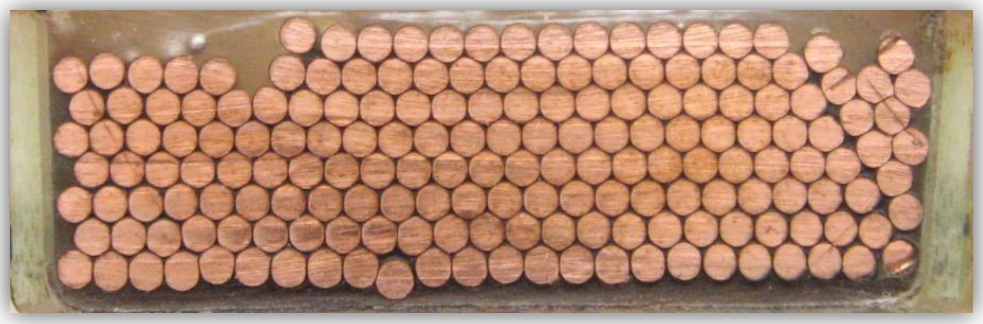

Figure 28: Cross sectional view of copper conductors in stator slot

3.2.4 Pole-Slot Combination

The pole-slot combination of surface mounted PM machines with concentrated windings determines the winding factor which is directly proportional to the average electromagnetic torque produced in the air gap. If the stator coils are fed with sinusoidal currents, the average electromagnetic torque produced can be approximated by [59]

$$T = \frac{1}{4\pi} k_w n_l n_t Q_s \hat{B}_{\delta 10} A_\delta \hat{I} \cos(\theta) \tag{3.7}$$

where k_w is the fundamental winding factor, n_l is the number of layers in each slot (1 or 2), n_t is the number of turns around each tooth, Q_s is the number of slots, $B_{\delta 10}$ is the peak value of the fundamental no-load air gap flux density, A_δ is the air gap area, Î is the peak value of the phase current to the machine and θ is the current angle [59]. To compensate for a poor winding factor, either the number of coil turns, n_t or the coil current, Î needs to increase which both increases the copper losses. It is therefore desirable to find a pole-slot combination with a good winding factor. Equation (3.7) also shows that by using double-layer concentrated windings, the same electromagnetic torque can be produced as with single-layer concentrated windings, but with fewer coil turns (less copper), lower air gap flux density (less magnet material), or lower current (less losses).

In order to calculate the winding factor of a pole-slot combination, it is necessary to consider the induced electromotive force (EMF) of the copper conductors. The per unit electromotive force (EMF) phasor for each coil side or winding element, i is defined as [58][59]

$$\vec{E}_i = e^{j\frac{\pi p}{Q_s} \cdot i} \tag{3.8}$$

Winding elements that share a stator slot have that same phasors and therefore only one phasor can be assigned to each slot. Each winding element is assigned to a phase and hence their EMF phasors add to the resulting phase EMF phasor. The winding factor can therefore be considered as the ratio of the resultant phase EMF phasor magnitude to the sum of the individual winding element phasor magnitudes. Thus, the more appropriate the winding elements are assigned to a phase, the better the winding factor becomes. For a three-phase machine, the winding factor is given by [58]

$$k_w = \frac{\left|\sum_{i=1}^{S/3} \vec{E}_i\right|}{S/3} \tag{3.9}$$

where S is the number of winding elements, and E_i is the electromotive force (EMF) phasor for each winding element, i. Since the coils of double-layer winding configurations are wound around a stator tooth, the two winding elements closest to a stator tooth belongs to the same phase. Another constraint is that the slot number, Q_s must be a multiple of the number of phases, m. This method used to calculate the winding factor and determine the winding phase sequence is presented in detail in [58] and [59].

Since the number of poles, p is fixed, only the slot number, Q_s can be varied to obtain different possible pole-slot combinations When selecting a slot number, factors such as the magneto-motive force (MMF), harmonics, torque quality and magnetic noise should be taken into consideration. The harmonics cause the magnetic fields in the rotor yokes to alternate and consequently, as explained earlier, give rise to eddy currents in the permanent magnets and iron losses in the rotor yokes. Machine winding arrangements with asymmetries (no common denominator for pole and slot numbers) present many more harmonics in the MMF than machines with symmetries.

The selection of a pole-slot combination also has an influence on both the cogging torque and torque ripple. Cogging torque, also known as "no-current" torque, is a result of the magnetic interaction between the PMs on the rotor and the iron-cored stator. Cogging is therefore defined as the torque ripple about zero torque when the electric machine is not energised (when there is no developed torque in the air gap). Torque ripple is defined as the ripple about the nominal torque at full load. It is proposed that combinations with a large least common multiple (LCM) have a high cogging frequency and therefore lower cogging amplitude [59]. The closer the number of slots is to the number of poles, the higher the LCM becomes [58]. However, further studies have shown that machines with high cogging torque can exhibit lower torque ripple than a design with lower cogging torque [58] as shown in Table 4 on the next page.

Machines with asymmetric windings also experience unbalanced forces distributed in the air gap. These forces add up to a resultant force that acts on the stator and moves around the air gap with time, causing the stator to vibrate and in turn generating acoustic noise. The moving resultant force also causes the strain in the mechanical structure to fluctuate, making the support structure prone to fatigue failure.

From the above discussion it must be noticed that a good winding factor, k_w should not be the only objective when selecting a pole-slot combination. A good pole-slot combination is therefore only obtained when the MMF, harmonics, torque quality and magnetic noise for all the different combinations are investigated. Table 5 shows the possible slot numbers, Q_s for the 40 pole machine. The number of slots per phase per pole is indicated by q in its simplest fractional form. The greatest common devisor (gcd) of the number of poles, p and the number of stator coils, Q_c gives the number winding sections, W_s in each machine [60]. Both q and W_s indicate how many repeating sections exist in an electrical machine.

For this study Q_s is chosen to be 48 which then gives a 40-48 pole-slot combination. This pole-slot combination has a relatively high winding factor, k_w and offers a symmetric winding layout as indicated by the even W_s. The symmetric winding layout has the advantage of fewer harmonics which results in fewer losses in rotor and balanced forces in the air gap [58]. This specific pole-slot combination choice is based on the results of studies presented in literature – no detailed investigation was done beforehand with regards to harmonics, vibration or torque quality.

Table 4: Torque quality of different PM electrical machines.

p, Qs, q	kw	LCM	Cogging torque in % of rated torque	Torque ripple in % of rated torque
p=60, Qs=72, q=2/5	0.933	360	1.4	2.6
p=64, Qs=72, q=3/8	0.945	576	0.3	3.4
p=64, Qs=60, q=5/14	0.951	960	0.03	3.2
p=64, Qs=66, q=11/32	0.954	2112	0.003	3.4
p=60, Qs=63, q=21/62	0.955	3906	0.003	4.4

Table 5: Possible slot numbers for a 40 pole machine

$p = 40$	Q_s	30	36	42	45	48	54	60	66	72
	q	1/4	3/10	7/20	3/8	2/5	9/20	1/2	11/20	3/5
	k_w	0.866	0.945	0.953	0.945	0.933	0.877	0.866	0.778	0.735
	w_s	10	4	2	5	8	2	20	2	8

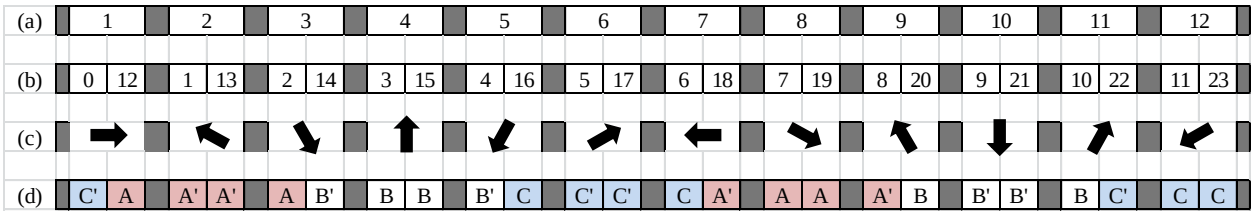

Figure 29: (a) Slot number, (b) layer number, (c) EMF phasor, and (d) phase sequence for a 40-48 pole-slot combination.

The winding layout or phase sequence for the selected pole-slot combination is presented in Figure 29. Twelve slots of the chosen machine is shown, each with a slot number, numbered winding elements and a per unit EMF phasor allocated to it. With the winding layout as determined by [58] it is clear that two adjacent phase coils are connected in series to form a phase pole. These series connected coils are in turn connected in parallel with the other seven pole forming serie connected coils of the same phase. The three phases are finally connected in Y. The resulting phase EMF phasors of the twelve slots are as shown in Figure 29c whilst Figure 29d winding layout or phase sequence.

3.3 Optimisation and Simulation Tools

Steady-state condition is assumed for the examination of the double-sided rotor PM machine. This section describes the FE model and the optimisation procedure followed. Some results regarding the output quality is also discussed.

3.3.1 The FE model description

The analysis of the double-sided rotor PMSG with non-overlap windings can be divided into its 8 winding or repeating sections. By simulating only one eighth of the machine, the computation time of the FE model significantly reduces and the calculated results can simply be applied for the remaining sections. The FE model thus consists of inner and outer rotor iron yoke sections, each with five surface mounted PM pairs which radial magnetised direction alternates. Since the number of magnet pairs is uneven, an odd or negative periodical boundary condition is applied to the radial planes at the two ends of the FE model [60]. The six stator coils represents the three-phase winding layout that repeats itself throughout the machine.

An important aspect of the FE double-sided rotor PMSG model is to determine the initial position of the rotor, relative to the stator and phase coils, and in combination with the applied currents. Maximum torque is achieved for a PM machine when the angle between the PM flux vector and the current vector is 90 electrical degrees. Therefore, since the current in phase A is chosen to be zero when the rotor is in its initial starting position, the flux density should be at its maximum. This

means that the *d*-axis of the rotor (that is the centre of a magnet) should be aligned to the phase-axis of phase A (that is the slot containing two A-phase layers)[26].

The flux path in the active part of a radial flux machine primarily moves in two dimensions, namely the radial and tangential directions. The flux variation in the axial direction is insignificant in comparison and therefore it is adequate to simulate the model in 2D only. This saves FE computation time. A two dimensional cross sectional plain, perpendicular to the axial direction and through the active section of the rotor and stator configuration, is therefore selected for modelling purposes. Figure 30 shows the FE model and its solved flux field plot for the starting position.

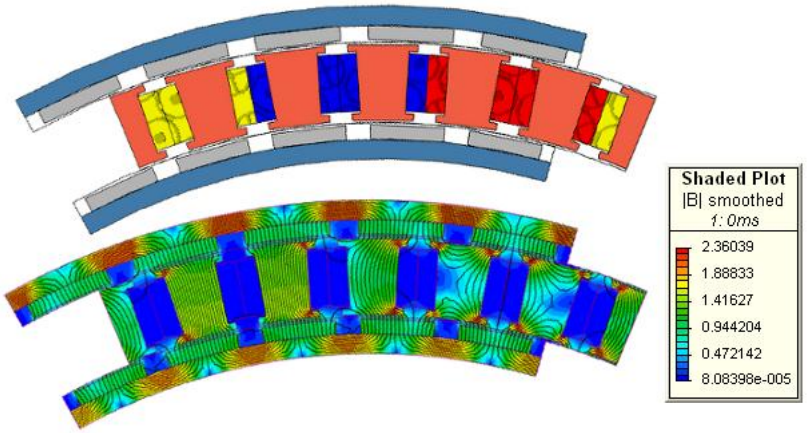

Figure 30: FE model - solid and with field plot

3.3.2 Optimising/design algorithm

It should be mentioned again that the aim of the study is to find a machine design, as a first design iteration, that is in the proximity of an optimum machine to prove the feasibility of the double-sided rotor topology for direct-drive wind applications. With this said, the design algorithm is essentially a line minimisation technique that is applied to each of the five dimensional parameters, x_k independently and minimises the objective function M = f(x_k), where M is the active mass of the PMSG. The FE package's scripting language is used to define all the machine parameters and write the design algorithm. The schematic is shown in Figure 31.

The design algorithm starts with the same initial machine variables as those of the single-sided rotor RFPM generator presented in [53]. The active mass, M_i is calculated for the initial machine dimensions and then they are varied one at a time. One machine parameter, x_k is incremented by a fixed step, Δx_k and the M_i recalculated. If the new active mass, M_i is higher than the initial active mass, M_{i-1} on the first step, then the increment direction is changed. After each incrementing a machine parameter value, the FE model is modified and simulated. To ensure that the developed air

gap torque stays above the rated torque value, the magnetic flux linkage, λ_{abc} results of each simulation, together with the phase currents, i_{abc} are transformed to their dq values by means of Park's transformation. The developed torque in the air gap is then defined as [45]

$$T = \frac{3}{2}\, p\, (\lambda_d\, I_q - \lambda_q\, I_d) \tag{3.10}$$

If the produced air gap torque is above the specified rating, then x_k is incremented, the FE model redrawn with the new value of x_k and the simulation repeated. However, if the developed air gap torque, T is below its specified value of 1000 Nm, then the active mass of the model is penalised as

$$M_i(x_k, w_k) = M_{gen}(x_k) + w_k\, \varepsilon \tag{3.11}$$

were w_k is a weighing factor for each parameter, x_k in $\boldsymbol{X}$ and ε is the penalty function defined as

$$\varepsilon = \begin{cases} 0 & : T \geq T_0 \\ (T - T_0)^2 & : T < T_0 \end{cases} \tag{3.12}$$

The values of $(x_k)_i$ and $(x_k)_{i+1}$ should then bracket the optimum value for x_k. By taking $(x_k)_i$, $(x_k)_{i+1}$ and $(x_k)_{i+2}$ to be the closest to the optimal active mass value, second degree polynomial of the Newton form is fitted to these three values. This polynomial has the form

$$f(x) = c_1 + c_2\,(x - x_i) + c_3\,(x - x_i)(x - x_{i+1}) \tag{3.13}$$

where

$$c_1 = f(x_i) \tag{3.14}$$

$$c_2 = \frac{f(x_i) - f(x_{i-1})}{(x_i - x_{i+1})} \tag{3.15}$$

$$c_3 = \frac{c_2}{x_i - x_{i+2}} - \frac{f(x_{i+1}) - f(x_{i+2})}{(x_{i+1} - x_{i+2})(x_i - x_{i+2})} \tag{3.16}$$

Figure 32 is a graphical representation of this process. The solid linear line is the calculated active mass of the generator. The diamond shaped markers indicate panelised mass function as in Equation (3.11). The minimum value of the polynomial, fitted through the last three data points, is obtained by setting the derivative of Equation (3.13) equal to zero. The x_k value (represented by b) that satisfies this expression is taken to be the optimum value, since it is close enough to the optimum value (represented by a). The optimum x_k value is therefore defined as

$$x_{opt} = \frac{1}{2}\left(x_{i+1} + x_i - \frac{c_2}{c_3}\right) \tag{3.17}$$

Since the optimum x_k value can be unrealistic when construction is considered, a lower boundary, x_{k0} is placed on each dimensional variable. This value is then taken as the optimum value when the lower boundary is violated in the optimisation process. After one of the dimensions has been optimised, the next dimension is optimised.

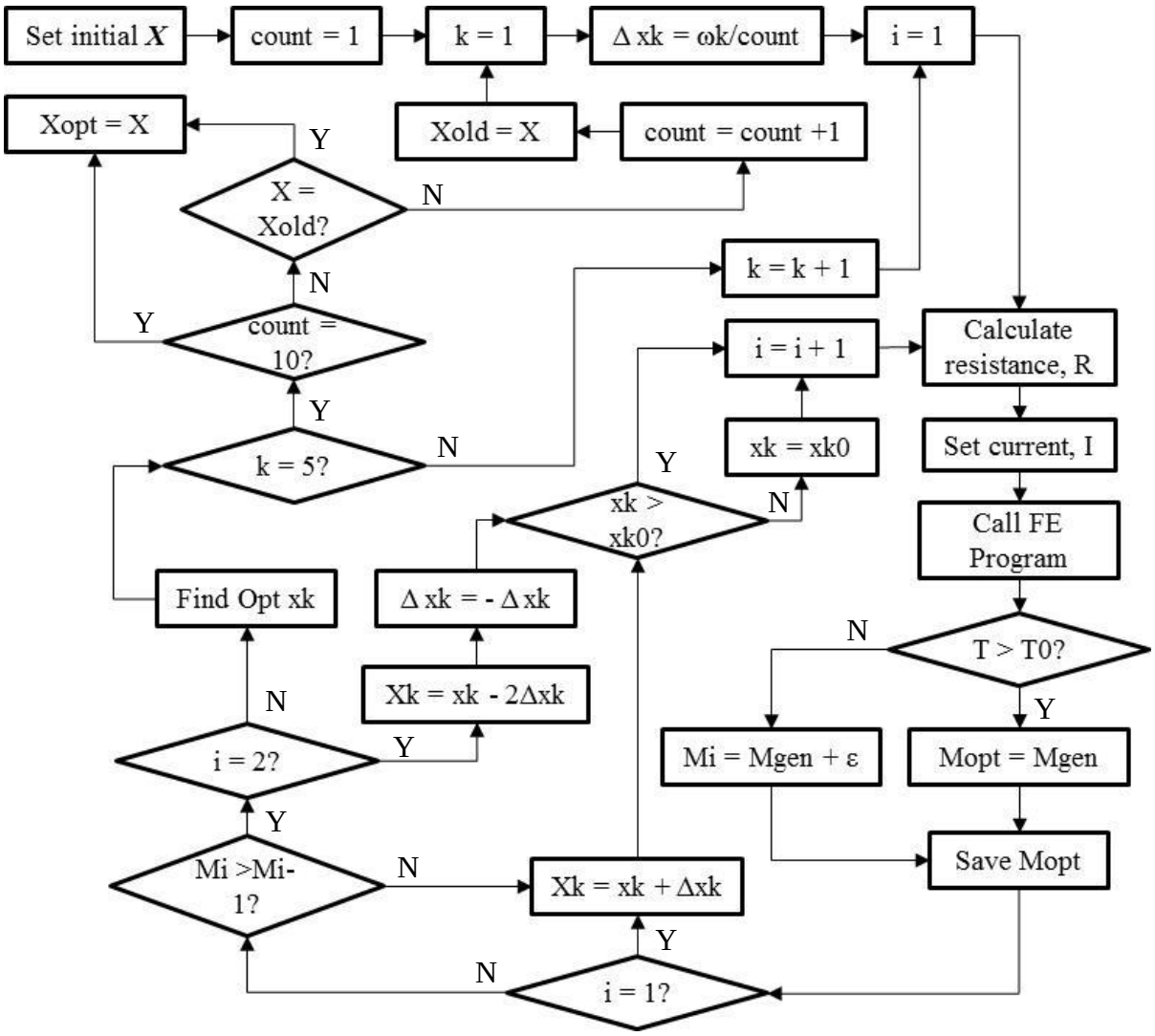

Figure 31: Diagram of optimisation procedure

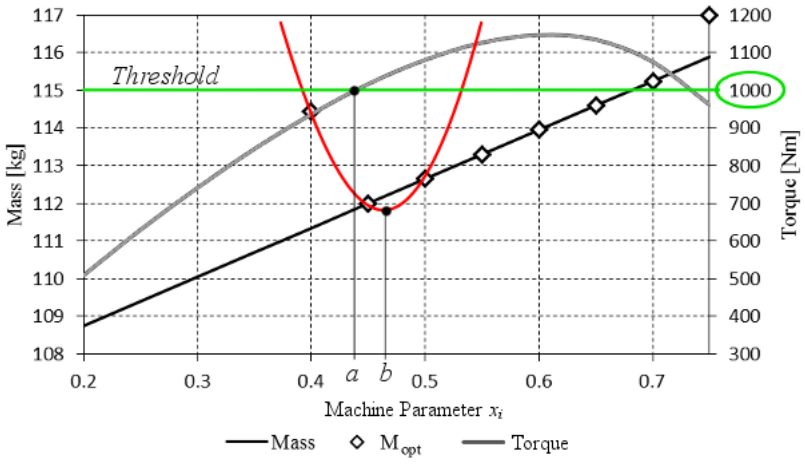

Figure 32: Finding optimum machine parameter, *x*.

Once the parameters contained in $\boldsymbol{X}$ each have an optimum value, these values are set as the new design parameters and the algorithm repeats the process. To improve the search for optimum machine parameters, the increment value of each parameter is reduced in order to make the steps smaller. The algorithm only terminates once the 10th optimum parameter set is found or when the change in two consecutive optimum parameter sets are negligible. This ensures a near optimum value for each machine parameter.

3.3.3 Further Optimisation of FE model

The design optimisation as described above is based on the average value of the performance torque. Dimension variations such as σ_m and σ_g, have shown to have a minimal effect on the average generated torque, τ_{ave}. On the contrary, cogging torque, $\Delta\tau$ has shown to have a high sensitivity to such dimensional variations [39][53]. Since turbine torque at low wind speeds is very low, a wind turbine generator with high cogging torque can result in total failure of start-up [46]. Torque ripple is another aspect of torque quality. The fluctuating forces that exist between the rotor and stator during operation can also have a devastating effect on the cantilever-like stator proposed for the double-sided rotor topology. Therefore, in search for improving the performance quality of the double-sided rotor generator, minimizing torque ripple, ΔT, by varying the magnet pitch, σ_m, slot pitch, σ_g, and slot opening, σ_w, is chosen above minimising the cogging torque, $\Delta\tau$, and is further investigated in this section.

The same method described in [39] for the minimisation of $\Delta\tau$ is followed for minimising ΔT. In short, single parameter variation for each of the above mentioned dimensional parameters is done, while all other machine parameters are kept constant. By using magneto static solutions for each FE model, low torque ripple regions are identified which allows optimum values to be chosen for each of the dimensional machine parameter investigated. This is done without drastically affecting the average generator torque, T_{ave} of the machine.

Figure 33 shows how the ΔT is affected by linearly varying the slot width for four predetermined magnet pitch values. A magnet pitch to pole pitch ratio of 0.95 proves to produce the least per unit (pu) torque ripple at 0.029. However, when cost is considered, a pu torque ripple of 0.047 is still acceptable since 21% less magnetic material is required. From this data the magnet pitch of σ_m = 0.75 and a slot width of σ_g = 0.42 is chosen for the double-sided rotor PMSG.

With the slot width fixed, the slot opening, σ_w, is also varied and its influence on the torque ripple plotted in Figure 35. It is evident that there is not much difference in the torque ripple of a machine with fully open slots, semi closed slots and fully closed slots. Even though the fully open slots uses the least amount of active material, the semi closed slot design, with its I-shaped coil cores, provides support for the coil sides, gives the casting material more grip on the stator iron and reduces the pu

torque ripple further to 0.04. A slot opening of 0.57 is thus selected for the double-sided rotor prototype.

A final aspect of the machine design that is considered is skewing. Traditionally skewing is applied so that the magnet or stator slot angular position changes, gradually or in steps, along the axial length. For the double-sided rotor topology, magnets and stator slots are aligned in the axial direction, but the magnets on the two rotor yokes are skewed relative to each other – the outer magnets are misaligned relative to the inner magnets with an angle β as shown in Figure 35.

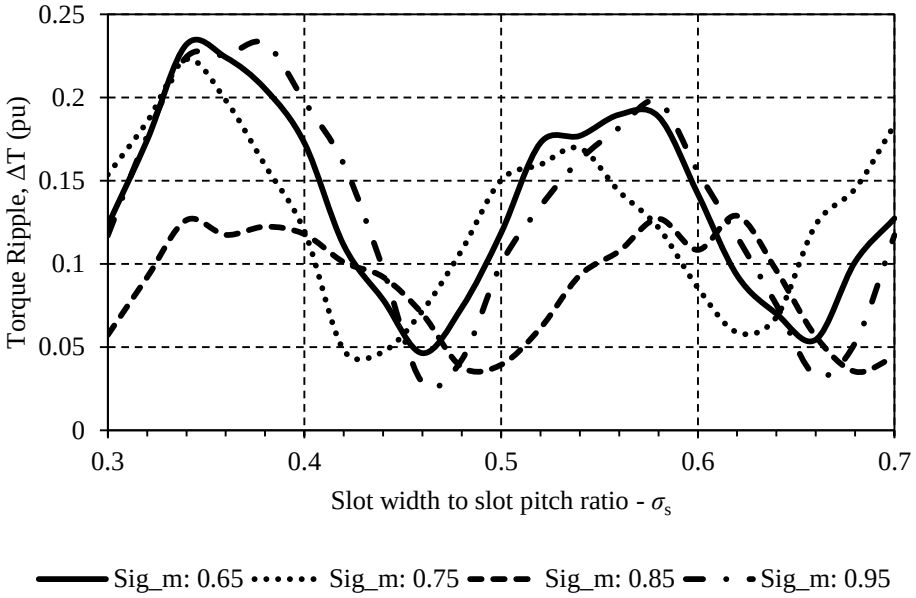

Figure 33: Varying slot width

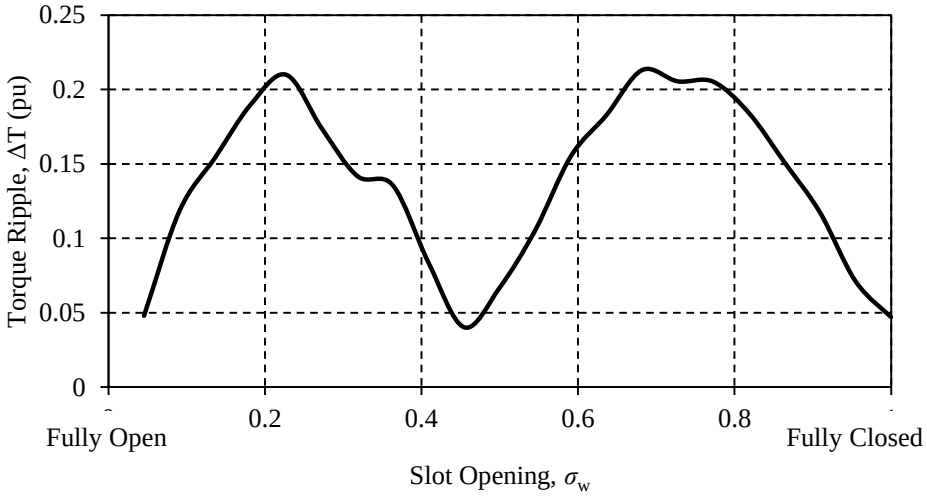

Figure 34: Varying slot opening

Figure 36 shows the developed outer and inner rotor torque for the FE model with its refined machine dimensions thus far. The total developed torque is the sum of the torque on the two rotors. The ripple effect is thus often magnified by this addition of the torque ripples of the two air gaps. Since the frequency of the two torque ripples are the same, their ripple effect is maximum when the outer and inner air gap ripples are in phase. When the ripples of the two air gaps are 180 degrees out of phase, then the peaks and valleys of the two waveforms are added, resulting in a minimum torque ripple. From Figure 36 it is noticeable that the non-skewed rotor torque ripple is slightly out of phase. It is expected that a phase shift of about 0.3 ms for the outer air gap torque ripple will approximately put the waveforms 180 degrees out of phase, resulting in a minimum torque ripple condition. This is verified by simulations which indicate that by skewing the rotors by 0.3 mechanical degrees, a further 43% reduction in the torque ripple of the double-sided rotor PMSG is reached.

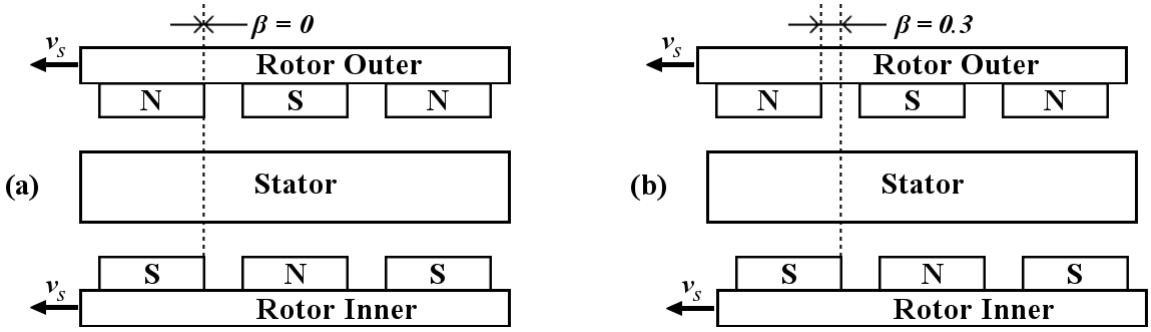

Figure 35: Double-sided rotor PMSG, (a) Non-skewed (b) Skewed.

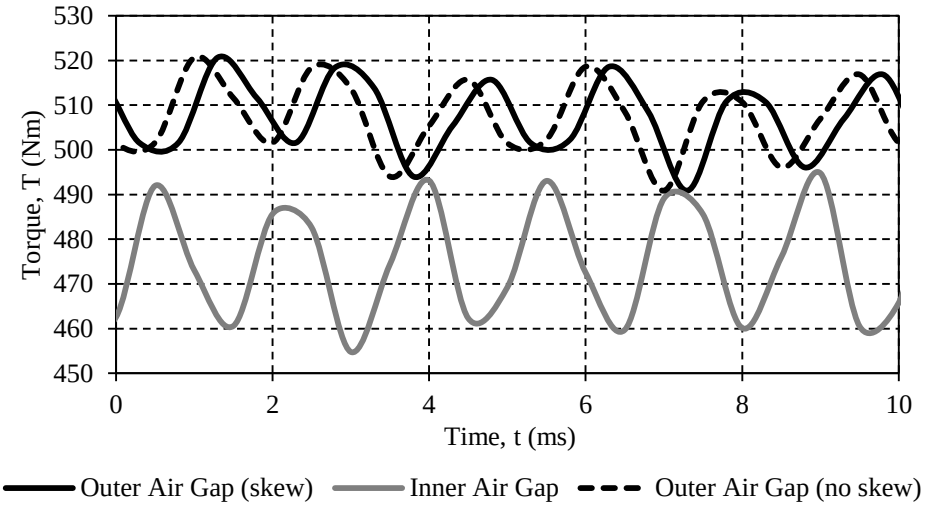

Figure 36: Minimizing developed torque ripple through rotor skewing.

3.3.4 FE Modeling Results and Performance Evaluation

The final and near optimum model parameters are contained in X'. The first five machine parameters were obtained through the optimisation of the model for average torque. The slot opening, σ_w and rotor skewing angle, β were obtained in the search for lower torque ripple at rated speed.

$$\boldsymbol{X'} = \begin{bmatrix} h_y \\ h_m \\ h_s \\ \sigma_m \\ \sigma_g \\ \sigma_w \\ \beta \end{bmatrix} = \begin{bmatrix} 8.47 \\ 6.32 \\ 33 \\ 0.75 \\ 0.42 \\ 0.57 \\ 0.3 \end{bmatrix} \tag{3.18}$$

In Chapter 2, two assumptions are made whilst the nature of different magnetic flux paths were investigated. The first assumption was that no leakage flux exists. This was however said to be idealistic. Magnetic attraction between rotor and stator, due to leakage flux, will always exist, though it can be minimized to a great extent through the altering the rotor-stator arrangement as shown in Chapter 2. The second assumption was that the section of the 300 kW RFPM wind generator in consideration, can be considered as linear because of its large air gap radius. As a result the magnets on both rotor yokes were considered to be of equal size, while in reality they are not.

With a constant magnet pitch, the volume of the outer and inner magnets of any double-sided rotor machine becomes very close to being equal as the air gap radius becomes bigger. On the other hand, the smaller the air gap radius becomes, the more significant becomes the difference in inner and outer magnetic material. A difference in magnet volume translates to a difference in the stored energy of the two air gaps, given that the lengths of the air gaps are identical. This is clearly seen in Figure 37, showing that the field force in the outer air gap is slightly more dominant than that of the inner air gap at different positions for a specific time instant. The stator of the double-sided rotor PMSG consequently experiences a resultant force radially outward. The axial distributed force in the stator is shown in

It is expected that the resultant radial force on the stator can be eradicated by either considering the outer and inner air gap clearances individually and finding their unique values that balances the outer and inner air gap field forces. Magnet height and pitch could also be considered for the outer and inner individually for this purpose, but such particular refining is irrelevant to the focus of this study. Figure 38 shows the FE estimation of the instantaneous radial force on the iron-cored stator of the double-sided rotor PMSG. Since the magnitude of these forces are manageable, finding a solution for dealing with the existing resultant force on the stator is left for the mechanical design, discussed in the next chapter.

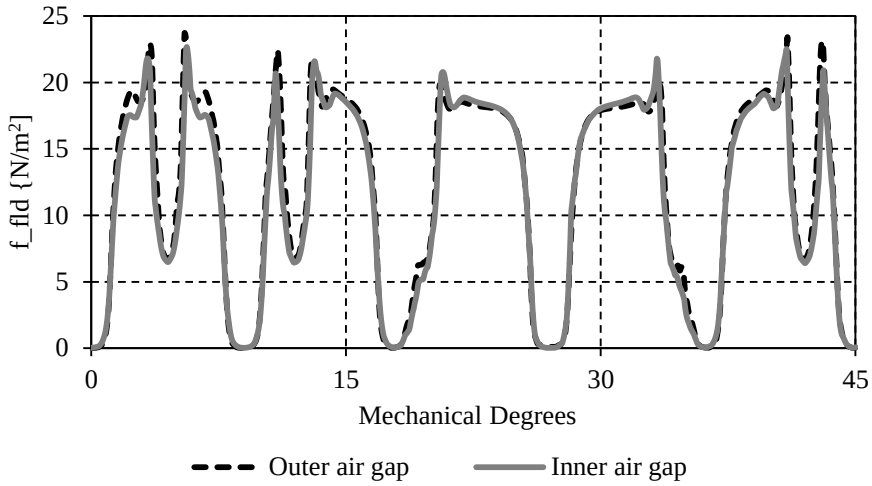

Figure 37: Field force distribution of inner and outer air gap

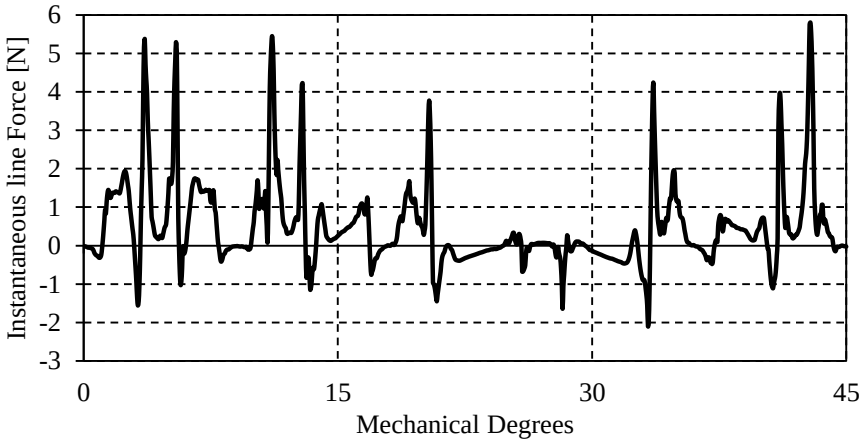

Figure 38: Instantaneous radial force on iron-cored stator at different positions.

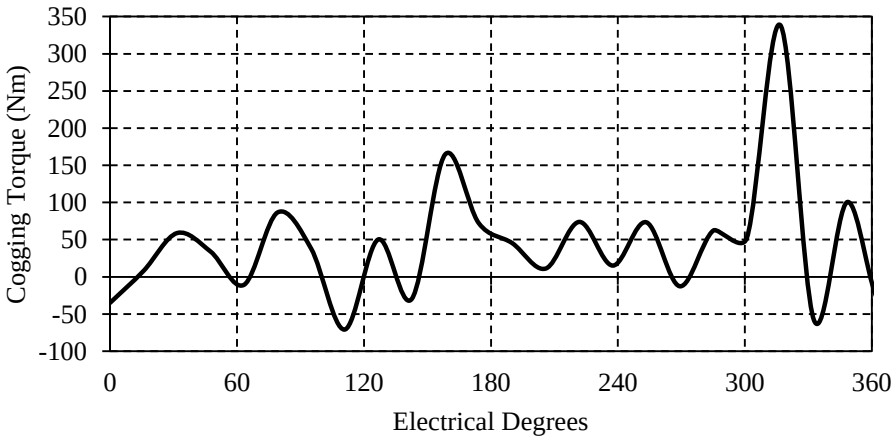

Figure 39: FE predicted cogging torque.

A final FE evaluation of the cogging torque is shown in Figure 39. The two peaks at about 160 and 315 electrical degrees respectively cannot be explained, except by inaccuracy of the FE software. With these two points ignored, the FE predicted cogging is 17% of the rated torque. For practical purposes such high cogging is unacceptable, but since minimising cogging is not an objective of this study, the building of the prototype is commenced to evaluate the performance of the proposed topology.

3.4 Design Conclusions

The overall goal of designing a well performing, light weight PMSG, by reducing the resultant force on the stator, is reached. The method followed first optimises the machine by minimising its mass, while still maintaining the averages developed torque above the minimum torque threshold. The optimum machine's performance is refined with slight parameter changes. This is done without significantly affecting the average torque of the machine.

The field forces in an air gap cannot be eliminated, but is addressed by introducing a second air gap, as with the double-sided rotor topology, which offers the opportunity of counteract the forces on the stator and greatly reduce the resultant force. The dual air gaps also eliminate the need for the iron stator yoke, which brings a significant reduction in the mass of the machine. This yokeless stator design furthermore allows the selection of a non-overlap, double layer, preformed winding configuration. A great advantage of this stator configuration is that the copper conductors can be wound directly onto/around the stator teeth, which gives a higher slot fill factor compared to performing the coils and then inserting them into the stator slots.

As the stator can only be inserted in between the two concentric rotor yoke and magnets arrays from one end and in the axial direction, the mounting of the stator can only occur at the tailing end, which gives the stator a cantilever-like structure. Because the strength of the non-ferrous material, used to support the suspended iron-cored coils between the inner and outer magnet arrays, are of concern, fluctuating radial forces and vibration is minimised. Minimising cogging torque and ensuring an easy start-up is jeopardised to safeguard the machine from possible failure during operation as a result of fluctuating radial forces and vibration. Simulations done on the double-sided rotor FE model, with the optimum machine parameters, predict a minimised torque ripple of 2.3% at rated conditions, while the cogging torque is estimated to be 17% of rated developed torque. The active mass is also expected to be about 7% less than that of the conventional single-sided rotor PMSG.

Chapter 4
Mechanical Design and Manufacture

With the focus on reducing manufacturing and maintenance costs, it goes without saying that the mass optimisation process extends further than just the electrical design of the generator. The mechanical design process pursues a simple and original structural topology with inherent light weight attributes for the experimental small-scale direct-drive generator, purposed for wind turbine applications.

The mechanical design of large wind turbines can be a daunting task that requires various specialised engineering skills. The design of small- to medium-scale turbines however is simplified and made less demanding by merely considering the major load carrying components of the generator, which are inclined to failure. Since the iron-cored stator coils are suspended between the rotor's two surface-mounted PM yokes, some controversial opinions will undoubtedly arise, which cannot be overlooked. For this reason this chapter will include mechanical design, strength analysis and manufacturing aspects of the double-sided rotor PMSG illustrated in Figure 40 to prove its feasibility.

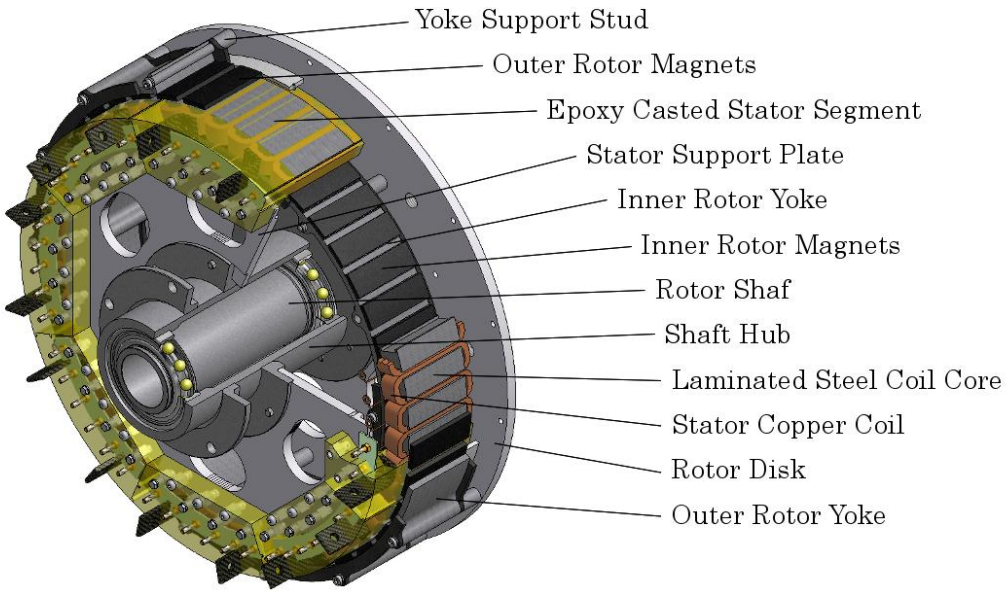

Figure 40: A CAD illustration of the double-sided rotor PMSG and its various parts

4.1 Rotor Design

4.1.1 Yoke height

From the previous chapter it is clear that the rotor comprises of two cylindrical laminated-steel yokes with different diameters, mounted concentrically on the same rotating shaft, one in the other. The yoke height, h_y is determined by the electro-magnetic requirements of the machine. Since the optimum yoke height, obtained from the electrical design, is the lowest possible value, it is necessary to examine whether the yokes will have sufficient structural rigidity to maintain the designed air gap clearance during operating and non-operating conditions. Figure 41 shows the operational forces acting on each of the two rotor yokes. The field force obtained from the electromagnetic analysis in the previous chapter is applied to the outer and inner surfaces of the inner and outer rotors respectively. Centrifugal forces are ignored because of the low operational rotation speed. The steady state torque, also obtained from the electromagnetic FE simulations, has a trivial influence on the yokes, yet is a major load component for the yokes' support frame, examined in the next section.

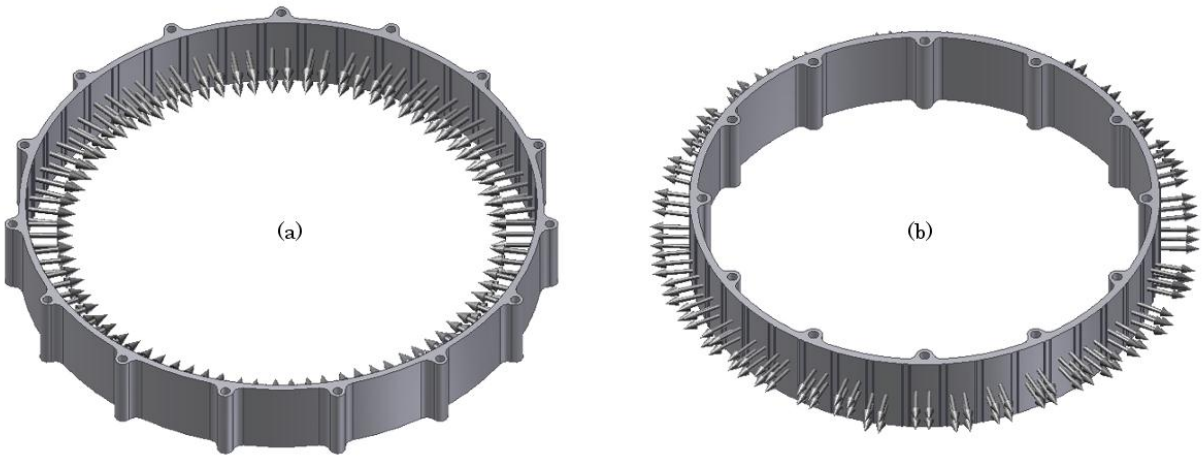

Figure 41: Rotor yokes with their respective loads.

The inner rotor yoke can be considered as a thin-walled cylinder subject to internal pressure, since the ratio of yoke height, h_y to yoke inner diameter, D_i is less than one-twentieth [61]. The maximum tangential stress, σ_t, also known as hoop stress, outweighs the radial stress, σ_r in such applications and can be approximated as [61]

$$(\sigma_t)_{max} = \frac{p_i(D_i + h_y)}{2\,h_y} \tag{4.1}$$

where p_i is the internal pressure and determined by dividing the average magnetic field force, f_{fld} over each magnet by the magnet's surface area, A_m as

$$p_i = \frac{(f_{fld})_{ave}}{A_m} \tag{4.2}$$

Comparing this maximum stress against the yield strength, S_y of the rotor yoke material, gives the design a safety factor, n_d of 13.43 for the inner rotor yoke, which is more than satisfactory. The outer yoke on the other hand, experiences a resultant external "pressure" which disqualifies it from using the same criteria. The magnitudes of the tangential stress and radial stress that exist in the outer yoke is approximated as [61]

$$\sigma_t = \frac{p_i r_i^2 - p_o r_o^2 - r_i^2 r_o^2 (p_o - p_i)/r^2}{r_o^2 - r_i^2} \tag{4.3}$$

and

$$\sigma_r = \frac{p_i r_i^2 - p_o r_o^2 + r_i^2 r_o^2 (p_o - p_i)/r^2}{r_o^2 - r_i^2} \tag{4.4}$$

In this case p_i is taken as zero while the external/outer pressure, p_o is calculated using Equation (4.2) with the relevant field force and air gap area. The outer and inner yoke radius is donated as r_o and r_i respectively while r is the radius to the stress element under consideration. It is assumed that maximum stress will occur at the inner surface of the yoke and therefore r is taken to be equal to r_i. Once again the yoke height protects the outer rotor yoke against yielding or plastic deformation and calculated safety factors coincide with the FE results for the same conditions.

It should be noted that even though the yokes, under the considered loads, will never experience yielding, deformation or deflection can still occur. Although the deformation is not permanent, it does result in a closing of the air gap clearance which could be detrimental during operation. A mechanical FE analysis is performed to determine this reversible deformation of the yokes under load. The magnetic attraction force or field force that exists in the air gap is applied to the appropriate surfaces of the two rotor yokes. Figure 42 and Figure 43 represents the deformation of the rotor yokes under two conditions. For the first condition the yoke can expand or contract freely as with pressure vessels. For the second condition it is assumed that the support frame will add to the stiffness of the structure and a fixed constraint is therefore placed on the keyholes of the yokes. The FE results as illustrated in Figure 42 and Figure 43 predict that the maximum deformation or displacement for the outer and inner yoke will be 0.019 mm and 0.013 mm respectively under the first conditions and 0.011 mm and 0.009 mm with the fixed keyhole condition. This is a satisfactory result since it is far below the 10% threshold.

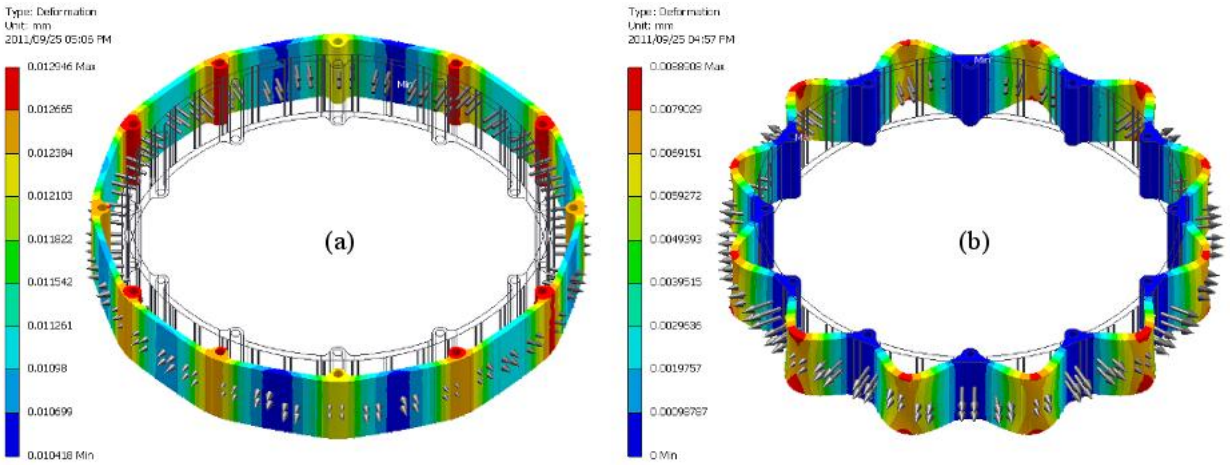

Figure 42: Deformation of inner rotor yoke with (a) no constraint and (b) fixed constraints

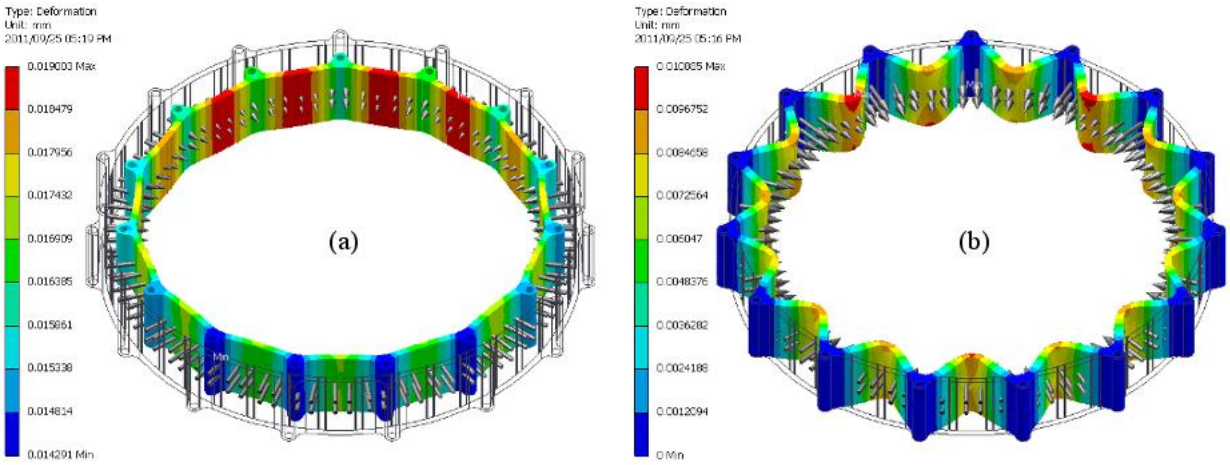

Figure 43: Deformation of outer rotor yoke with (a) no constraint and (b) fixed constraints

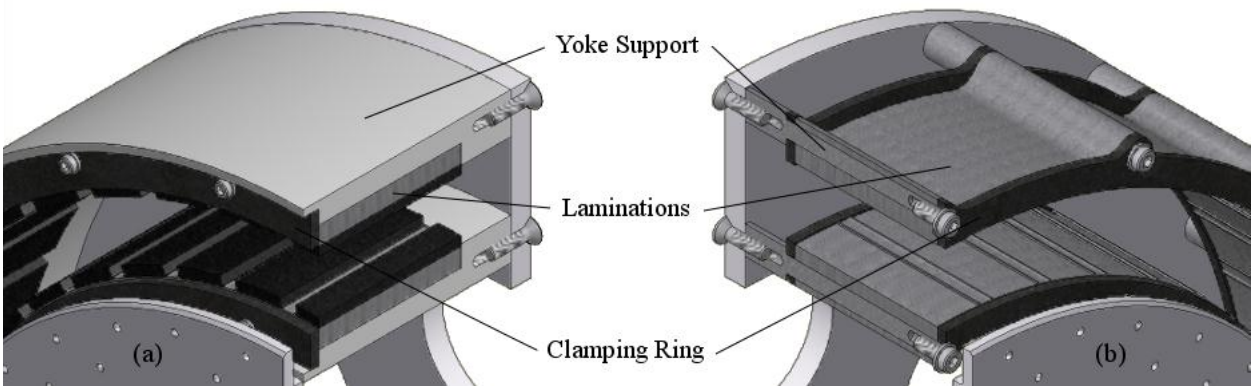

Figure 44: Solid support frame for rotor laminations

4.1.2 Lamination support frame

Since the yoke iron is laminated, the laminated steel stack of the rotor must be clamped and held tightly together in its compressed state to provide the rotor with rigidity and to prevent loose laminations from vibrating and producing noise. The laminations are generally held together with a series of welds axially along the yoke back, while the laminations are firmly clamped together in a holding fixture. This is done to keep the laminations together until it is installed and welded to the support frame. Another method commonly used in practice, particularly when the laminations are segmented, is to key the steel laminations to bars that form part of the support structure, before clamping and welding the stack [62]. The bars therefore aid in the proper alignment of the laminations and prevent any radial movement of the yoke.

For small- to medium-scale synchronous generators it is also common to key the laminations into a solid, circular support frame and clamp it down with a steel ring and bolts. The CAD in Figure 44 shows such a type of support frame. The laminations are clamped between the step/shoulder, cut into the solid support frame and the clamping ring. In an attempt to reduce the additional mass of the yoke support frame, the light weight material, aluminium, is used, but the material and manufacturing costs of this support structure is still steep.

In an effort to optimise the inactive structural mass, the solid support frame is done away with and support studs, machined from N8 bright steel, are used to support the yoke laminations. These studs are fixed onto a rotor disk, which serve as a common connector between the two rotor yokes and the rotating shaft. The yoke laminations, modified with keyholes, are sandwiched between two steel end rings and are keyed to the support studs. A step in the stud provides a shoulder for the first end ring to press against when the laminations are clamped and gives the lamination stack the desired axial placement from the rotor disk. The laminations fit tight to the stud, which requires that the laminations are clamped periodically as the stack is built up. A bolt tightened on the threaded end of each stud, presses down on the last end ring and holds the stack in compression.

Figure 45 shows photos taken at different time periods during the assembly process of the rotor. Clearly seen in the photos are the support studs (bolted to the rotor disk), the rotor yoke laminations which are sandwiched between the end rings, keyed to the stud and clamped to the studs' shoulders by the clamping bolts. The length of the stud's key section is designed so that the desired axial stack length is achieved when the clamping bolt and washer is tightened to the stud's end. 205 silicone steel laminations, with 0.5 mm thickness, were used to achieve a satisfactory rotor yoke compaction pressure.

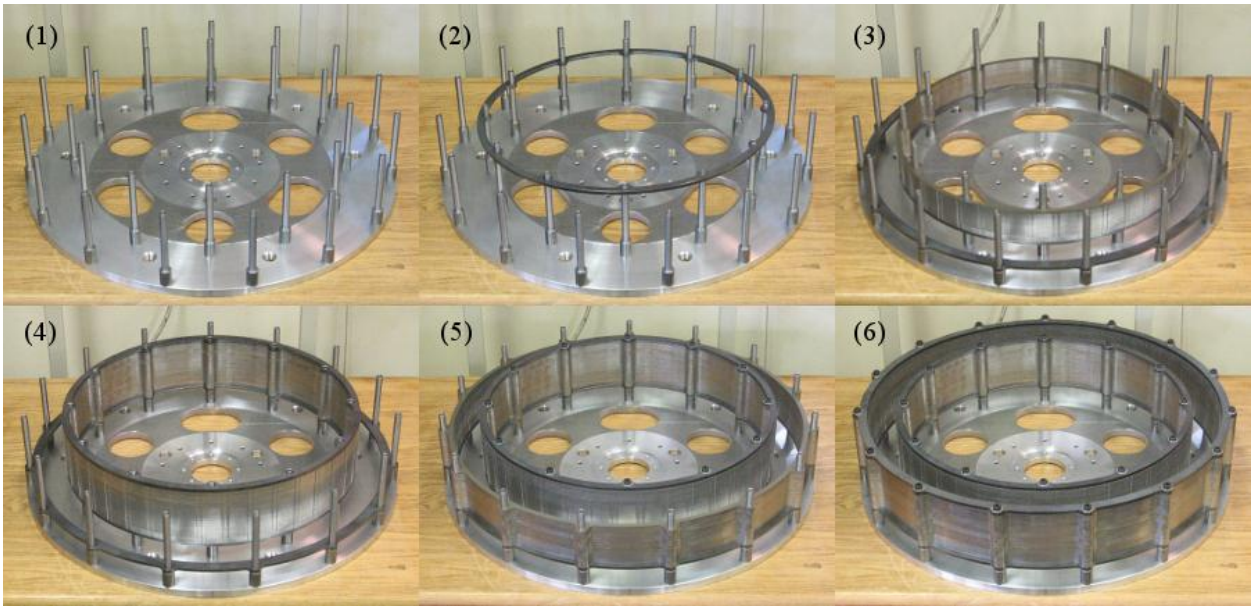

Figure 45: Rotor building sequence.

Since the rotor yokes have proved to withstand the magnetic field forces, torque is the only major load that the rotor studs have to withstand. As the electromagnetic simulations have shown, the outer rotor experiences a slightly greater torque at rated conditions than the inner yoke, but failure is expected to occur at the inner yoke supports since fewer stud are used for its support. Analysis is done on a stud, assuming 1000 Nm torque in the inner air gap. Furthermore, the torque ripple is accounted for in the analytical analysis, since failure due to both static and fluctuating load conditions are considered. Figure 46 shows the torque load acting on the rotor stud. Failure is expected to occur at A since this is where the tension stress is the greatest. Calculations for static failure have shown that the design safety factor is 5.4 for studs made of EN8 grade steel. Considering both the Gerber and Langer criteria of failure, the calculations for fatigue failure have resulted in a design safety factor of nearly 6 for the studs supporting the inner yoke.

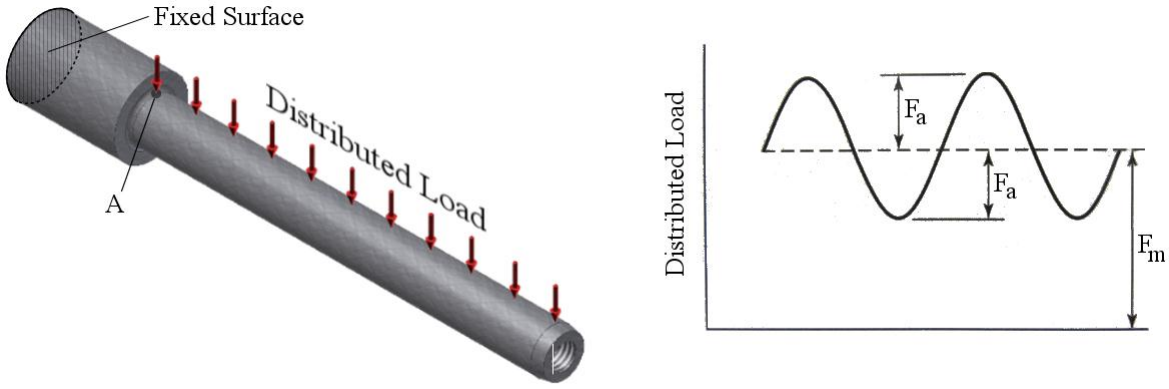

Figure 46: Load on rotor studs

4.1.3 Magnet mounting

The generator design considered in this study utilizes surface mounted magnets which, due to the stepping rotor surface profile it creates, produces turbulent air flow in the air gap and thus enhances the air cooling capability on the stator surface. The low operating speed of the generator allows the magnets to be bonded onto the rotor yokes with an epoxy adhesive which permits sufficient strength to withstand the centrifugal and magnetic field forces. The placement of the permanent magnets however, is a critical aspect in electrical machine construction. If it is not precisely placed it has a severe effect on the quality of the machine's output, since a misalignment of one mechanical degree for the 40 pole machine translates to a 20 electrical degree offset.

The use of embedded or even semi-embedded magnets makes this task much simpler, as the yoke profile can ensure the accurate placement of the magnets. With surface mounted magnets however, it is much more difficult to guarantee their precise placement, especially when they are glued to the rotor yoke surface. Too much glue between the magnets and yoke creates a significant closing in the air gap clearance. For this reason pressure is required to make sure that the layer of glue between the magnet and yoke surfaces is not excessive. If the pressure is not applied perpendicularly to the surface, the magnets tend to creep to the point where the force is perpendicular.

One way to overcome this creeping effect is to use spacers or a magnet jig when placing the magnets. This method can be very effective, but experience has shown that an expensive jig is required, since cheaper alternatives are susceptible to imperfections. The best alternative for the accurate placement of surface mounted magnets is to introduce burrs to the lamination profile which locate the magnets without having to embed them into the rotor yoke. The burrs on both sides give the securing glue more magnet-to-yoke surface area to act on. As these burrs are very small, it is assumed that it has no effect on flux leakage.

4.2 Stator Design and Manufacturing

The purpose of the iron stator back-yoke in conventional iron-cored generators is not only to provide a return path for the magnetic flux, but it also serves as a support structure for the stator teeth and copper conductors located in the slots. Without the stator back-yoke, the different stator components of the double-sided rotor topology are cast in an epoxy resin to locate them concentrically between the two rotor yokes and serve as a support structure for the stator's active components. This section discusses the various design aspects and manufacturing procedures for the iron-cored stator for the double-sided rotor direct-drive synchronous generator.

Due to the nature of the double-sided rotor topology, during the assembly of the generator, the stator needs to be inserted axially in between the two rotor yokes and secured on one end only for the

sake of simplicity. For this to be possible, the thickness or height of the unsecured, inactive section may not exceed the height of the active section.

4.2.1 Armature Iron Cores

The stator core has an I-profile, as determined from the electrical design and optimisation. Because the stator iron core experiences a full reversal flux density fluctuation, eddy currents and thus iron losses are prominent in the stator. For this reason the stator cores are constructed from laminated silicone steel. Conventional iron-cored machines are equipped with keyholes in the laminated stator yoke for assembly, alignment and structural support purposes. Since the double-sided rotor topology has no stator yoke, an alternative method for constructing the laminated cores should be investigated.

Three methods for the core assembly are found in practice. The first requires a keyhole, preferably two, axially through the laminated coil core. A steel bar/rod is then keyed through each hole and, while the lamination stack is clamped in a holding fixture, the rod ends are welded to the two end laminations. This method is not recommended, as the keyholes, located in the stator teeth, are expected to excessively increase iron losses due to higher saturation in the cores and the solid steel rods which will harbour large eddy currents. The second method of assembling the stator cores entails them being welded axially along the core sides while keeping them in a holding fixture. The electrical short-circuit created by the weldment on large laminated stators has a trivial effect on the performance of the machine. For small cores, the weldment can pose a more degrading effect to the machines performance. A third method, probably more common in small DC motors, is to bond the individual core laminations with some form of epoxy glue. The glue is allowed to cure while the lamination stack is clamped. The bond between laminations are not very strong, but since the copper coil is wound around the core and then cast in epoxy, the bond strength is only essential in keeping the core form until the casting process.

4.2.2 Armature coils

With the stator iron yoke removed it is possible for the armature coils to be wound directly onto the individual coil cores or stator teeth. The laminated coil core stack is clamped into a special fixture mounted on a winding machine. Because the slots are semi-closed, fibreglass strips, 0.75 mm thick, are glued to the core to provide support for the coil suspending above the iron flanges of the core. Insulation sheets are used to insulate the coils from the iron cores and prevent damage incurred during the winding process or with the removal of the coil module from the winding clamp.

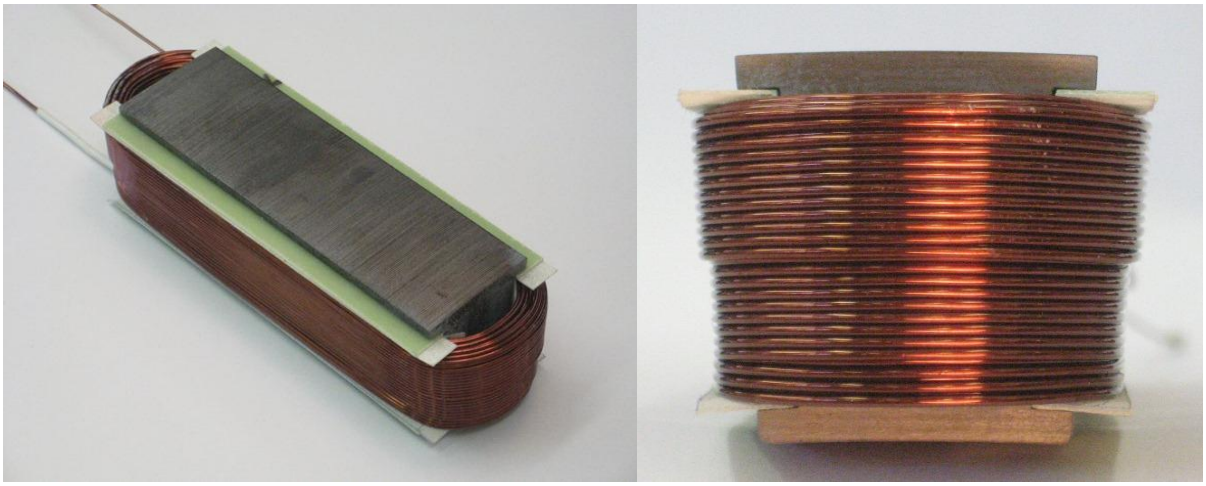

Figure 47: Copper coil module.

Calculations suggested and test coils confirmed that a 180 turn of 0.9 mm round annealed copper wire fills the available slot area the best. Cross sectional wire profiles, other than round, was not considered. The pure copper core of the wire is covered with a double layer of polyamide coating to insulate the coil winding strands from each other. Figure 47 shows a completed coil module that has been removed from the winding clamp.

After the winding process is complete, the coil module is tested for any possible damage to the coil insulation that would cause short-circuit between coil strands, the coil and the iron core or even between the phase coils sharing a slot. Each coil module is tightly wrapped in aluminium foil, then with a device call a Megger, and a potential of 1000 V is put across the coil and the foil. Any short circuit is an indication of damage to the copper wire's insulation. The completed coil module is now ready for casting.

4.2.3 Mould design

One of the advantages that the yokeless stator with its double-layer non-overlap windings offers is that segmentation of the stator is possible. Since one phase pole consists of two adjacent, serie connected coils, it is practical that the modular stator sections contain a number of coils that is a multiple two. The stator can therefore comprise of fifteen modular sections, each with a one phase pole. Since the roundness and geometric tolerances of the assembled stator become difficult to maintain with such a high number of stator modules, it is advisable to opt for fewer sections. For this study a modular stator segment is adopted which contains three stator poles (one for each phase) and represents an eighth of the assembled stator.

Even though the stator mould does not form part of the actual machine, it is nevertheless a very important part of the machine design. Several aspects regarding the positioning of the individual coil

modules become a concern when they have to be suspended between the rotors. These concerns may include the axial positioning, the radial positioning and the equal spacing of the coil modules around the stator circumference. For these reasons special attention is given to the design of the stator mould.

The mould consists of five parts – a convexed base, sides, a concaved top and a bottom plate. Slots (A) are cut in the axial direction in the mould's convexed base to guarantee the iron core's exact placement so that 48 cores are evenly spaced around the circumference of the complete stator. The slightest physical misalignment of the cores, as with the magnets, produces an electrical misalignment that is multiplied by a factor $p/2$ and thus has a deteriorating effect on the electrical characteristics of the machine. The concaved top section of the mould is designed with a shoulder (B), so that the radial thickness of the mould's cavity decrease, preventing the stator iron cores to move past the predetermined point. The shoulder therefor aligns the iron core with each other and determines their axial position.

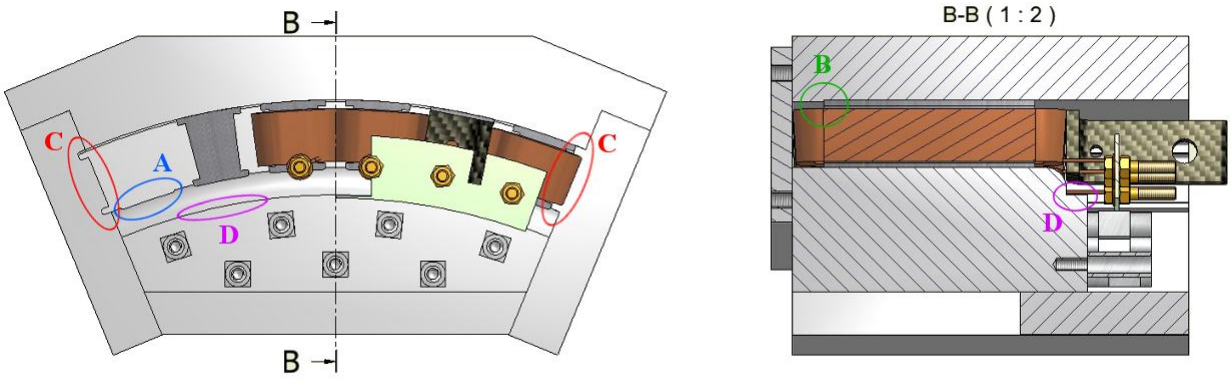

Figure 48: Assembled stator mould.

The stator mould is furthermore equipped with slots in both of its sides (C) – one side the inverse of the other, allowing the adjacent stator segments to slot into each other. These slots serve two purposes. Firstly it provides a guide for the stator segment when they are inserted or removed from the machine. These slots are crucial in preventing the iron-core stator segments from latching to either the inner or outer rotors' magnets. Secondly, it prevents the individual stator segments from vibrating individually under the fluctuating magnetic forces.

The mould design has a feature that gives the stator casting a curved shoulder (D) perpendicular to its mounting surface that is bolted to the stator supporting disk. The supporting disk is machined to exactly the radial dimension of the stators inherent shoulder, positioning the segment radially, precisely between the two rotors and also giving the elbow of the L-shaped segment some support.

The stator's radial placement is further ensured by using three shoulder bolts that fits snug in three of the spacers casted in the segment.

One of the curing stages of the epoxy resin, which is used to cast the stator components with, requires the cast to be exposed to high temperatures for a specified time period. Because epoxy resin tends to become soft at high temperatures, it goes without saying that the casting stays in the mould, which will be exposed to the same temperatures. High temperatures can cause the mould to swell or elongate excessively and in turn undesirable distorting of the curing epoxy resin may occur. A distorted stator section leads to a non-circular completed stator and non-uniform air gaps, which has a negative effect on machine performance, on quality and puts strain on the structural components. For these reasons it is important to consider thermal expansion properties when selecting a material to make the mould from. A common material used for mould is 6068 aluminium. It is strong, machined with ease, and has good thermal properties.

Finally, dowels and dowel holes are incorporated in the mould design to aid in the proper alignment of the different parts and to ensure an accurate and precise fit once assembled. Threaded holes are also provided to ease the disassembling of the mould when the stator casting is ready for ejection.

4.2.4 Stator casting process

The mould is prepared for casting by cleaning all surfaces properly with acetone. A silicone based grease in then smeared on all interior surfaces of the mould to ease the removal of the casted stator section later on in the casting process. The six coil modules are then placed in their positioning slots on the base of the semi assembled mould. The three phase coils are formed by paring two adjacent coil modules and connecting them in series as explained in chapter 3. This connection is done while the coil modules are positioned in the mould to ensure as short a series connection as possible. Following this the mould top is positioned on the coils and semi secured by the bolts. Before these bolts are tightened, the coils are pushed down onto the shoulder that is cut into the mould's top to ensure precise axial positioning of the stator iron cores. Next the bottom of the mould, containing the end-windings are filled with fibreglass fibres to help increase this section's strength and rigidity before the moulds base plate is secured. The mould is now fully assembled.

At the top open-end of the mould, the phase coils are connected to the outgoing electrical phase terminals and the L-shaped connection point, for inserting and ejecting the stator sections, are inserted. The spacers, needed for bolting the stator segments to its support structure, is secured in position with shoulder bolts for precise locating before the top section of the mould is finally also filled fibreglass fibres. The stator components are now ready for the epoxy resin casting process.

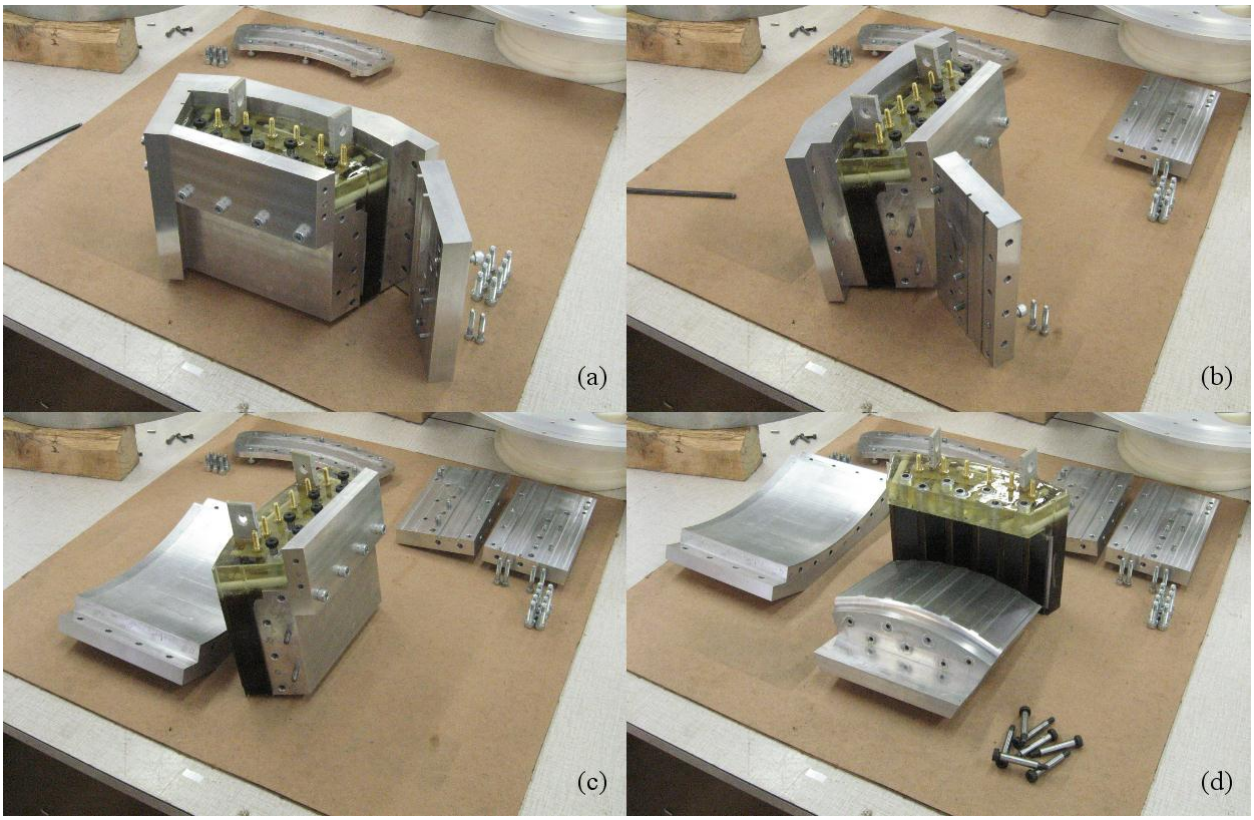

Figure 49: Ejecting the casted stator section.

The epoxy resin mixture is prepared by mixing the ratio of epoxy and its corresponding hardener in a separate container. The liquid mixture is then slowly poured into the mould and allowed to fill the mould from the bottom up, permitting air to escape. Once the desired level is reached, the mould is placed in a vacuum chamber to make sure that no air bubbles are trapped between the moulds content. This process also guarantees good penetration of epoxy resin between the coil's individual wire strands, adding strength to the casted end product. Usually the epoxy resin level lowers quite a bit and therefor it is needed to top it up to the desired level. The air extraction and topping up of epoxy resin is repeated until no noticeable drop in the resin level is noticed, before the casting is allowed to cure.

Curing resides in two stages. Initial curing takes place at room temperature for a 24 hour period. There after a second curing period of 4 hours takes place in a high temperature oven. Finally the finished section is removed from the mould and is tested for quality. Fig. 42 (right) shows a finished peace. An interesting occurrence was detected during the first curing stage of the stator casting. In the upper 20 – 30 mm of the casting the epoxy resin pulls away from the interior surfaces of the aluminium mould. This is anticipated to be due to capillary action effects, where the cohesive forces within the epoxy resin liquid in stronger than the adhesive forces between the liquid and the thin layer of silicone grease on the mould's surfaces. Because the silicone grease is only used for the

initial two or three casts, the effect of capillary action lessened, but where still undesirably dominant. This is overcome by pouring the epoxy resin liquid in two stages – only filling the mould to about 95 % the final cast volume and then after it cured, casting the other 5%.

4.2.5 Strength considerations

In the previous chapter it was shown that the field force in the outer air gap is slightly greater than that in the inner air gap. This resultant force is therefore applied to the inner surface of the stator segments as a pressure. The content of the casting will have a significant influence on the strength properties of the stator castings, but to find an approximation of the behavior of the stator segments, a pure epoxy casting is assumed as seen in Figure 50a. Figure 50b shows the predicted deformation of a pure epoxy casting, which is estimated to result in a 25% air gap closing. Such a large deformation of the free end of the stator segment will consequently increase field force and eventually result in a total air gap closing. The regions with notches which experience the greatest stresses are modified with large fillets as seen in Figure 50c.

To prevent the stator segments from deforming and resulting in a closing of the outer air gap, a stainless steel ring is used to clamp the assembled stator at the free end. The stainless steel ring is a robust solution to address the deformation of the stator segments and is expected to increase the eddy current losses of the machine, since its location is very close to the magnets.

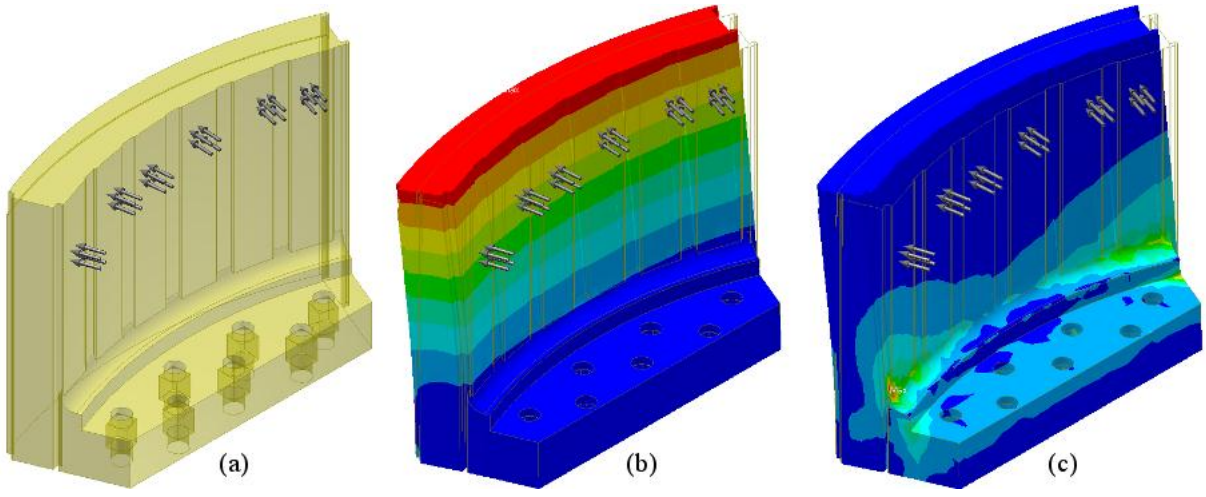

Figure 50: Prediction of stator segment deformation

4.3 Sub-assembly

In order to do a comparative study between the two generator topologies, that is the conventional single-sided rotor topology and the double-sided rotor topology, it is necessary to ensure that only the effect of the active material arrangement are compared. Care is taken to ensure that differences in the subassemblies of the two topologies limited. The same subassembly used for the conventional single-sided rotor generator is therefore implemented into the double-sided rotor generator's mechanical structure. No optimization is done on the sub-assembly of the double-sided rotor generator in order to prevent any possible mass reduction gained

The subassembly consists of a bearing hub, mechanical bearings, rotor shaft, rotor support disk and stator support disk. The bearing hub is modified by moving the flange, on which the central axis stator support disk is mounted, closer to the nacelle for the mounting of the cantilever stator support disk required for the double-sided rotor topology. The rotor shaft is mounted and located in the hub by two deep-groove mechanical bearings which are press-fitted to both the bearing hub and rotor shaft.

To ensure that the subassembly will adequately withstand the operational forces of the wind generator, FE analyses are done on the different sub-assembly components ensure that the deformation and stress concentrations due to loading is within acceptable limits.

4.4 Assembling of the double-sided rotor PMSG

Figure 51 shows the assembly of the two completed rotor yokes with magnets. Steel rods are used to guide the inner rotor yoke during the assembly and prevent the two rotors from latching to each other. As a safety measure, non-ferrous materials are used as a buffer between the two rotor yokes. Figure 51c shows the completed PMSG rotor with the hub, shaft and stator disk mounted. The skewing of the rotors can be seen in Figure 51d.

Figure 52 shows how the stator segments are inserted into the PMSG. Two non-ferrous dummy segments are used to serve as guides during the insertion of the first segment. This can be seen in Figure 52a. Once the stator segment is secured, the dummy segments are moved to provide support for the next stator segment to be inserted (Figure 52b). Eventually the secured stator segments provide the necessary support and guides for the last segments to be inserted. Figure 52c shows how the last stator is inserted. The final, completed PMSG with all the stator segments secure and phase terminals connected is shown in Figure 52d.

Figure 53a shows the stainless steel clamping ring used to prevent stator segment deformation. A standard size stainless steel flat bar is rolled and welded to the desired size. No further machining or

cutting is performed to save costs. The ring is press fitted to the assembled stator end. The ring is provided with threaded holes are, seen in Figure 53a, while a locating hole is drilled into each stator segment, as seen in is Figure 53b. Figure 53c show the grub screw used to locate the stainless steel ring on the stator. The 2 mm clearance between the rotor and stator clamping ring, seen in Figure 53d, is evidence of the tight clearances and need for precise positioning of components.

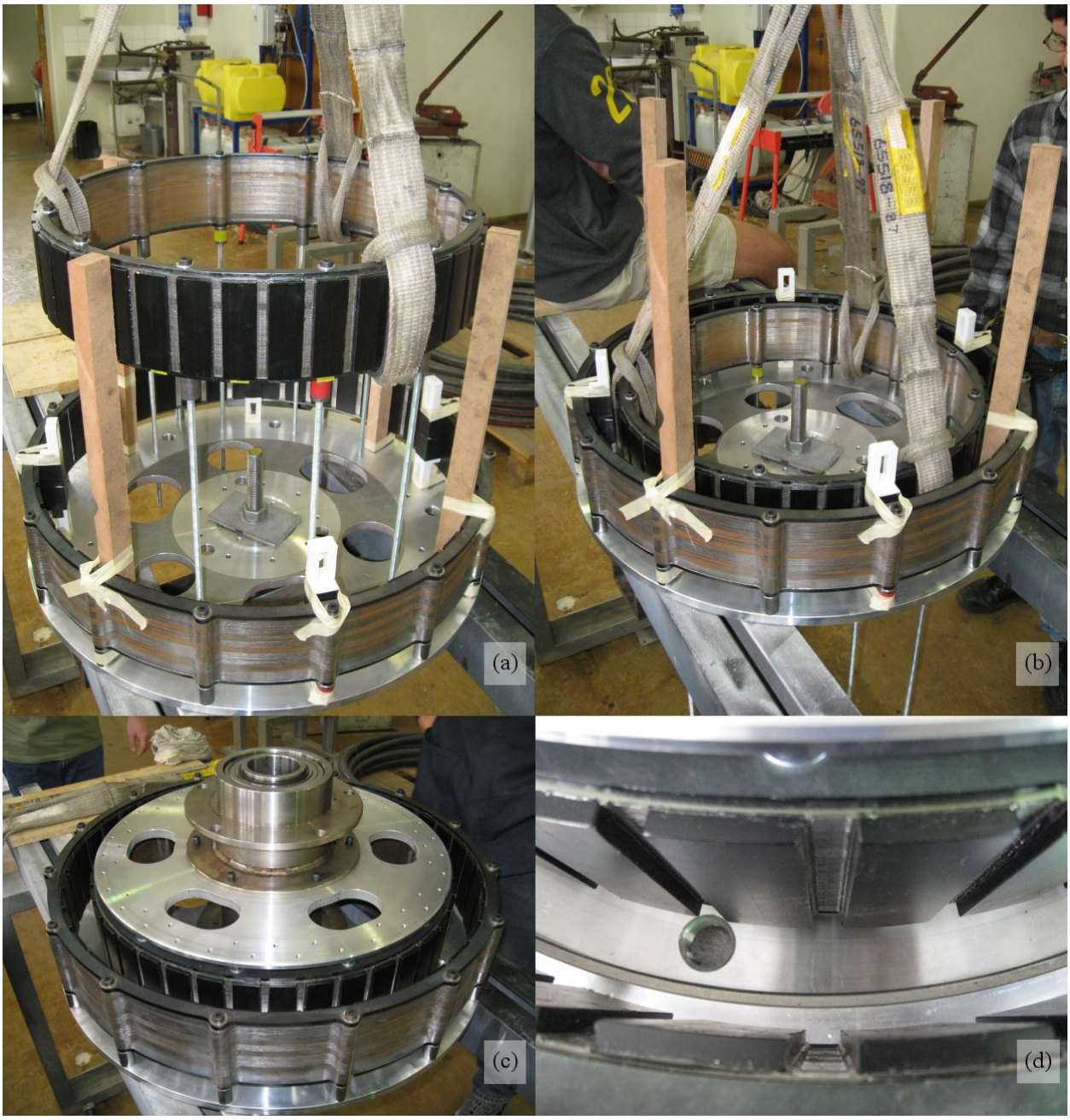

Figure 51: Rotor assembly.

Figure 52: Inserting stator segments into the double-sided rotor PMSG.

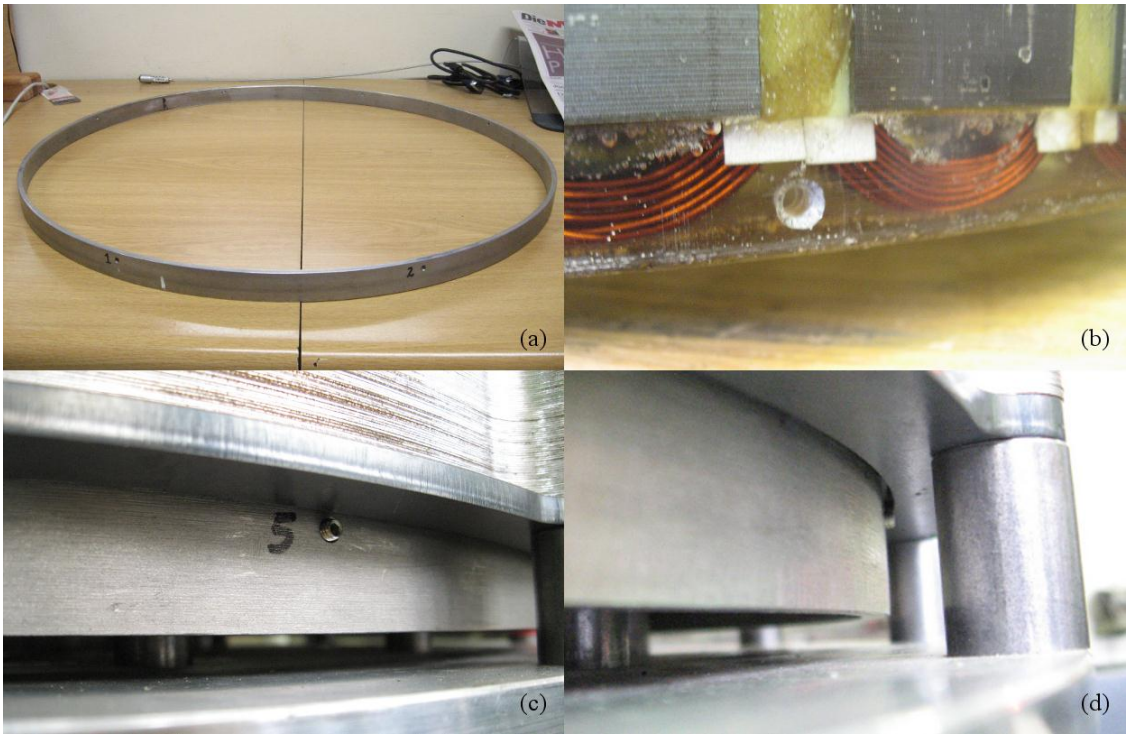

Figure 53: Clamping stainless steel ring for stator segments.

4.5 Mechanical Design Conclusions

The mechanical design of the double-sided rotor PMSG proved to simplify the assembly process while still maintaining the required precise placement of the different machine components. The stator segments also satisfactory complied with the tight design constraints and tolerances place on it and maintained an even clearance all around the air gap. Further confidence is gained in the mould design of the stator segments.

The studded rotor yoke support structure offers various advantages over that of the solid support frame. For one, air flows freely over the backs of both rotor yokes which enhance the dissipation of heat caused by iron losses in the yokes. Another is that much less material is needed for the support frame of the rotor yokes, promising a light weight structure. The manufacturing of the studs is also less laborious and much cheaper than that of the solid frame. With the rotor yoke rings suspended away from the rotor disk, the stator end-windings on both ends are exposed to sufficient air flow.

Furthermore, with cool air accessible from both ends of the yokes, the fanning effect of the surface mounted magnets enhances the cool-hot air exchange over the stator cores which have a positive effect on the machine's losses. The stator design and stator mould design also proved to be practical in keeping the inner and outer surfaces of the stator coil cores exposed to the air flow in the air gaps to shed excess heat as a result of its iron losses.

Chapter 5
Comparative Study and Evaluation

The content of this chapter is focused on the performance evaluation of two iron-cored direct-drive permanent magnet wind generators. The optimum designed 3rd generation conventional single-sided rotor wind generator, presented in [39], [46] and [53], and the near optimum 1st generation double-sided rotor wind generators are compared on a 15 kW power level. The machine dimensional parameters of these two machines are shown in Table 6. Since the purpose of the newly proposed double-sided rotor topology is to bring about a reduction in its structural mass, mass differences between the two generator topologies are considered after which other performance aspects such as induced voltage quality, per unit impedance, torque quality, magnet demagnetization and temperature rise and cooling of the magnets and windings.

Table 6: Parameters of the compared PMSGs

MACHINE PARAMETERS	DOUBLE-ROTOR	SINGLE-ROTOR	UNIT
Machine outer diameter, D_o	653.5	653.5	mm
Machine inner diameter, D_i	520.34	494	mm
Rotor height, h_y	8.47	7.25	mm
Magnet height, h_m	6.32	6	mm
Magnet pitch, σ_m	0.75	0.73	pu
Stator height, h_s	33	64.5	mm
Stator yoke height	_	10	mm
Slot width, σ_g	0.42	0.44	pu
Axial length, l	100	100	mm

5.1 Mass Comparison

The mass differences of the two PMSGs are shown in Figure 54. As expected, the magnet material and rotor iron usage is about two times more for the double-sided rotor topology than for the single-sided rotor topology, since it has a second rotor yoke with surface mounted magnets. Furthermore both the yoke and magnet heights are larger than that of the single-sided rotor PMSG. On the other hand, the stator iron usage of the double-sided rotor is 44% less compared to the conventional single-sided rotor machine. This was anticipated since the double-sided rotor topology has a yokeless stator. However, the large reduction in stator mass is not only a result of the yokeless stator, but also because its tooth height is shorter than that of the conventional yoked stator. Interestingly the optimisation algorithm has reduced the stator/tooth height of the yokeless stator design by 40%, which consequently also greatly reduced the copper volume of the machine as seen in Figure 54.

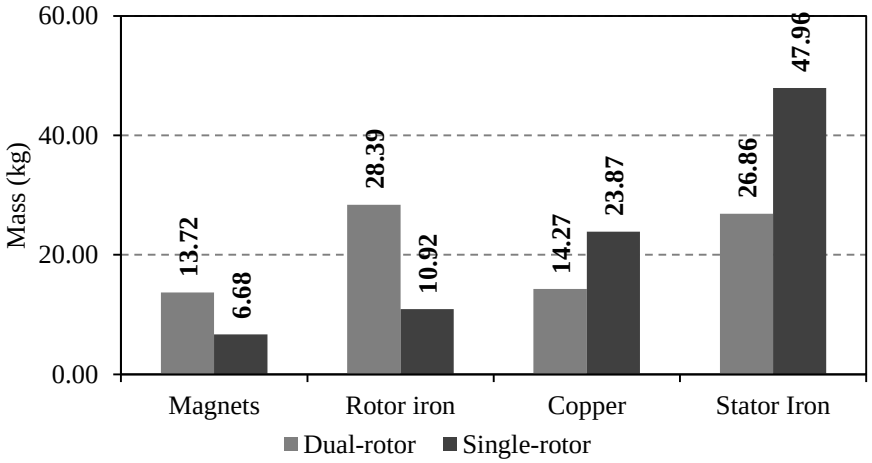

Figure 54: Active mass comparison of the double-sided rotor and single-rotor PMSGs.

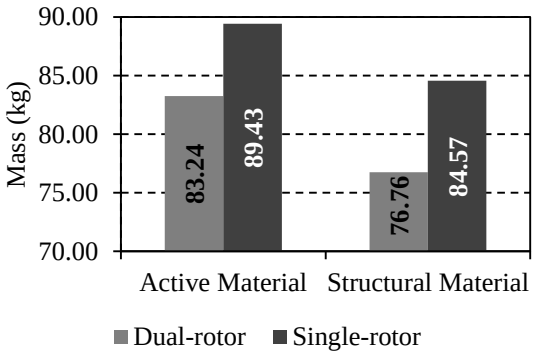

Figure 55: Active and structural mass comparison of the double-sided rotor and single-rotor PMSGs.

Figure 55 shows the active material and structural material differences of the two generator topologies. The double-sided rotor topology utilises less material both for the active components and

for the structural components. Although this topology uses more or less twice as much magnets and rotor yoke iron, its yokeless stator design and shorter stator teeth/slots height brings about the great reduction in active material. This large reduction in stator material can be explained by looking at Equation (3.7) again. Since both generators are designed to develop the same air gap torque value at rated speed, the double-sided rotor topology has the advantage of having a higher slot fill factor, two layers in each slot, a higher peak value for the fundamental no-load air gap flux density and a total air gap area that is nearly twice that of the conventional topology's. This allows the fewer number of copper coil turns around each stator tooth (48 coils with 180 turns each, compared to 24 coils with 424 turns each) and is expected to be the reason for the narrower and shorter stator slots.

As the sub assembly of the both machines are basically identical, the mass difference seen in Figure 55 for the structural material is primarily owed to the rotor and stator support structures of the double-sided rotor machine. Figure 56 shows the difference in the two rotor support structures. The 27 support bars that serve as support structure for the two rotor yokes and illustrated in (a), clearly use less material than the yoke support structure used in the single-sided rotor machine and illustrated in (b).

A similar solid support structure, as seen in Figure 56b, is used for the stator yoke lamination stack of the single-sided rotor machine. Since the stator coil core laminations of the double-sided rotor machine are bonded, coils wound directly on it and then permanently casted in an epoxy and fibreglass stator casting, there is no need to clamp the core lamination stacks. The stator design also uses the less dense fibreglass-epoxy casting as a support structure that is mounted to the stator support disk and contributes to the structural mass reduction seen in Figure 55. There is however concerns and uncertainty regarding the behaviour of the epoxy castings over time, that need to be investigated further.

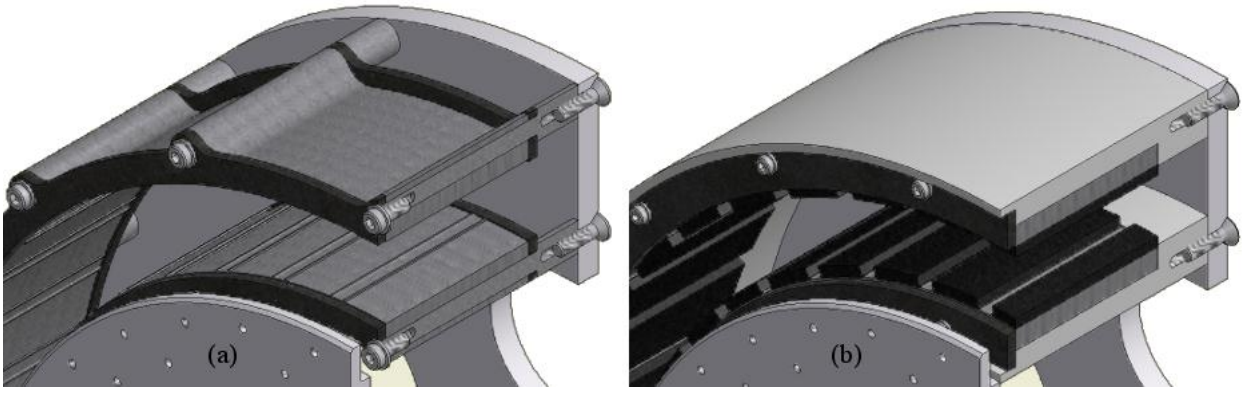

Figure 56: Two rotor yoke support structures.

5.2 Laboratory Test Setup

The test bench setup for the testing of the double-sided rotor generator is shown in Figure 57. A 4 pole, 45 kW induction machine, with a rated speed of 1475 rpm, is connected to the utility grid via an *Allan Bradley* variable speed drive (VSD), which allows variable speed operation. The induction machine is connected to a gearbox, with a gear ratio of i = 7.6, to match the torque and speed characteristics of the low speed, high torque synchronous PM wind generator. Prop shafts are used to transfer the torque between the gearbox and the PM synchronous generator. A *Lorenz* torque sensor is placed in the connection between the gearbox and electrical generator to measure the developed torque. This measured data is read through a USB connection and stored on a notepad computer. Finally the electrical wind generator tested can be connected to a resistive load or short-circuited.

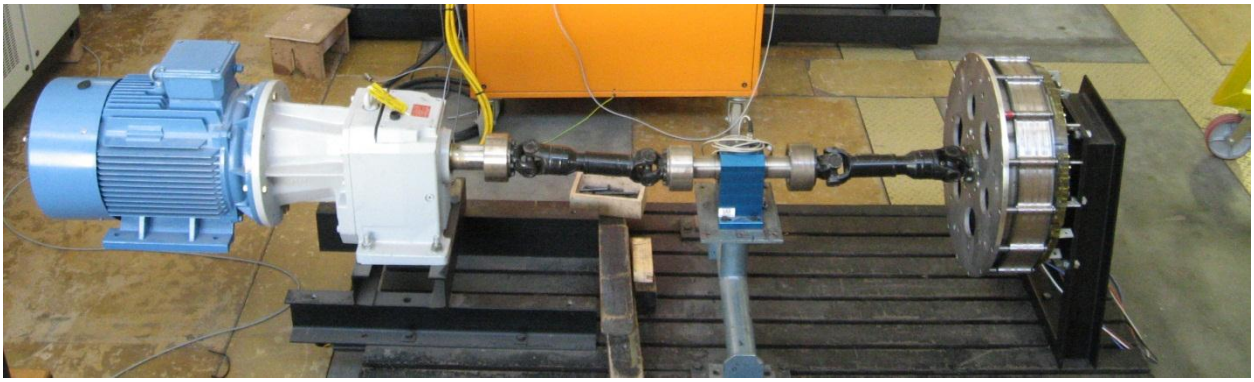

Figure 57: Test bench setup.

5.3 Performance Evaluation

In this section the practical measurements attempts to validate the predicted performance results from the electrical design in Chapters 3.

5.3.1 Voltage Quality

The voltage quality of the double-sided rotor PM generator, with its double layer non-overlap windings, is expected to be better than that of its single-sided rotor counterpart, with single layer non-overlap windings. It is known that non-overlap windings with a double layer arrangement have a lower harmonic content than those with a single layer arrangement. Figure 58 shows the induced voltage wave forms of the two machines, at rated speed, are shown in the time domain. From Figure 58 it seem as if the double-sided rotor PM machine has a generated back-EMF voltage that is closer to being pure sinusoidal, compared to the single-sided PM machine.

The amplitude of each of the harmonics present in the measured induced voltage, is obtained by applying a Fast Fourier Transform (FFT) on the measured data points. The first 22 harmonics in the open circuit induced voltages of both PMSG's are plotted in the frequency domain in Figure 59. From this plot is evident that the double-sided rotor has fewer harmonics than the single-sided rotor PMSG, although it has a very dominant 3rd harmonic. The first harmonic is omitted in Figure 59 since it only indicates the amplitude of the fundamental voltage component.

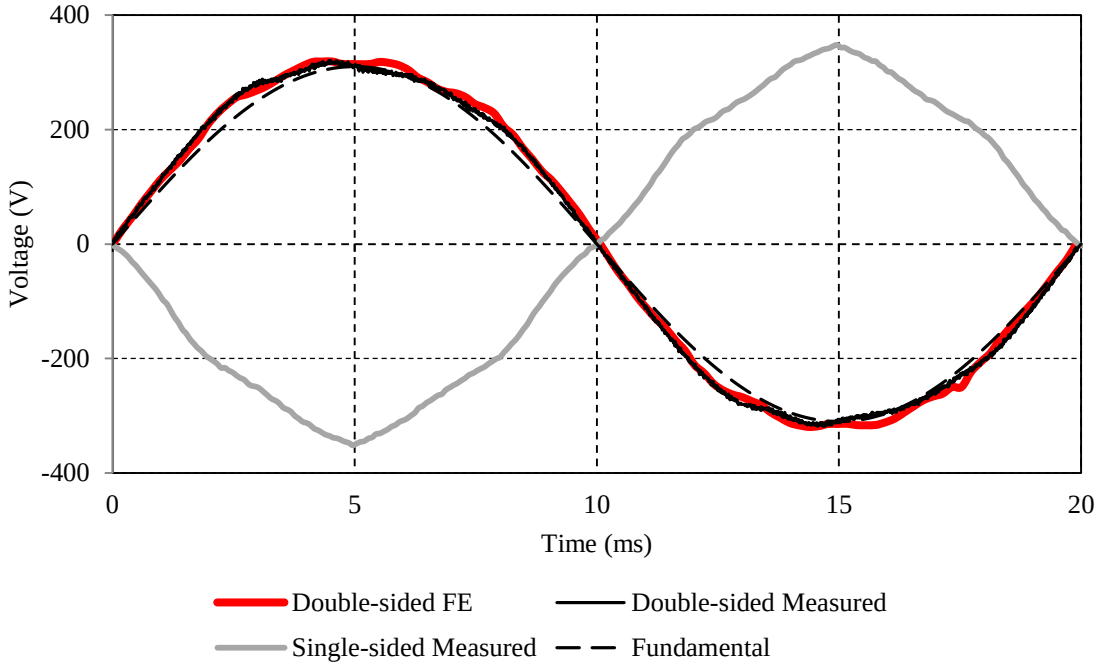

Figure 58: FE-calculated and measured open circuit induced voltages at rated speed.

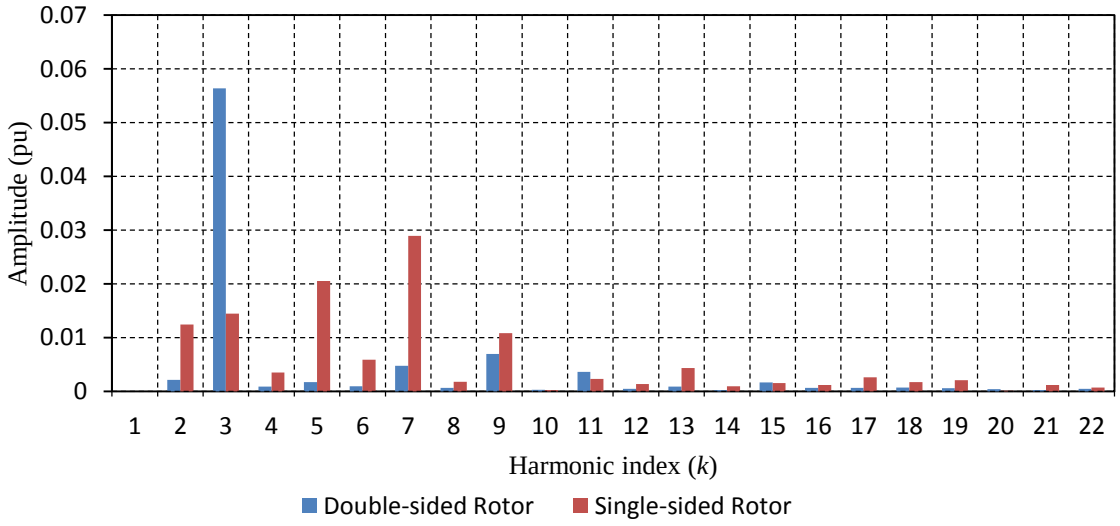

Figure 59: Amplitudes of the harmonics present in the no-load voltage waveform.

Since the induced voltage waveform is not perfectly sinusoidal, the total harmonic distortion (THD) index gives some indication of the amount of distortion in the voltage. The THD of the induced voltage can be calculated by [47]

$$THD_V(\%) = \frac{\sqrt{\sum_{n=2}^{\infty} V_n^2}}{V_1} \tag{5.1}$$

where V_n is the voltage amplitude of the n-th order harmonic frequency and V_1 is the voltage amplitude of the fundamental frequency. The THDv caused by the first 40 harmonics is calculated to be 5.72%. Interestingly this is more than the 4.29% THDv of the single-sided rotor PMSG.

The phase voltage and current waveforms at rated load is shown in Figure 60. The load test was done with the PMSG connected to a resistance load. The THD of the rated load voltage and currents are calculated to be 5.42% and 0.83% respectively.

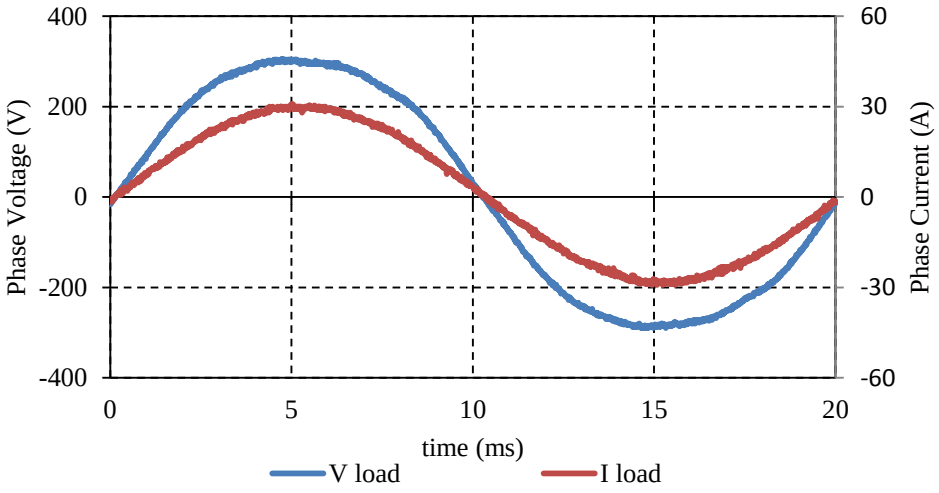

Figure 60: Phase voltage and current measured at rated speed with a resistive load.

5.3.2 Determining Phase Circuit Parameters

Figure 61 shows a schematic of the equivalent circuit of a single phase with its parameters. The internal phase resistance, R_i, obtained by connecting the terminals of a milli-ohm meter to the phase and neutral terminals of the PMSG. The internal phase inductance, L_i, value is determined by first obtaining the internal phase impedance, Z_i, which is given by

$$Z_i = \frac{E_{OC}}{I_{SC}}. \tag{5.2}$$

Thus the open-circuit (OC) induced phase voltage and short-circuit (SC) phase current, at the same rotor rotational speed, n, is required to obtain Z_i, of the double-sided rotor PM generator. Once Z_i is determined, the internal phase reactance, X_i, is accordingly determined by

$$X_i = \sqrt{{Z_i}^2 - {R_i}^2}. \tag{5.3}$$

Finally, with X_i known, the internal phase inductance is calculated with the expression

$$L_i = \frac{X_i}{2\pi f}. \tag{5.4}$$

In this study a milli-ohm meter is used to obtain R_i for each phase. The value for R_i is found to be 333 mΩ for each phase. The resistance of the FE model is corrected so that its total R_i equals the actual measured R_i value of the double-sided rotor PMSG. With this amended FE model, the OC phase voltage and SC phase current is obtained at various rotor speeds and the L_i calculated. Figure 62 shows the calculated L_i values for a range of operating speeds.

Laboratory test measurements could not verify this parameter value since the rotor speed was limited to about 14.5 rpm. This limit is imposed by the torque sensor which reached its rated torque of 2 kN at this rotor speed. Transient FE simulation results predict that the maximum developed SC pull-out torque of the double-sided rotor PMSG to occur at about one third of its rated speed and to have a magnitude three times that of its rated value.

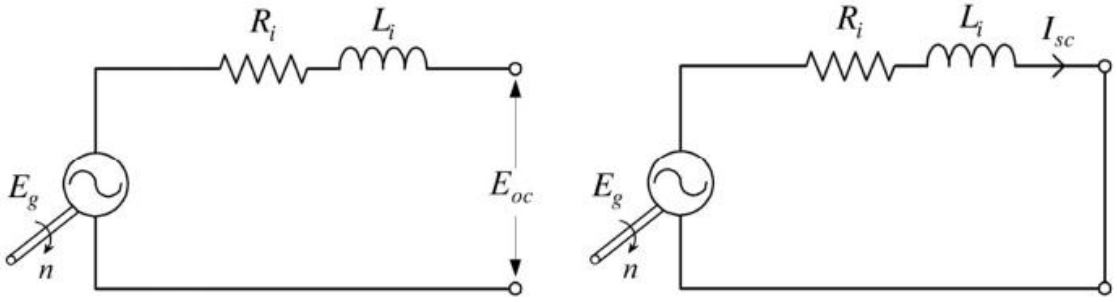

Figure 61: Schematic for the open circuit (left) and short circuit (right) test [47].

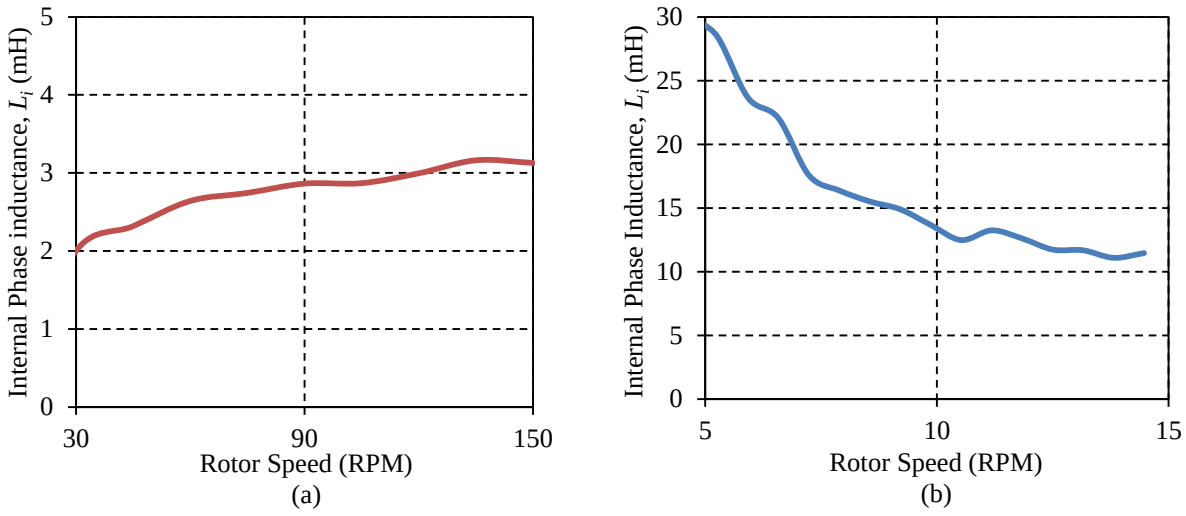

Figure 62: FE calculated internal inductance (a) FE calculated and (b) Measured.

Determining the machine inductance has shown to be a greater challenge than what initially was expected. The FE calculated inductance is much lower than the value calculated from the measured results. This can be explained, since in the case of the 2D FE calculation the end winding inductance is ignored, which will significantly lower calculated inductance value. In this regard the FE calculated inductance is too low. At the same time it is expected that both the measurement and FE way of calculations give too high inductance values. The reason for this is that the armature reaction effect is ignored in both methods. The armature reaction effect reduces the air gap flux and hence E_{oc}.

Finally, the difference in the FE and measured results seen in Figure 62 can be explained by a difference in the magnet BH characteristic used in the FE calculation and the actual magnet's characteristic in the machine. Although the measured open circuit voltage E_{oc} can be close to the FE calculated value, this is not a guarantee that the magnet characteristics in both are the same.

5.3.3 Torque Quality

Two machine parameters in wind generators that quantifies the quality of the machine's torque, is its torque ripple and the cogging torque. Chapter 3 showed that slight dimensional parameter changes have a significant effect on the torque ripple and greatly improve it with trivial changes in the average generator torque. FE modeling of the double-sided rotor PMSG with its optimum machine parameters estimated a 2% ripple in the developed torque. Although the torque ripple is considered to be more of a concern in safeguarding the generator during operation, the cogging torque is also investigated here.

Because of dynamic effects contained within the drive train of the test setup, it is not possible to accurately measure the cogging torque in a dynamic test. A static cogging torque test setup, as proposed in [39] and illustrated in Figure 63, is thus used to obtain cogging measurements. In this setup a torque beam is connected to the torque sensor, on the prime mover's side. Knowing the length of the beam and by controlling the height of its loose end, the electrical machine's rotor can be positioned to any mechanical angle and corresponding torque measurements taken. Since the cogging torque fluctuates about zero, applying a counter weight to the rotor will give the measurements a positive offset and simplify the mechanical rotor angle adjustments. The torque offset is subtracted afterward to obtain the cogging values about zero the torque.

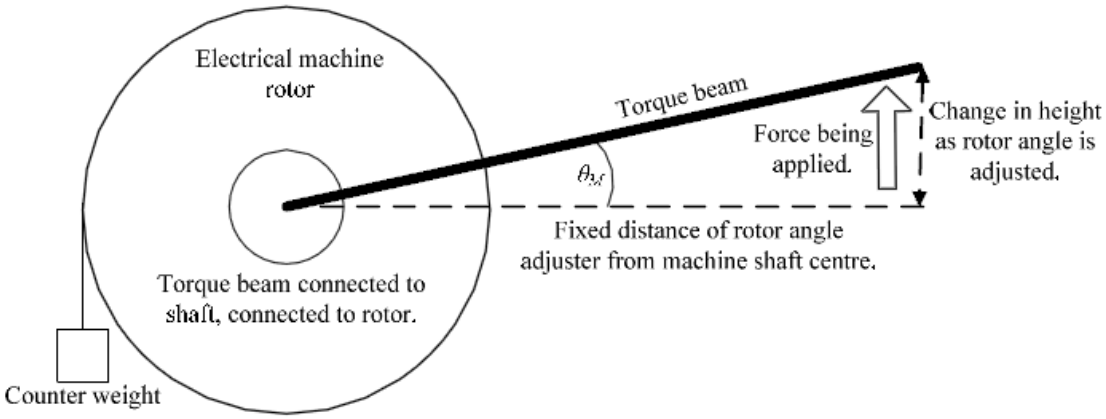

Figure 63: Illustration of the static cogging torque measurement setup [39].

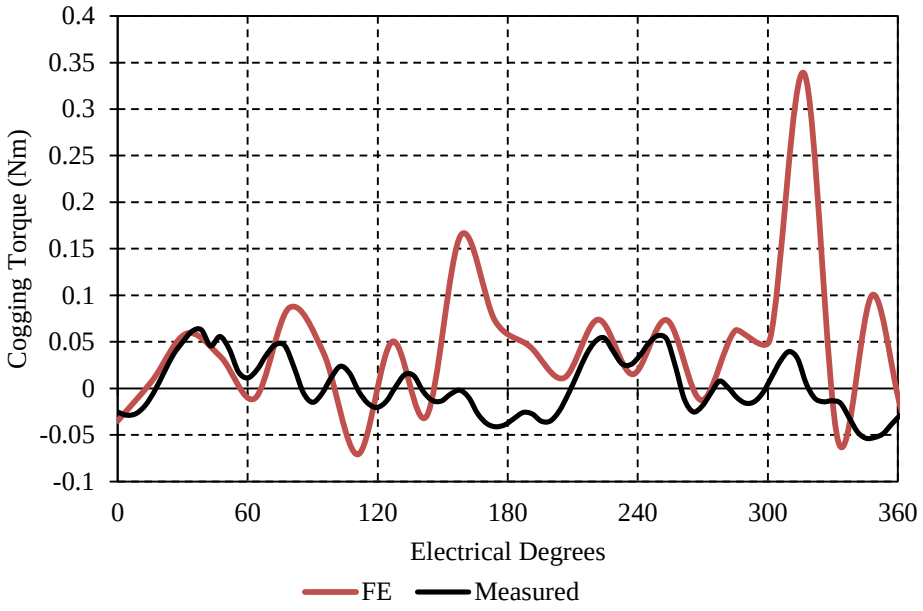

Figure 64: Cogging torque simulated and measured results.

The measured cogging torque and FE calculated cogging torque is presented in Figure 64. The measured cogging torque is 11% of the rated torque, is less than the FE predicted cogging and more consistent over the full electrical degree range. The total measure cogging is 11% of the rated torque.

5.3.4 Flux Density and Magnet Demagnetisation

Figure 65 shows the FE-calculated instantaneous air gap flux density in both air gaps of the double-sided rotor machine under full-load conditions. The effect of the armature reaction is clearly seen in flux density waveform. The higher magnet and rotor yoke heights of the double-sided rotor machine gives it the higher average air gap flux density of 0.9 T, compared to the 0.75 T of the single-sided rotor machine.

Although magnetic linearity was assumed for the electrical design of the double-sided rotor machine, several design choices were made to minimize the possibility of magnet demagnetisation. Since high machine operating temperatures increase the risk of demagnetization, design choices included segmenting the magnet to limit eddy currents, which is a source of heat, selecting a high magnet grade, and ensuring sufficient air flow over magnet and stator core surfaces. The larger magnet height also gives the magnets some protection. The *dq*-currents together with the phase current are shown in Figure 66. The values of i_d and i_q are 49% and 108% of the rated steady state current peak value respectively.

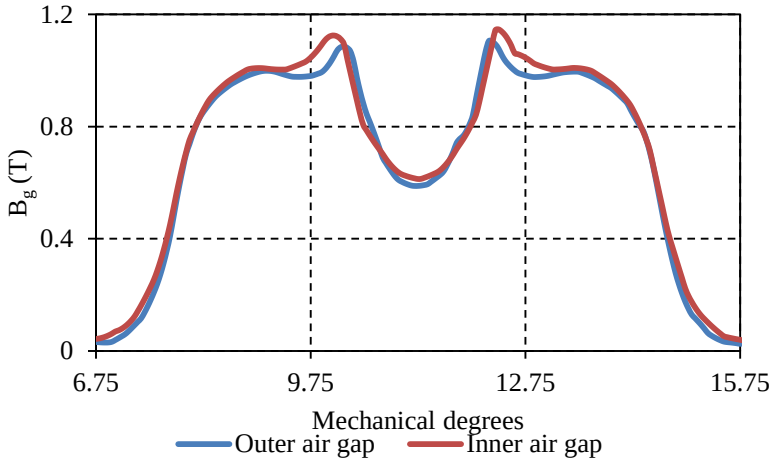

Figure 65: FE-calculated magnitude of the flux density in both air gaps of the double-sided rotor PMSG

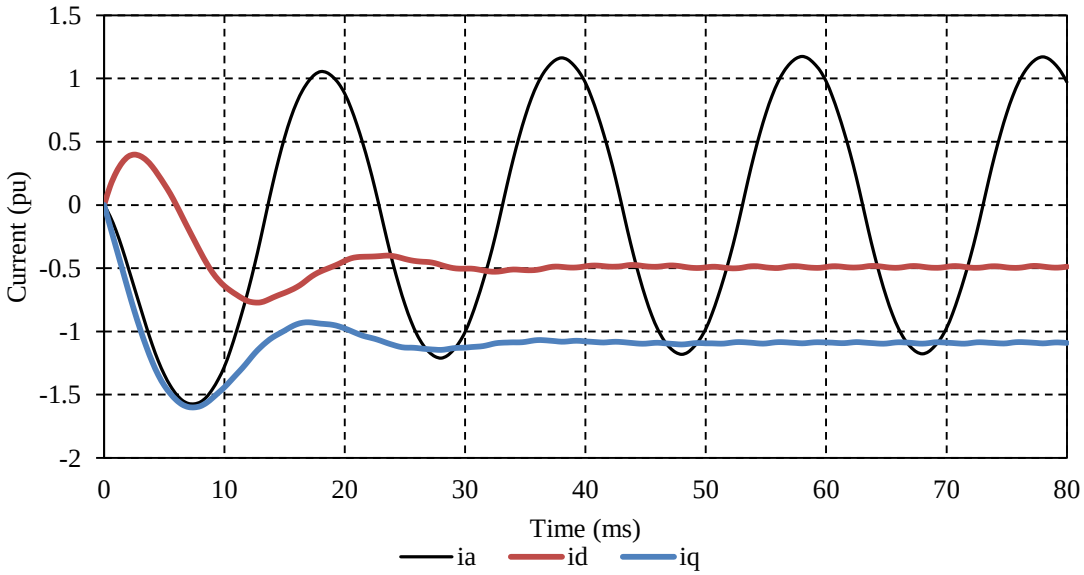

Figure 66: Transient FE-simulated short-circuit phase current of the double-sided rotor PMSG at rated speed

5.3.5 Temperature Rise and Cooling

Throughout the entire testing period of the double-sided rotor PMSG, the temperature of the stator coil cores and the magnets were monitored to prevent unwanted high temperatures that might cause failure or demagnetisation. A 60 minute continuous operating period, at rated speed and with a full resistive load, were performed to monitor the temperature rise of the different machine components. All tests were performed in a laboratory with an ambient temperature of about 20 °C and no air flow. The temperature monitored with a *FLUKE* Thermal Camera are expected to be higher than in real wind turbine applications where there is sufficient air flow to remove hot air near active component surfaces and replace it with cooler air. The results from the thermal images, taken after the 60 minutes of continuous testing, are shown in Figure 67 while the final temperatures of the different active components are tabulated in Table 7.

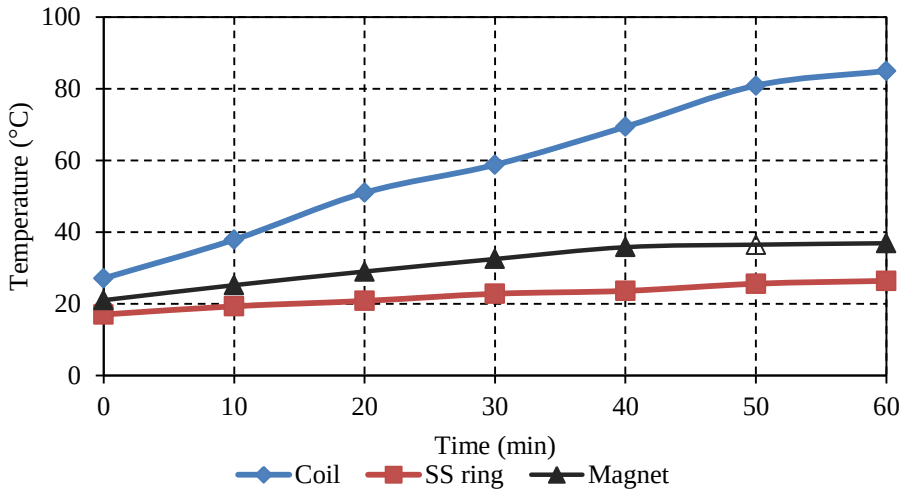

Figure 67: Temperature rise during a 60 min rated speed test with full resistive load.

Table 7: Final temperatures of PMSG components after a temperature test.

PMSG COMPONENTS	FINAL TEMPERATURE
Rotor Yoke	23.1 °C
Magnets	36.9 °C
Stator Coil Core	87.3 °C
Coil End Winding	63 °C
Stainless Steel Ring	29.2 °C

The temperature of the magnets seems to be linear for the first 40 minutes, with decreasing temperature increments of 4.2 °C – 3.3 °C every 10 minutes. The temperature increase of the magnets over the last 20 minutes of the test was a mere 1.1 °C, indicating the approach of a possible upper temperature limit which might be below 40°C. A similar knee is noticed in the temperature increase of the stator coil cores at 50 minutes. The temperature rise in the stainless steel ring is an indication of the unwanted eddy current losses in it. No particular flattening of the temperature rise in the stainless steel ring is noticed. The unequal initial temperatures of the different noticed in Figure 67 is owed to a few short test performed beforehand. Figure 68 shows the thermal images taken of the final stator coil core and magnet temperatures.

The SC test, in which the rotor speed was gradually increased over a time period of 20 minutes, has also had a very small effect on the temperature of the magnets and coil cores. The SC test was also performed after some resistive load tests, yet the thermal images in Figure 69 shows that the final temperatures reached are only 41.4 °C and 25.9 °C for the cores and magnets respectively.

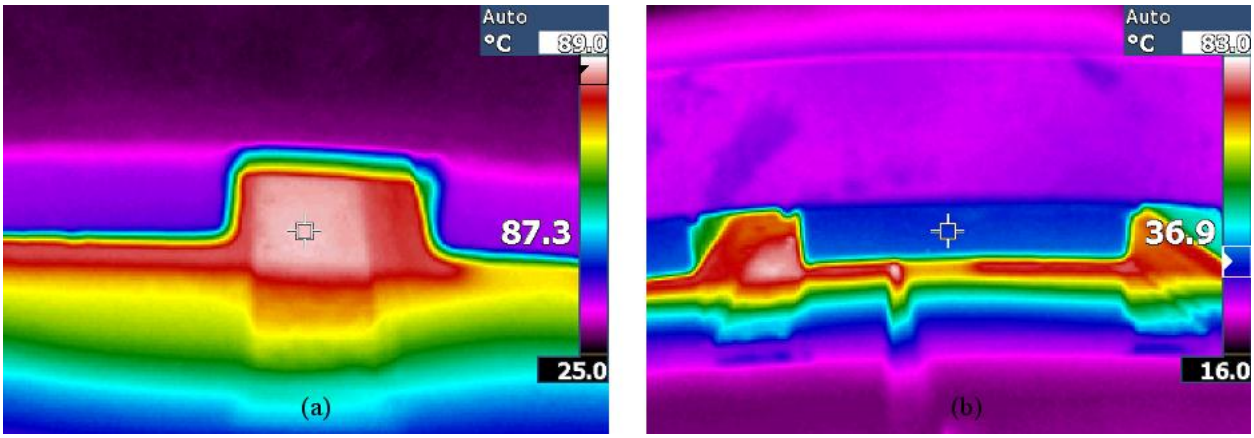

Figure 68: Thermal image for (a) the stator coil cores and (b) the magnets after 60 minutes operating at rated speed and with a full resistive load.

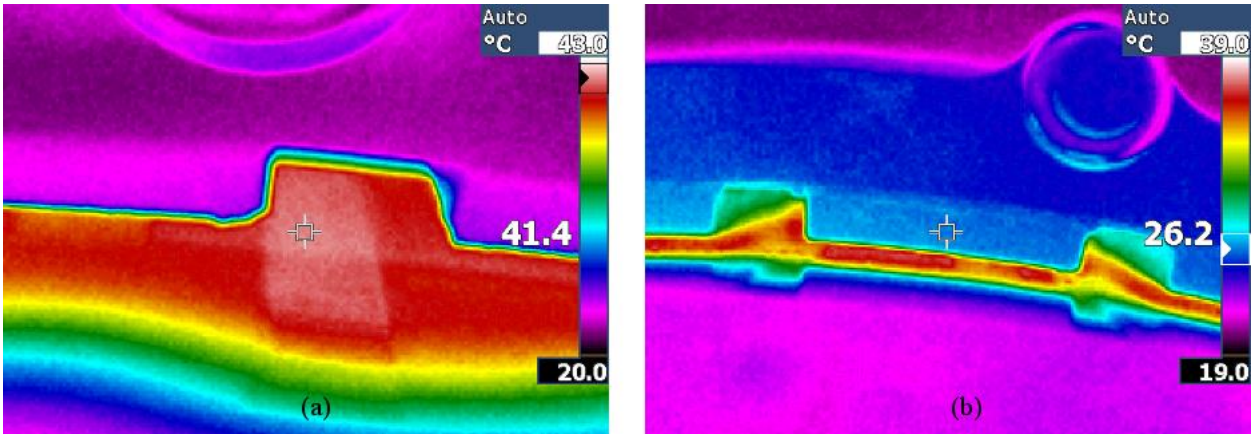

Figure 69: Thermal image of (a) stator coil core and (b) magnet after short circuit test.

The relatively low temperatures of the double-sided rotor PMSG is greatly owed to the mechanical design and construction of the machine. The rotor bar supports, suspending the rotor yokes the desired distance from the rotor disk, allows sufficient air flow through the two air gaps and continually replaces the heated air in the air gaps with cool air. The fanning effect of the surface mounted PMs also creates turbulent air flow in the air gaps and thus over the surfaces of the magnets and stator coil cores, which greatly enhances the machine's cooling ability. The rotor bar supports furthermore allows the rotor yoke backs to be exposed to the atmosphere. Air can thus flow directly over the laminated rotor yoke backs and maintaining its near ambient temperature.

5.4 Conclusion

Apart from the high cogging torque, the double-sided rotor PMSG topology has an acceptable induced voltage waveform, a high SC torque, low torque ripple and hence low noise, are well safeguarded against demagnetisation, and has excellent cooling properties. Furthermore this proposed machine's efficiency is greater than 90% from one fifth of its rated speed with a full resistive load, and 95.2% at rated speed. The efficiency of the double-sided rotor PMSG is shown in Figure 70.

The design results of the double-sided rotor and single-sided rotor PMSGs are summarised in Table 8. For interest sake, the design results of an air-cored PMSG of the same size and power rating is also included in Table 8. From the summarised data it is clear that the double-sided rotor topology is best topology choice for reducing generator mass and maintaining a high efficiency.

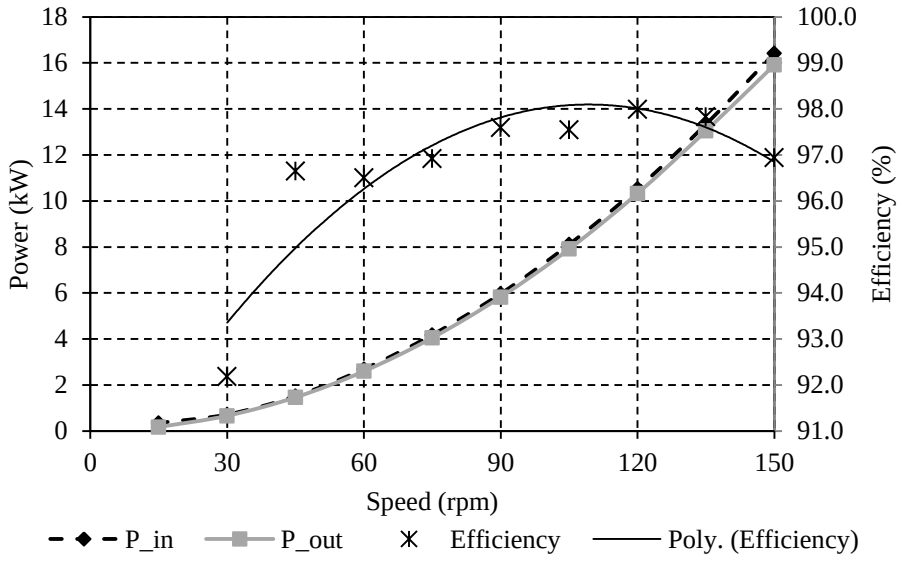

Figure 70: Efficiency of the double-sided rotor PMSG at rated speed and full load.

Table 8: Design results of two iron-cored and an air-cored direct-drive wind PMSG.

PARAMETERS ↓	Single-sided Rotor Iron-Cored	Double-sided rotor Iron-Cored	Double-sided rotor Air-Cored
Outer diameter, do (mm)	653.5	653.5	678
Inner diameter, di (mm)	494	520.34	576
Active axial length, ℓ (mm)	100	100	149
Magnet height, hm (mm)	6.0	6.32	9.7
Stator (slot) height, h (mm)	53	33	11.42
Copper mass (kg)	23.9	14.3	15.5
Active iron mass (kg)	58.9	55.3	43.9
Magnet mass (kg)	6.5	13.7	30.1
Total active mass (kg)	89.4	83.2	89.5
Total mass {structural + active} (kg)	174	160	164.4
Synchronous reactance *Xs* (p.u.)	0.471	0.103*	0.063
Phase resistance *Rs* (p.u.)	0.034	0.035	0.072
Current density (A/mm^2)	3.39	4.71	6.0
Power factor {*Id* = 0 A}	0.934	0.999	0.998
Efficiency (%) {*Id* = 0 A}	93.5	96.7	92.6
Copper losses (W)	749	574	1124
Stator eddy current loss (W)	_	_	34.4
Stator core losses (W)	246	110	_
Stator loss / stator volume(kW/m^3)	90	112	345

** Value obtained from FE calculations – The real synchronous reactance is anticipated to be higher, but still much lower than that of the single-sided rotor PMSG's reactance value.*

Chapter 6
Conclusions and Recommendations

To reduce the overall mass of wind turbine generators, a double-sided rotor PMSG with iron-cored stator coils is proposed. A 15 kW prototype is successfully designed and built with satisfactory performance. The double-sided rotor topology is evaluated in a comparative study against a conventional single-sided rotor generator. In this chapter the findings of the study is summarised and areas for further study are recommended.

6.1 Conclusions

In this study the origin of the radial magnetic attraction forces that exist in conventional single-sided rotor electrical generators is investigated. To better understand these forces, the electromechanical energy conversion and magnetic flux paths in such machines are considered. Specific conclusions of this study are summarised as follows:

- The magnetic attraction forces that exist in conventional iron-cored PM machines are a result of the stored energy in the air gap, which greatly depends on the air gap length. The slightest eccentricity of the rotor-stator arrangement has a quadratic effect on the magnitude of the resultant magnetic force.
- Adopting a dual air gap topology and removing the stator yoke greatly minimises the resultant magnetic attraction force on the stator. Since flux leakage exists around each air gap, the field forces of the two air gaps are still dependent on the air gap lengths, but oppose each other and so reduce the resultant force on the iron-cored stator.
- An analytical investigation suggests that a C-shaped modular rotor yoke topology can greatly reduce the flux leakage that makes the air gap field forces dependent on the stator position. Each C-shaped rotor yoke module, isolated from the neighbouring module, provides an alternative, transversal path for the magnetic flux which has shown to make the air gap field forces insensitive to any air gap closing/opening as a result of stator eccentricity. Weighty C-shaped yoke modules, construction challenges and design limitations have made this topology

an unpractical option. A double-sided rotor PM topology, consisting of two concentric rotor yoke rings, is proposed for this study since it proved to reduce the effect of the magnetic field forces on the iron-cored stator, but requires proper and precise stator placement.

A complete electrical and mechanical design of a double-sided rotor 15 kW direct-drive PMSG is presented in this study. The design process optimised both the active and the inactive material, whilst manufacturability and assembly of the prototype generator are also considered. Experimental results of a prototype generator is summarised as follows:

- Although the double-sided rotor topology uses nearly twice as much rotor iron and magnet material, the optimisation reduced the stator volume to such an extent that the total active material usage is less than that in the conventional single-side-rotor PM machines. The total active mass is 7% less than that of the single-sided rotor iron-cored PMSG.
- The double-sided rotor iron-cored prototype proved to be lighter than both the single-sided rotor iron-cored PMSG and the double-sided air-cored PMSG. The total mass of the generator presented in this study is a mere 40% of the total mass of the 15 kW C-Gen prototype generator presented in [37]. This light weight attribute is owed to the yokeless stator design and the low cost rotor yoke support structure.
- Stator core losses are significantly reduced by removing the stator yoke. The double-layer stator winding configuration allowed a shorter stator slot height which contributed to the 55% less core losses in the yokeless stator, compared to the conventional yoked stator.
- The double-sided rotor topology has inherent cooling advantages which are evident in the low operating temperatures of the machine and its magnets. The rotor support structure, which allows sufficient air flow through both the air gaps, and the dual air gap, which nearly doubles the area for heat exchange, are the greatest contributors to this topology's excellent cooling characteristic.
- The yokeless stator design has the advantage that the copper can be wound directly onto the stator teeth/coil cores, which gives the topology a good slot fill factor of 0.53.
- A modular iron-cored stator design is implemented in this study. The designed stator mould is equipped with slots and brims to ensure precise placement of the stator coil core modules. Tight tolerances are applied to the mould to ensure that the outer and inner surfaces of the coil cores are not covered with epoxy during the casting and curing process, which will inhibit thermal exchange in the air gaps of the double-sided rotor PMSG.

- Using Epoxy to cast the stator coil core modules and keep them suspended between the two rotor yoke is possible, since the double-sided rotor topology proposed in this study greatly reduces the resultant magnetic force on the stator segments.
- The undesired and relatively high cogging torque of the double-sided rotor generator cannot be explained, since it is not a result of irregular stator coil placement, non-uniform air gap length in the machine or any other mechanical discrepancies.
- The performance efficiency is very high
- The short circuit pull-out torque of the double-sided rotor PM generator is expected to be at least double that of the single-sided rotor generator, because of the double-layer winding arrangement used. This is confirmed by the practical measurements that showed a 2 kN developed short circuit torque at a 10^{th} of the machines rated speed. A short circuit pull-out torque of nearly 3 times that of its conventional single-sided rotor counterpart is expected.

6.2 Recommended further study

Some of the shortcomings of this thesis are presented in this section and are suggested for further study.

- The optimisation of the double-sided rotor machine could be revised in two ways. Firstly, a more refined optimisation algorithm can be used to find the optimum machine parameters and secondly, cogging torque can be minimised together with torque ripple, since the performance of the proposed topology built further confidence in the cantilever stator design.
- Thermal deterioration of epoxy is a concern. Literature shows that sufficiently high temperatures of the stator coils and cores could cause chemical bonds in the epoxy to break due to thermally induced vibration of the bonds. Macroscopically the cast becomes brittle and becomes mechanically weaker.
- Material wastage can be reduced by segmenting the rotor yoke lamination profile. This will consequently reduce the manufacturing cost of the laminations, which is desirable. Caution should however be taken with the segmentation location to prevent unnecessary iron losses in the rotor yokes.

Bibliography

[1] E.W.Golding, "The Generation of Electricity by Wind Power", published by E. & F.N. Spon Limited, 22 Henrietta Street, London, W.C.2, 1955 (page v).

[2] G.L. Johnson, "Wind energy systems", published by Prentice-Hall Inc., Englewood, Cliffs, NJ, 1985.

[3] http://windenergyfacts.eu/brief-history-of-wind-energy.html accessed 6 Sept 2011.

[4] http://www.centreforenergy.com/AboutEnergy/Wind/History.asp accessed 7 June 2011.

[5] Christian Ngô, Joseph B. Natowitz, "Our Energy Future Resources, Alternatives and the Enviroment" published by John Wiley & Sons, Inc., Hoboken, New Jersey, 2009 page 8

[6] Review of Historical and Modern Utilization of Wind Power - http://130.226.56.153/rispubl/VEA/Review_Historical_Modern_Utilization_Wind_Power.pdf accessed 6 Sept 2011

[7] Christian Ngô, Joseph B. Natowitz, "Our Energy Future Resources, Alternatives and the Enviroment" published by John Wiley & Sons, Inc., Hoboken, New Jersey, 2009 page 10

[8] http://www.guardian.co.uk/environment/2008/oct/17/wind-power-renewable-energy accessed 7 June 2011

[9] http://www.guardian.co.uk/environment/2008/oct/17/wind-power-renewable-energy accessed 6 Sept 2011.

[10] http://alumnipaksima.com/home/index.php?option=com_content&view=article&id=74:wind-turbine&catid=37:green-technology&Itemid=34 accessed 6 Sept 2011

[11] http://telosnet.com/wind/20th.html accessed 6 Sept 2011

[12] Olano A, Moreno V, Molina J, Zubia I. Design and Construction of an Outer-Rotor PM Synchronous Generator for Small Wind Turbines; Comparing real results with those of FE Model. Proceedings of the International Conference on Electrical Machines, 2008.

[13] http://www.windpowerengineering.com/tag/gerald-fox/ accessed 7 Sept 2011

[14] http://www.envirothonpa.org/documents/The1973OilCrisis.pdf accessed 7 Sept 2011.

[15] http://www.gwec.net/index.php?id=13 accessed 7 Sept 2011

[16] http://www.gwec.net/fileadmin/images/Publications/GWEC_annual_market_update_2010_-_2nd_edition_April_2011.pdf accessed 7 Sept 2011

[17] H. Polinder, S. W. H. De Haan, M. R. Dubois. "Basic Operation Principles and Electrical Conversion Systems of Wind Turbines", *EPE Journal*, 15, pp. 43-50, (2005).

[18] H. Polinder, D.J. Bang, R.P.J.O.M. van Rooij, A.S. Mcdonald, M.A. Mueller, "10 MW Wind Turbine Direct-Drive Generator Design with Pitch or Active Speed Stall Control", Proceedings of IEEE International Electric Machines and Drives Conference, Antalya, Turkey, 3-5 May 2007.

[19] T. Wildi, Electrical machines drives, and power systems – Fifth edition. Pearson Education, New Jersy, 2002.

[20] R. Datta and V.T.Ranganathan," Variable Speed Wind Power Generation using Doubly-fed Wound Rotor Induction Machine - A Comparison with Alternative Schemes",IEEE Transactions on Energy Conversion, Vol.17, no.3, pp.414-421, September 2002.

[21] A.S. McDonald, M.A. Mueller, H. Polinder, "Structural mass in direct-drive permanent magnet electrical generators", IET Renewable Power, Vol. 2, Issue 1, pp3-15, 2008

[22] D. Bang, H. Polinder, G. Shresha, J.A. Ferreira, "Possible Solutions to Overcome Drawbacks of Direct-Drive Generator for Large Wind Turbines" *Proceedings of European Wind Energy Conference and Exhibition*, EWEA: Marseille, France, 2009.

[23] E. Spooner, P. Gordon, J.R. Bumby and C.D. French, "Lightweight ironless-stator PM generators for direct-drive wind turbines", *IEE Procedings – Electric Power Aplications*, vol. 152, pp. 17-26, Jan. 2005

[24] Engström S, lindgren S. Design of NewGen Direct-Drive Generator for Demonstration in a 3,5 MW Wind Turbine. Proceedings of European Wind Energy Conference and Exhibition, EWEA: Milan, Italy, 2007

[25] Y. Chen, P. Pillay, A. Khan, "PM Wind Generator Comparison of Different Topologies", Proc. 39th IAS Annu. Meeting Conf., vol. 3, p.1405, 2004.

[26] F. Libert, J.Soulard, "Design Study of Different Direct-Driven Permanent-Magnet Motors for a Low Speed Application", Conference: Nordic Workshop on Power and Industrial Electronics (NORpie), Trondheim, Norway, 12-14 June, 2004

[27] M.A. Meuller, A.S. McDonald, "A lightweight low speed permanent magnet electrical generator for direct drive wind turbines", EWEC, Brussels, 2008

[28] S. Jöckel. "Gearless Wind Energy Converters with Permanent Magnet Generators – An Option for the Future?",*Proc. European Union Wind Energy Conference*, 1996, pp. 422-428, Göteborg, Sweden, 20-24 May

[29] T. Hartkopf, M. Hofmann, S. Jöckel, "Direct-drive generator for megawatt wind turbines", European Wind Energy Conf., Dublin, Ireland, 1997, pp. 668-671

[30] T. Haring, K. Forsman, T. Huhtanen and M. Zawadzki, "Direct drive – opening a new era in many applications", *Pulp and Paper Industry Technical Conference*, pp. 171-179, 16-20 June 2003.

[31] S. Du, Y. Zhang, J. Jiang, "Research on A Novel Combined Permanent Magnet Electrical machine", *International Conference on Electrical Machines and Systems (ICEMS'08), pp.* 3564 - 3567, Volume: Issue: , 17-20 Oct. 2008

[32] H. Haraguchi, S. Morimoto, M. Sanada, "Suitable Design of a PMSG for a Large-scale Wind Power Generator", *Energy Conversion Congress and Exposition, 2009. ECCE 2009.* pp.2447-2452

[33] A. E. Fitzgerald, C. Kingsley (Jr.), A. Kusko, *Electrical Machinery*. 3rd Ed. New York: McGraw-Hill. pp. 289

[34] Y. Duan, R.G. Harley, "Present and Future Trends in Wind Turbine Generator Design", Proc. IEEE Power Electron. Mach. Wind Appl., Jun. 2009, pp. 1–6

[35] E. Spooner, P. Gordon, J.R. Bumby and C.D. French, "Lightweight, ironless-stator, PM generators for direct-drive wind turbines", IEE Proc.-Electr.Power Appl., Vol. 152, No. 1, pp. 17-26, January 2005.

[36] A.S. McDonald, "Structural analysis of low speed, high torque electrical generators for direct drive renewable energy converters", Ph.d. dissertation, School of Engineering and Electronics, University of Edinburgh, Edinburgh, UK, December 2008

[37] N. Hodgins, A. McDonald, J. Shek, O. Keysan and M. Mueller, "Current and future development of the C-Gen lightweight direct drive generator for wave and tidal energy", *European Wave and Tidal Energy Conference*, pp. 352-359, Uppsala, Sweden, 7-10 September 2009

[38] T. Epskamp, B. Hagenkort, T. Hartkopf, S. Jöckel, "No Gearing, No Converter – Assessing the Idea of Highly Reliable Permanent Magnet Induction Generators", Proc. EWEC, 1999, pp.813 – 816, Nice, France, March 1999.

[39] J.H.J. Potgieter, "Design and Analysis of Gearless Direct-Grid Permanent Magnet Induction Wind Generator" MSc.Eng. Dissertation, Department of Electrical Engineering, University of Stellenbosch, Matieland, South Africa, 2011.

[40] D. Bang, H. Polinder, J.A. Ferreira, S. Hong, "Structural mass minimisation of large direct-drive wind generators using a buoyant rotor structure", Proc. of the IEEE Energy Conversion Congress and Expo (ECCE), 2010, pp. 3561 – 3568.

[41] J.N. Stander, G. Venter, M.J. Kamper, (2011), "Review of direct-drive radial flux wind turbine generator mechanical design", Wind Energy. doi: 10.1002/we.484

[42] G. Shrestha, H. Polinder, D.J. Bang, J.A. Ferreira, "Direct Drive Wind Turbine Generator With Magnetic Bearing", Proceedings of European Wind Energy Assosiation (EWEA) Offshore Wind Conference and Exhibition, EWEA, 2007

[43] D. Bang, H. Polinder, G. Shrestha, J.A. Ferreira, "Review of Generator Systems for Direct-Drive Wind Turbines", Wind Power to the Grid – EPE Wind Energy Chapter 1st Seminar, 2008, EPE-WECS 2008, pp. 1 – 10, Identifier: 10.1109/EPEWECS.2008.4497321

[44] M. Krishnamurthy, B. Fahimi, "Qualitative Analysis of Force Distribution in a 3-Phase Permanent Magnet Synchronous Machine", IEEE Conference on Electric Machines and Drives, 2009, pp. 1105-1112

[45] A. E. Fitzgerald, C. Kingsley (Jr.), S. D. Umans, 2003. *Electrical Machinery*. 6th Ed. New York: McGraw-Hill. pp. 112-129

[46] M.J. Kamper, J.H.J. Potgieter, J.A. Stegmann, P. Bouwer, "Comparison of Air-cored and Iron-cored Non-overlap Winding Radial Flux Permanent Magnet Direct Drive Wind Generators", Proc. Energy Conversion Congress and Exposition (ECCE'11), 17-22 Sept. 2011, pp. 1620 – 1627.

[47] J.A.Stegmann, "Design and Analysis Aspects of Radial Flux Air-cored Permanent Magnet Wind Generator System for Battery Charging Applications" MSc.Eng. Dissertation, Department of Electrical Engineering, University of Stellenbosch, Matieland, South Africa, 2011.

[48] R. Qu, T.A. Lipo, "Dual-rotor, radial-flux, toroidally-wound, permanent-magnet machines", IEEE-IAS Conf. Rec. Pittsburgh, PA, Oct 2002, vol. 2, pp. 1281 - 1288

[49] R. Qu, M. Aydin, T.A. Lipo, "Performance Comparison of Dual-Rotor Radial-Flux and Axial-Flux Permanent-Magnet BLDC Machines", Proc. Electric Machines and Drives Conference (IEMDC'03), IEEE International, 1-4 June 2003, Vol. 3, pp. 1948 – 1954.

[50] Y. Yeh, M. Hsieh, D.G. Dorrell, "Different arrangements for Dual-Rotor Dual-Output Radial-Flux Motors", Energy Conversion Congress and Exposition (ECCE), 2010 IEEE, 12-16 Sept. 2010, pp. 2956 - 2962

[51] P. Sivachandran, P. Venkatesh, N. Kamaraj, "Cogging Torque Reduction in Dual-Rotor Permanent Magnet Generator for Direct Coupled Stand-Alone Wind Energy Systems", Conf. Record of IEEE 2008 International Conference on Sustainable Energy Technologies (ICSET), Nov. 2008, pp. 24 – 28.

[52] J.H. van Wijk, M.J. Kamper, "C - core topology for PM wind generators with non-overlap iron-cored stator windings ", in IET Int. Conf. Power Electron., Mach. and Drives, Brigthon, 2010, p. 6

[53] J.H.J Potgieter, M.J. Kamper, "Cogging Torque Sensitivity in Design Optimisation of Low Cost Non-Overlap Winding PM Wind Generator", Int. Conf. on Electrical Machines (ICEM'10), Rome, Italy, Sept. 2010.

[54] A.S. McDonald, M.A. Mueller, H. Polinder, "Structural mass in direct-drive permanent magnet electrical generators", Renewable Power Generation, IET, March 2008, Vol. 2, pp. 3 -15.

[55] D.A. Wills, M.J. Kamper, "Reducing Rotor Eddy Current Losses Using Partial Magnet and Rotor Yoke Segmentation", Proc. of Int. Conf. on Electrical Machines (ICEM'10), Rome, Italy, Sept, 2010.

[56] H. Polinder and M.J. Hoeijmakers, "Eddy-current losses in the segmented surface-mounted magnets of a PM machine", IEE Proc. – Electr. Power Appl., Vol 46, no. 3, May 1999

[57] H. Polinder, M.J. Hoeijmakers, M. Scuotto, "Eddy-current losses in the solid back-iron of PM machines for different concentrated fractional pitch windings", IEEE International Electric machines & Drives Conference, 2007. IEMDC '07, Vol 1, 3-5 May 2007, p. 652 – 657

[58] F. Liber, J. Soulard, "Investigation on Pole-Slot Combinations for Permanent-Magnet Machines with Concentrated Windings", Proc. of Int. Conf. on Electrical Machines (ICEM'04), Cracow, Poland, 5-8 September 2004.

[59] F. Magnussen, C. Sadarangani, "Winding Factors and Joule Losses of Permanent Magnet Machines with Concentrated Windings", Electric Machines and Drives Conference (IEMDC'03), vol. 1, pp. 333 – 339, June, 2003.

[60] M.J. Kamper, A.J. Rix, D.A. Wills, R. Wang, "Formulation, Finite-Element Modeling and Winding Factors of Non-Overlap Winding Permanent Magnet Machines", 18th International Conference on Electrical Machines, 2008. ICEM 2008. 6-9 Sept. 2008, pp. 1 – 5.

[61] J.E. Shigley, C.R. Mischke, R.G. Budynas, *Mechanical Engineering Design*, Seventh Edition, McGraw-Hill, New York, 2004, p.150.

[62] G. Stone, E.A. Boulter, I. Culbert, H. Dhirani, *Electrical insulation for rotating machines: design, evaluation, aging, testin and repair*, John Wiley & Sons, 2004, pp. 137 – 139.